OFFICE OF NAVAL RESEARCH
CONTRACT Nonr-1866(24)

NR-384-903

TECHNICAL MEMORANDUM
No. 55

SOLID TORSIONAL HORNS

BY

Robert W. Pyle, Jr.

MAY 1963

ACOUSTICS RESEARCH LABORATORY
DIVISION OF ENGINEERING AND APPLIED PHYSICS
HARVARD UNIVERSITY-CAMBRIDGE, MASSACHUSETTS

Office of Naval Research

Contract Nonr-1866(24)

Technical Memorandum No. 55

SOLID TORSIONAL HORNS

by

Robert W. Pyle Jr.

May 1963

Abstract

The propagation of torsional waves in tapered solid elastic rods has been studied both theoretically and experimentally from the viewpoint of acoustic horn theory. Such tapered rods in torsional vibration have been dubbed "torsional horns." Two differential equations are derived which describe the propagation of torsional waves. One of these is an "exact" wave equation which can be readily solved only when the horn boundaries fit a separable coordinate system. The other is an approximate wave equation based on the assumption that the wavefronts are plane cross sections of the horn. This equation is very similar to Webster's plane-wave equation for compressional waves in an acoustic horn.

For purposes of analysis, torsional horns are divided into three categories: those having smooth contours fitting separable coordinates, those having smooth contours not fitting separable coordinates, and those having piecewise-smooth contours. Experimental apparatus was devised and built for the measurement of the standing-wave patterns and resonance frequencies of experimental torsional horns made of brass or mild steel. The experimental data are compared with the solutions of the two wave equations for selected horn contours from each category. A quantitative estimate of the error introduced by the plane-wave approximation is obtained for the exponential horn.

Acoustics Research Laboratory

Division of Engineering and Applied Physics

Harvard University, Cambridge, Massachusetts

PREFACE

Acoustic horns have been in use since primitive man first discovered that his voice could be heard at a greater distance if he cupped his hands around his mouth while shouting. The development of horns as impedance transformers progressed empirically from that day to the early twentieth century, when A. G. Webster did his pioneering work on acoustic horns. In the period between the two World Wars, the use of Webster's plane-wave horn equation was extended to the analysis of horns of several types of contour for guiding sound waves in air. During World War II, W. P. Mason conceived of using tapered solid rods as impedance changers for compressional elastic waves, and he successfully adapted existing horn theory to these solid horns. Such devices found use in the new art of ultrasonic machining and impact grinding.

Mason's work suggested to Professor Frederick V. Hunt a new twist in solid horns: the possibility of torsional excitation. The research reported here was initiated when Prof. Hunt proposed that I undertake to find out whether tapered solid rods display typical "horn-like" behavior for torsional waves.

I would like to acknowledge the guidance of Prof. Hunt in the execution of this research project. His ready availability and willingness to discuss problems both large and small have been of no little help. I wish to thank collectively the staff of the Acoustics Research Laboratory for many fruitful discussions and helpful suggestions. I am particularly grateful to Fudlow Abdelahad for his expert machine work in the construction of the mechanical apparatus and the experimental horns, and to Miss Constance Demos for her tireless assistance with the

mechanics of manuscript production. Finally, I should like to acknowledge the partial support of this research by the Office of Naval Research, under Task Order 24 of Nonr-1866.

TABLE OF CONTENTS

LIST OF FIGURES

LIST OF TABLES

SYNOPSIS

This report and the research described herein is the author's answer to a query as to whether solid tapered rods display horn-like behavior for torsional waves as they do for compressional waves. The text of this report consists of seven chapters and two appendices.

Chapter I is an introduction giving some historical background of the present research and an outline indicating the main features of the remainder of the text.

Chapter II contains derivations of the differential equations and boundary conditions necessary for the mathematical description of torsional-wave propagation in solid horns. Torsional waves are defined in this chapter as rotationally symmetric shear waves, a definition which leads to the requirement that the boundary of a torsional horn must be a surface of revolution if torsional waves are to propagate in the horn without partial conversion to compressional waves.

Two wave equations are derived. One of these is "exact," a specialization of the general equations of small-amplitude motion in an elastic medium. It can be readily solved, however, only for horns whose boundaries fit coordinate surfaces in circular cylindrical or spherical coordinate systems. For the analysis of horns whose contours do not fit a separable coordinate system, such as the exponential horn, an approximate wave equation is derived based on the assumption that the wavefronts of the torsional waves are plane cross sections of the horn. This plane-wave equation for torsional horns is similar in form to the plane-wave equation for compressional-wave horns first derived* by Webster.[3] The

---

* Numbers refer to the list of references at the end of the text.

difference between the two is that the moment of the cross section of the horn appears in the torsional plane-wave equation where the area appears in the compressional plane-wave equation. The close relationship between the plane-wave equation for torsional and compressional waves was pointed out by the author[8] in a paper delivered before the Acoustical Society of America and was subsequently also noted by Kharitonov.[9]

The boundary condition that the normal derivative of the angular displacement must vanish at a free surface is also derived in Chapter II.

In Chapter III is a description of the techniques and apparatus developed for the experimental investigation of the properties of torsional horns. The goals of the experimental program were the measurement of the resonance frequencies and standing-wave patterns at resonance of finite solid horns. To measure a standing-wave pattern, the specimen horn is excited at the corresponding resonance frequency and the amplitude of vibration at a movable measurement point is compared with the amplitude at a fixed reference point. Conventional phonograph pickups are used as the vibration-sensing elements. Torque is exerted on the specimen horn by an eddy-current driver developed for the purpose. This driver has no mechanical connection to the specimen horn. It exerts torque on the specimen horn at two frequencies which are the sum and difference of the frequencies of the currents in its two field windings. An approximate analysis of the driver operation indicates that approximately twice as much torque is exerted on ferrous as on nonferrous specimen horns. This was verified experimentally. The fact that the torque is induced at frequencies other than the driving-current frequencies permits isolation of desired signal from interference coupled

magnetically directly from driver to phonograph pickup. The horn under study is used as the frequency-determining element in a self-excited oscillator to insure that the drive is applied to the specimen horn at the resonance frequency.

The Q
~~Measurement~~ of a resonance of a specimen horn can be calculated from the resonance frequency and the measured decay rate of free vibrations at that frequency.

Using the methods covered in Chapters II and III, Chapters IV, V, and VI are devoted to the theoretical and experimental study of three different classes of horns.

Chapter IV deals with horns which fit separable coordinate systems. The exact wave equation is separated and solved for the normal modes of vibration of cylinders and cones. Of special interest are the one-parameter modes which are functions of only one space coordinate. Appendix A contains a demonstration that no coordinate systems other than cylindrical and spherical allow one-parameter solutions. The compound modes, for which the angular displacement is a function of two space coordinates, are analyzed for both cylinder and cone. Results of numerical computations are presented in graphical form showing the relation between the dimensions of a cone and the resonance frequency of its lowest mode. This information is believed to be unavailable elsewhere. The numerical method for finding the resonance frequencies is outlined in Appendix B. Resonance frequencies and standing-wave patterns were measured for both conical and cylindrical horns. The results are presented in graphical and tabular form in Chapter IV. The agreement between theory and experiment is very good to excellent in all cases.

Chapter V is concerned with horns, such as the exponential, whose contours are smooth but do not fit separable coordinate systems. The plane-wave equation derived in Chapter II is solved for cylindrical, conical, and exponential horns. The first two shapes were included to show that the plane-wave equation gives the same solution as the exact wave equation in the cases for which axially directed true one-parameter waves can exist. A torsional-wave impedance is defined as the ratio of torque to angular velocity and its value is found to vary as the moment of the cross section (proportional to the fourth power of the radius) as compared with the analogous mechanical impedance in compressional-wave horns, which varies as the area of the cross section (proportional to the square of the radius). A quantitative estimate of the error incurred by the use of the approximate plane-wave equation for the exponential horn was obtained from the discrepancy between the observed resonance frequencies and the predicted values. This discrepancy was interpreted in terms of an effective length based on the assumption that the observed resonance frequencies could be described by the approximate plane-wave frequency equation if the length of the horn were taken to be different from its physical length. This approach when applied to exponential horns gave consistent results, and it was found that the length correction, the difference between the effective length and the physical length, could be decomposed into the sum of two end corrections, each of which is proportional to the product of the radius of the horn and the slope of its contour at the end in question. The plane-wave frequency equation for an exponential horn could therefore be modified by the incorporation of end-correction terms in order to improve its accuracy in predicting the resonance frequencies of a horn of given dimensions.

However, it was discovered that in practice this would be of little avail since small errors in the contour of the horn cause far greater departures from the predicted resonance frequencies than does the inaccuracy inherent in the assumption of plane waves.

Chapter VI contains an extension of the plane-wave analysis to include the effects of discontinuities in the horn contour or its slope. Attention is focused on horns composed of cylinders of different diameters and lengths. Equations are derived for the resonance frequencies of double and triple cylinders. Experimental results are presented showing reasonably good agreement with the predicted values of gain and resonance frequencies. The presence of a step causes the greatest departure from the assumed plane wavefronts when the step is at a node of angular displacement. Measured resonance frequencies for modes of this type were quite perceptibly lower than the values predicted using the plane-wave assumption. The discrepancy is qualitatively explained in terms of mode conversion at the boundary.

Chapter VII is a summary of the results of the investigation and an indication of some possible applications for torsional horns. There is also a brief discussion of some areas for further investigation.

Chapter I

INTRODUCTION

"The horn, the horn, the lusty horn
Is not a thing to laugh to scorn."

As You Like It
Shakespeare

This report and the research described therein is the author's answer to a query as to whether tapered solid rods display horn-like behavior for torsional waves as well as compressional waves.

1.1 Historical background

The theory of solid horns as concentrators of elastic energy or impedance transformers is a comparatively recent development in acoustics. Although G. W. Pierce[1] had used tapered solid couplers for the transfer of acoustic energy as early as 1933, Warren P. Mason[2] of Bell Laboratories seems to have been the first to conceive of a tapered solid rod as a horn. He successfully adapted Webster's theory[3] of horns for compressional waves in air to compressional elastic waves in a solid.

In the years since the Second World War, such solid horns have found applications in ultrasonic machining and welding, and in fatigue

---

1. U. S. Patent No. 2,044,807, issued June 23, 1936, to Atherton Noyes, Jr., assignor to G. W. Pierce. Application filed on June 30, 1933.

2. U. S. Patent No. 2,514,080, issued July 4, 1950, to W. P. Mason. Application filed on January 10, 1945.

3. A. G. Webster, Proc. Natl. Acad. Sci. U. S. 5 (1919), p. 275.

and wear testing of materials.[4] Work in this field has by no means been confined to the United States. Merkulov[5] in the Soviet Union and Neppiras[6,7] in England have been particularly active in the development of the theory of solid compressional-wave horns.

In their analysis of solid horns, all of the above authors have ignored the ability of a solid to sustain a shear stress, that property which differentiates it from a fluid. The existence of shear stresses is implicitly acknowledged through the use of Young's modulus for the calculation of the compressional-wave propagation speed, but nowhere do the shear stresses enter explicitly into the analysis. One might well ask, therefore, whether it is possible to find modes of vibration for solid horns in which the shear stresses predominate. Such an approach then leads quite naturally to consideration of the torsional vibrations which form the subject of this report.

This research project was undertaken in the belief that no one had previously approached torsional vibrations from the standpoint of acoustic horn theory. This writer delivered a paper before the Acoustical Society of America in 1960 reporting preliminary results of his investigations.[8] In the audience was Warren P. Mason, who later remarked that he had a patent application pending on torsional horns! Dr. Mason was

---

4. Mason, W. P., Physical Acoustics and the Properties of Solids (Van Nostrand, New York, 1958), Chapter VI. See also W. P. Mason and R. F. Wick, J. Acoust. Soc. Am. 25 (1951), p. 209.

5. L. G. Merkulov, Soviet Phys. - Acoustics 3 (1957), p. 246.

6. E. A. Neppiras, Brit. J. Appl. Phys. 11 (1960), p. 143.

7. E. A. Neppiras and R. D. Foskett, Philips Tech. Rev. 18 (1956-57), p. 325. See also E. A. Neppiras, J. Sci. Inst. 30 (1953), p. 72.

8. R. W. Pyle Jr., "Torsional Horns," paper I9, Sixtieth Meeting of the Acoustical Society of America, October 20-22, 1960. An abstract of this paper appears in J. Acoust. Soc. Am. 32 (1960), p. 1504.

kind enough to lend the author a copy of this patent application which deals almost exclusively with applications of torsional horns and very little with the analysis of their vibratory properties. A later conversation with Mr. E. A. Neppiras of Mullard Laboratories, England, revealed that he also had engaged in some unpublished research on torsional horns. He too was concerned more with practical applications than with theory.

Recently, at least two papers on torsional horns have come from the Soviet Union.[9,10] Kharitonov points out the same analogy between torsional horn theory and normal acoustic horn theory which this writer had shown previously in the paper cited above. Marakov's paper is chiefly concerned with an approximate analysis of exponential and double cylindrical horns.

1.2 The present investigation

The study of the propagation of torsional waves in solid horns, like most problems in the physical sciences, may be approached in two ways, theoretically and experimentally. The theoretical approach consists of mathematical analysis based on the linear theory of elasticity. The experimental approach consists of the construction of solid horns and the measurement of their pertinent properties. Both avenues have been explored and have proven complementary: Experimental results have served not only to verify the theoretical analysis, but also to indicate fruitful directions in which to extend the analysis.

The following exposition is divided into three main sections. The first, consisting of Chapters II and III, deals with the tools, both

---

9. A. V. Kharitonov, Soviet Phys. - Acoustics 7 (1962), p. 310.
10. L. O. Marakov, Soviet Phys. - Acoustics 7 (1962), p. 364.

theoretical and experimental, which are necessary for the investigation of torsional horns. The second section, Chapters IV, V, and VI, presents both analytical and experimental results for various specific types of horn contour. Chapter VII is the third section, a discussion of the significance of the results and of possible fruitful paths for further investigation.

Two differential equations which describe the propagation of torsional waves are derived in Chapter II. The first of these is "exact," a specialization of the small-signal equations of elastic motion. This equation can be solved easily if at all only for cylindrical and conical horns, however. The second equation is only approximate but it can be solved for a wide variety of horn contours. These two types of mathematical description led to the classification of horns into three categories: those whose contours fit separable coordinate systems (cylinder, cone); those whose contours are continuous and smooth but do not fit separable coordinates (e.g., exponential, catenoidal horns); and those whose contours, though piecewise belonging to one or the other of the first two categories, are characterized by one or more discontinuities of the contour or its derivative (e.g., coupled cylinders, coupled exponential horns). Selected examples from each category have been studied in detail. Chapter IV deals with cylinders and cones, Chapter V with the exponential horn, and Chapter VI with coupled cylinders. Fig. 1-1 is a photograph of some representative samples from each group which were fabricated for experimental purposes.

A horn is often analyzed in terms of the change in amplitude and phase of a progressive wave transmitted along the horn. However, for reasons discussed in Chapter III, it was found more convenient experi-

mentally to deal with standing waves rather than with progressive waves. Chapter III is a discussion of experimental technique and a description of the apparatus developed for measuring the torsional standing-wave patterns and resonance frequencies of the normal modes of finite horns. As a consequence of the selection of this type of experiment, the major object of the theoretical analysis in Chapters IV, V, and VI has been to delineate the essential features of torsional standing waves, although some attention has been paid to the behavior of progressive waves.

Chapter VII contains an evaluation of the validity of the approximate mathematical method used for the theoretical analysis in Chapters V and VI, and provides a summary of the results obtained in this investigation. Also in this chapter is a discussion of some further problems suggested by the work reported here and some speculation about possible applications of torsional horns.

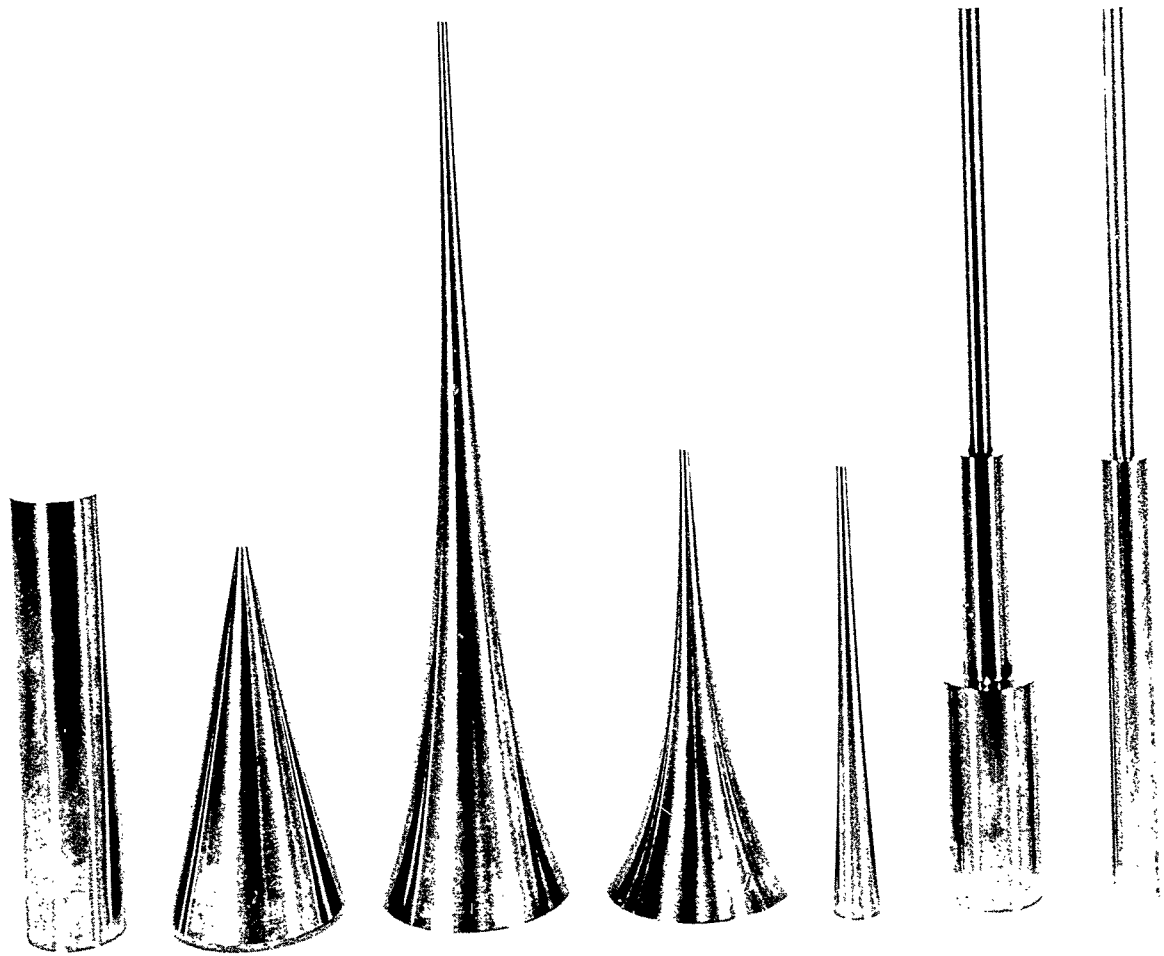

Fig. 1-1. Some typical experimental torsional horns. From left to right: cylinder, cone, three exponential horns, two stepped cylinders.

Chapter II

WAVE EQUATIONS AND BOUNDARY CONDITIONS

2.1 Definition of torsional vibrations

Before proceeding to the wave equations and their associated boundary conditions which constitute the major topic of this chapter, we must first define torsional vibrations. Hereafter, the term torsional vibrations refers to rotationally symmetric vibrations of an elastic body for which the only particle displacement is oscillatory rotation about the axis of rotational symmetry. This can be concisely phrased in mathematical terms. Let the axis of rotation be the z-axis of a circular cylindrical coordinate system (r,z,φ), and let $\underline{u} = (u_r, u_z, u_\varphi)$ be the instantaneous particle displacement vector. Then torsional vibrations are those for which

$$u_r = u_z = 0 \quad \text{and} \quad \frac{\partial u_\varphi}{\partial \varphi} = 0 \ ;$$

i.e.,

$$u_\varphi = u_\varphi(r,z,t) \ . \tag{2-1}$$

It is possible to deduce some further properties of torsional vibrations directly from the definition (2-1).

In cylindrical coordinates, the dilatation, div $\underline{u}$, a measure of the relative volume change within the medium due to the vibration, is

$$\operatorname{div} \underline{u} = \frac{1}{r}\frac{\partial (r u_r)}{\partial r} + \frac{1}{r}\frac{\partial u_\varphi}{\partial \varphi} + \frac{\partial u_z}{\partial z} \ . \tag{2-2}$$

From Eq. (2-1), it is obvious that div $\underline{u} = 0$ for any torsional vibration; i.e., torsional vibrations are equivoluminal.

If the displacement is small enough so that the usual small-signal relations between strain and displacement are valid, then we find that for torsional vibrations only two of the six independent components of strain[11] are nonzero, the shear strains

$$e_{r\varphi} = \frac{1}{2}\left(\frac{\partial u_\varphi}{\partial r} - \frac{u_\varphi}{r}\right)$$

and (2-3)

$$e_{z\varphi} = \frac{1}{2}\frac{\partial u_\varphi}{\partial z} \quad .$$

If we assume that the relationship between stress and strain is linear (generalized Hooke's law) and that the elastic medium is isotropic, homogeneous, and lossless, it follows that the only nonvanishing components of stress are the corresponding shear stresses*

$$\tau_{r\varphi} = 2\mu e_{r\varphi} = \mu\left(\frac{\partial u_\varphi}{\partial r} - \frac{u_\varphi}{r}\right)$$

and (2-4)

$$\tau_{z\varphi} = 2\mu e_{z\varphi} = \mu\frac{\partial u_\varphi}{\partial z}$$

where μ is the shear modulus.

2.2 The exact wave equation

2.2.1 Derivation from the general equation of motion

The small-signal equation of motion[12] in a lossless, isotropic homogeneous, elastic medium is

---

11. Sokolnikoff, I. S., Mathematical Theory of Elasticity (McGraw-Hill, New York, 1956), p. 183.

* p. 180 of Ref. 11, cited above.

12. Kolsky, H., Stress Waves in Solids (Oxford U. Press, London, 1953), p. 199.

$$(\lambda + 2\mu)\ \text{grad div}\ \underline{u} - \mu\ \text{curl curl}\ \underline{u} = \rho \frac{\partial^2 \underline{u}}{\partial t^2} \quad , \tag{2-5}$$

where $\underline{u}$ is the particle displacement vector and μ the shear modulus, as before, and ρ is the density of the medium.

It can readily be shown that torsional waves can exist, satisfying both the differential equation of motion (2-5) and the defining conditions for torsional vibrations (2-1). Since it follows from Eq. (2-1) that the dilatation div $\underline{u}$ vanishes identically, the first term on the left-hand side of (2-5) is zero. Applying the curl operator twice, subject to the conditions (2-1), we obtain after some routine manipulation the torsional wave equation for the particle displacement u_φ (a scalar equation since $u_r = u_z = 0$),

$$\frac{\partial^2 u_\varphi}{\partial r^2} + \frac{1}{r}\frac{\partial u_\varphi}{\partial r} + \frac{\partial^2 u_\varphi}{\partial z^2} - \frac{u_\varphi}{r^2} - \frac{1}{c^2}\frac{\partial^2 u_\varphi}{\partial t^2} = 0 \quad , \tag{2-6}$$

where $c^2 = \frac{\mu}{\rho}$; c is the shear-wave propagation speed for the medium. This equation was apparently first stated by Pochhammer in 1876.[13]

It will prove preferable later to work with the angular displacement $\Psi = u_\varphi / r$ rather than with the particle displacement u_φ. Equation (2-6), rewritten with Ψ as the dependent variable, becomes

$$\Psi_{rr} + \frac{3}{r}\Psi_r + \Psi_{zz} - \frac{1}{c^2}\Psi_{tt} = 0 \quad , \tag{2-7}$$

where subscripts on Ψ denote <u>partial derivatives</u>.

---

13. L. Pochhammer, J. reine angew. Math. 81 (1876), p. 324. For a more readily obtainable account of Pochhammer's work, see Chapter III of Ref. 12, cited on p. 8.

Since Fourier showed that an arbitrary time-variation can be represented as the superposition of simple-harmonic terms, we can assume sinusoidal time dependence through the definition $\psi(r,z)e^{j\omega t} = \Psi(r,z,t)$ with no loss of generality because of the linearity of Eq. (2-7). Making this substitution in (2-7), we obtain the Helmholtz form of the wave equation,

$$\psi_{rr} + \frac{3}{r}\psi_r + \psi_{zz} + k^2\psi = 0 \quad , \tag{2-8}$$

where the subscripts again denote partial derivatives.

2.2.2 Derivation from Hamilton's principle

We can also derive Eq. (2-7) from Hamilton's principle, using the calculus of variations. Hamilton's principle states that the dynamical behavior of a conservative system will be such that the integral

$$J = \int_{t_1}^{t_2} L\,dt = \int_{t_1}^{t_2} (T - V)\,dt \tag{2-9}$$

is extremized, where L, the Lagrangian, is equal to the difference of T, the kinetic energy of the system, and V, the potential energy of the system.

The kinetic energy may be written as the volume integral over the domain of the system, G, of a kinetic energy density; that is,

$$\begin{aligned} T &= \iiint_G \frac{1}{2}\rho\,(r\Psi_t)^2 r\,d\varphi\,dr\,dz \\ &= \rho\pi \iint_{G'} (r\Psi_t)^2 r\,dr\,dz \quad , \end{aligned} \tag{2-10}$$

where G' is the reduced domain in r and z, the integration over φ having

been carried out explicitly since by Eq. (2-1) the integrand is not a function of φ.

Assuming adiabatic vibration, the potential energy will be the volume integral over G of the volume density of strain energy* W; in this case,

$$W = \tau_{r\varphi}\, e_{r\varphi} + \tau_{z\varphi}\, e_{z\varphi} \,. \tag{2-11}$$

We can express the two nonzero components of strain in terms of the angular displacement as

$$e_{r\varphi} = \frac{1}{2}\, r\, \Psi_r$$

and (2-12)

$$e_{z\varphi} = \frac{1}{2}\, r\, \Psi_z \quad ,$$

where subscripts on e denote the component of strain and the subscripts on Ψ indicate partial derivatives, as before.

Combining Eqs. (2-4), (2-11), and (2-12), we can write

$$W = \frac{1}{2}\, \mu \left[(r\Psi_r)^2 + (r\Psi_z)^2 \right]. \tag{2-13}$$

Hence the total potential energy is

$$V = \iiint_G W r d\varphi dr dz = \mu\pi \iint_{G'} \left[(r\Psi_r)^2 + (r\Psi_z)^2 \right] r dr dz \,. \tag{2-14}$$

The integral, J, to be extremized now can be written in terms of Ψ as

---

* p. 81 ff. of Ref. 11, cited on p. 8.

$$J = \pi \int_{t_1}^{t_2} \iint_{G'} \left\{ \rho (r\dot{\Psi}_t)^2 - \mu \left[(r\Psi_r)^2 + (r\Psi_z)^2 \right] \right\} r \, dr \, dz \, dt$$

$$= \pi \int_{t_1}^{t_2} \iint_{G'} \left[\rho \dot{\Psi}_t^2 - \mu (\Psi_r^2 + \Psi_z^2) \right] r^3 \, dr \, dz \, dt \quad . \tag{2-15}$$

We have not hitherto specified anything about conditions at the boundary. It has been shown[14,15] that the type of boundary conditions does not affect the necessity for satisfying within the domain the Euler differential equation for the problem. (A discussion of boundary conditions follows in section 2.3.)

The integrand of J is

$$F(\Psi_r, \Psi_z, \dot{\Psi}_t, r, z, t) = r^3 \left[\rho \dot{\Psi}_t^2 - \mu (\Psi_r^2 + \Psi_z^2) \right] . \tag{2-16}$$

For an integrand of this form, the Euler equation (which must be satisfied in order to extremize J) is*

$$\frac{\partial}{\partial r} \left(\frac{\partial F}{\partial \Psi_r} \right) + \frac{\partial}{\partial z} \left(\frac{\partial F}{\partial \Psi_z} \right) + \frac{\partial}{\partial t} \left(\frac{\partial F}{\partial \dot{\Psi}_t} \right) = 0$$

$$= \frac{\partial}{\partial r} (-2\mu r^3 \Psi_r) + \frac{\partial}{\partial z} (-2\mu r^3 \Psi_z) + \frac{\partial}{\partial t} (2\rho r^3 \dot{\Psi}_t) \quad . \tag{2-17}$$

Completing the indicated differentiations and dividing by μr^3, we obtain

$$\Psi_{rr} + \frac{3}{r} \Psi_r + \Psi_{zz} - \frac{\rho}{\mu} \ddot{\Psi}_{tt} = 0, \tag{2-18}$$

which is, as we expected, the same as Eq. (2-7).

---

14. Courant, R., and D. Hilbert, Methods of Mathematical Physics (Interscience, New York, 1953), vol. I, pp. 208-11.

15. Forsyth, A. R., Calculus of Variations (Dover, New York, 1960), p. 606.

* p. 606 of Ref. 15, cited above.

2.3 Boundary conditions

2.3.1 At a free surface

Another way of saying that a boundary surface is free from external constraint is to require that the traction across the surface vanish. In cylindrical coordinates, we can express this requirement through the three equations*

$$\begin{aligned} \tau_{rr}\cos(n,r) + \tau_{rz}\cos(n,z) + \tau_{r\varphi}\cos(n,\varphi) &= T_r = 0 \ , \\ \tau_{rz}\cos(n,r) + \tau_{zz}\cos(n,z) + \tau_{z\varphi}\cos(n,\varphi) &= T_z = 0 \ , \\ \tau_{r\varphi}\cos(n,r) + \tau_{z\varphi}\cos(n,z) + \tau_{\varphi\varphi}\cos(n,\varphi) &= T_\varphi = 0 \ , \end{aligned} \qquad (2\text{-}19)$$

where T_r, T_z, and T_φ are the three components of the traction, and (n,r), (n,z), and (n,φ) represent the angles between the outward-directed normal to the surface and the r-, z-, and φ-directions, respectively.

The first two of Eqs. (2-19) lead to an interesting restriction on the shape of the boundary. It is well known that the reflection of a shear wave at a free boundary is in general accompanied by a partial (or in some cases, total) conversion of the incident energy to longitudinal wave motion.** We desire here that torsional waves propagate as such, without mode conversion. We saw in section 2.1 that this implied the vanishing of all stress components except the shear stresses $\tau_{r\varphi}$ and $\tau_{z\varphi}$. If we set $\tau_{rr} = \tau_{rz} = \tau_{zz} = 0$ in the first two of Eqs. (2-19), we obtain

$$\cos(n,\varphi) = 0 \ . \qquad (2\text{-}20)$$

In other words, the normal to the surface is perpendicular to the

---

* p. 181 of Ref. 11, cited on p. 8.

** pp. 24-31 of Ref. 12, cited on p. 9.

φ-direction, implying that the boundary is a surface of revolution. In order that torsional waves may propagate as torsional waves, therefore, it is necessary that any free boundaries be parallel to the direction of particle displacement; this same requirement must be met if plane shear waves are to be reflected from a plane boundary as shear waves.*

Combining Eq. (2-20) and the third of Eqs. (2-19) we obtain

$$\tau_{r\varphi} \cos(n,r) + \tau_{z\varphi} \cos(n,z) = 0 \ , \qquad (2\text{-}21)$$

which, by the use of Eqs. (2-4) and (2-12), becomes

$$\Psi_r \cos(n,r) + \Psi_z \cos(n,z) = 0 \ . \qquad (2\text{-}22)$$

The left-hand side of (2-22), however, is just the normal derivative of Ψ, since $\cos(n,\varphi) = 0$. Thus the boundary condition for use with the wave equation (2-7) at a free surface is simply that the normal derivative of Ψ vanish at the surface. Obviously, the same boundary condition applies to ψ of (2-8), the wave function with the time dependence removed.

2.3.2 On the axis of rotation

Everywhere in an elastic medium undergoing oscillatory vibration the particle displacement must be bounded and continuous; violation of these conditions would imply either infinite energy or fracture of the medium. The stress must be continuous if we are not to permit infinite localized forces. If the elastic medium is homogeneous and isotropic, it follows from Hooke's law that the stress is also bounded (and the particle displacement is then twice differentiable). We can utilize these facts to derive a condition on Ψ at the "boundary" $r = 0$.

---

* p. 30 of Ref. 12, cited on p. 9.

In any rotational coordinate system, the axis of rotation is a singular line since the unique correspondence between coordinate values and points described breaks down there[16] (the azimuthal angle φ may take on any value, yet the point described is still the same). We shall hence have an easier time if we transform from cylindrical to cartesian coordinates through the relations

$$x = r \cos \varphi \ , \quad y = r \sin \varphi \ , \quad z = z \ . \tag{2-23}$$

Let u, v, and w be the x-, y-, and z-components of the particle displacement in the cartesian system. We can then write the cartesian version of Eq. (2-1),

$$u = -u_\varphi \sin \varphi \ , \quad v = u_\varphi \cos \varphi \ , \quad w = 0 \ . \tag{2-24}$$

We have from (2-23) and (2-24)

$$\Psi = \frac{u_\varphi}{r} = - \frac{u}{y} = \frac{v}{x} \ , \tag{2-25}$$

and, from the chain rule for partial derivatives, the differential operator relationship

$$\frac{\partial}{\partial r} = \cos \varphi \frac{\partial}{\partial x} + \sin \varphi \frac{\partial}{\partial y} \ . \tag{2-26}$$

Using Eqs. (2-4), (2-12), (2-23), (2-25), and (2-26), we can write

$$\begin{aligned} \frac{\tau_{r\varphi}}{\mu} &= r \Psi_r = r \cos \varphi \, \Psi_x + \sin \varphi \, \Psi_y \\ &= x \Psi_x + y \Psi_y = x \frac{\partial}{\partial x} \left(\frac{v}{x} \right) + y \frac{\partial}{\partial y} \left(-\frac{u}{y} \right) \\ &= \frac{\partial v}{\partial x} - \frac{\partial u}{\partial y} + \frac{u}{y} - \frac{v}{x} = \frac{\partial v}{\partial x} - \frac{\partial u}{\partial y} - 2 \Psi \ . \end{aligned} \tag{2-27}$$

---

16. Kaplan, W., Advanced Calculus (Addison-Wesley, Cambridge, Mass., 1953), p. 157.

Invoking the conditions in the first paragraph of this section, we can now see from (2-27) that Ψ is bounded. This, together with the boundedness and continuity of $\tau_{r\varphi} = \mu r \Psi_r$, implies that Ψ_r is bounded and continuous; hence, Ψ_{rr} must be bounded. By a similar argument, Ψ_{zz} is bounded. Barring infinite accelerations (or frequencies) means that Ψ_{tt} must also be bounded. We can rewrite the torsional wave equation as

$$\Psi_{rr} + \Psi_{zz} - \frac{1}{c^2}\Psi_{tt} = -\frac{3}{r}\Psi_r \ . \qquad (2\text{-}28)$$

Since each term on the left-hand side of (2-28) is bounded everywhere, including the axis, $r = 0$, we see that as r approaches zero, Ψ_r must approach zero in such a way that $\frac{1}{r}\Psi_r$ remains bounded. Thus the "boundary" on the axis is very much like a free surface.

2.4 An approximate wave equation for horns of arbitrary contour

The exact wave equation (2-7) can be easily solved only when the boundaries of the horn are coordinate surfaces of a separable coordinate system. The relatively few horn shapes which meet this criterion are discussed in Chapter IV and Appendix A. We can, however, derive an approximate wave equation which will be comparatively easy to solve for a wide range of horn contours.

In order to gain some insight into the nature of the approximation to be used, we shall begin by examining the boundary condition at a free surface, Eq. (2-22), which we write again here:

$$\Psi_r \cos(n,r) + \Psi_z \cos(n,z) = 0 \ . \qquad (2\text{-}22)$$

If the slope of the horn contour is small, then $\cos(n,z) \ll \cos(n,r)$ and it follows that $|\Psi_z| \gg |\Psi_r|$ at the surface. If the length of the horn is much greater than its diameter, then it is likely that the frequency range

of interest will be the range for which the wavelength is comparable to the length, and thus the diameter will be much less than a wavelength. In this case Ψ will not vary appreciably over a cross section, and we see that $|\Psi_z| \gg |\Psi_r|$ everywhere within the horn. These conditions on the geometry of the horn are met by most typical horns vibrating in their lower modes.

We therefore assume that $\Psi_r \equiv 0$, i.e., that any plane cross section of the horn rotates as a whole (since Ψ is not a function of r). This assumption permits us to derive a simplified wave equation whose solutions will not quite satisfy boundary condition (2-22), except for the case of a cylinder, discussed in Chapter IV. If the conditions given in the preceding paragraph hold, the solutions will presumably be not far different from the actual vibrations of the horn under study. Chapter VII contains a discussion of the range of validity of the plane-wave assumption.

This assumption of plane wavefronts is essentially the same as the plane-wave assumption frequently used in the analysis of horns designed to guide sound waves in air,[17] first suggested by Webster* in a paper read in 1914 (but not published until 1919).

By incorporating the constraint $\Psi_r = 0$ in the integrand for the Lagrangian, we can derive the approximate wave equation from a variational integral in a manner similar to that used for the derivation of the exact wave equation in section 2.2.2.

---

17. See for example P. M. Morse, Vibration and Sound (McGraw-Hill, New York, 1948), 2nd ed., pp. 265-88.

* Ref. 3, cited on p. 1.

We wish, then, to extremize the integral

$$J = \int_{t_1}^{t_2} dt \int_{z_1}^{z_2} dz \int_0^{R(z)} dr \int_0^{2\pi} \left[\frac{1}{2} \rho (r \Psi_t)^2 - \frac{1}{2} \mu (r \Psi_z)^2 \right] r \, d\varphi \qquad (2\text{-}29)$$

where the horn now extends from z_1 to z_2 and is bounded laterally by the contour $r = R(z)$. Since Ψ is not a function of either r or φ, we can explicitly integrate over these two variables and obtain

$$J = \int_{t_1}^{t_2} dt \int_{z_1}^{z_2} \frac{I_s(z)}{2} \left[\rho \Psi_t^2 - \mu \Psi_z^2 \right] dz \quad , \qquad (2\text{-}30)$$

where

$$I_s(z) = \int_0^{R(z)} \int_0^{2\pi} r^3 \, d\varphi \, dr = \frac{\pi}{2} R^4(z) \quad . \qquad (2\text{-}31)$$

The quantity $I_s(z)$ is the <u>moment</u> of the cross section at z. Invoking Eq. (2-17), we see that the Euler equation for (2-30) is

$$\frac{\partial}{\partial t} \left[\rho \, I_s(z) \Psi_t \right] - \frac{\partial}{\partial z} \left[\mu \, I_s(z) \Psi_z \right] = 0 \quad , \qquad (2\text{-}32)$$

or, after performing the indicated operations,

$$\Psi_{zz} + \frac{I_s'(z)}{I_s(z)} \Psi_z - \frac{1}{c^2} \Psi_{tt} = 0 \quad , \qquad (2\text{-}33)$$

where $I_s'(z)$ is the derivative of $I_s(z)$ with respect to its argument z and $c^2 = \mu/\rho$, as before. The time dependence may be removed from Eq. (2-33) by assuming sinusoidal time variation, just as for the wave equation. This gives the plane-wave Helmholtz equation

$$\psi_{zz} + \frac{I_s'(z)}{I_s(z)} \psi_z + k^2 \psi = 0 \quad . \qquad (2\text{-}34)$$

The boundary condition at a free end, $z = z_1$, is that $\Psi_z(z_1) = 0$ for Eq. (2-33) and $\psi_z(z_1) = 0$ for Eq. (2-34), since Ψ_z and ψ_z are the appropriate normal derivatives.

Equation (2-34) is of exactly the same form as Webster's original plane-wave equation, save that the moment of the cross section of the horn has been substituted for the area of the cross section. Hence, all the results obtained for horns for acoustic pressure waves can be adapted to torsional horns by choosing the moment of the cross section of a torsional horn so that it varies with distance along the axis in the same manner as does the cross-sectional area of the corresponding pressure horn.*

Equation (2-33) was derived by constraining the form of the wave function Ψ, which is equivalent to stiffening the medium. Hence we know from Rayleigh's principle[18] that any resonance frequencies calculated from (2-33) (or (2-34), for that matter) will be upper bounds on the true resonance frequencies.

---

* Ref. 8, cited on p. 2, and Ref. 9, cited on p. 3.

18. Temple, G., and W. G. Bickley, Rayleigh's Principle (Dover, New York, 1956).

Chapter III

EXPERIMENTAL TECHNIQUES AND APPARATUS

3.1 Objectives of the experiment

The apparatus necessary for any experimental study of the propagation of torsional waves in a solid horn will consist of three parts: a driver for exciting the horn torsionally, a mechanical system for supporting and loading the horn, and a means for sensing and measuring the vibrations of the horn. If we think of the system in terms of the driver transmitting energy through the horn to the load, then for analytical purposes it is often convenient to divide the total vibration of the horn into a transmitted wave traveling from driver to load and a reflected wave traveling from load to driver. The relation between the transmitted and reflected waves depends upon conditions at the boundaries of the horn; e.g., the percentage of the incident energy absorbed by the load, the reaction of driver and load upon the horn, and the like. We desire here to study the properties of the horn, in which case we must know the relation between the transmitted and reflected waves since we cannot measure them independently. We must isolate the behavior of the horn from the behavior of the driver and load.

There are two ways often used to accomplish this. The first is to terminate the horn with a load which absorbs all the transmitted wave, thus eliminating the reflected wave. The total vibration of the horn is then a progressive wave propagating from driver to load. The second method is to terminate the horn in such a way that the transmitted wave is totally reflected. In the absence of elastic losses in the horn itself, this would give rise to a stationary wave, since the transmitted

and reflected waves would have equal intensity at any given point along the horn. If the driving torque is suitably applied at the natural frequency of one of the normal modes of the horn, the amplitude of vibration will rise to a value limited only by the energy losses in the horn. At such a resonance, if the losses are low, far less driving power is required to maintain a given amplitude of vibration in a standing-wave than is needed to produce the same amplitude in a progressive wave. However, the driver must not react appreciably on the horn if the normal modes of the combination are to be essentially the same as the normal modes of the horn alone.

The second method was adopted for this investigation. Since the axis of rotation is always a nodal line for torsional vibrations, the specimen horns are supported at the ends of the axis, leaving them essentially unconstrained (for torsional vibrations). With "nothing to twist against," waves propagating within the horn are completely reflected at the boundaries. The experimental horns are made of metals with low internal elastic losses. This insures that excitation at a resonance frequency of the horn produces vibrations of adequate amplitude for observation with relatively small driving torque.

The experimental scheme is then to simulate the normal modes of free vibration of a lossless horn by supplying enough energy to make up for that dissipated within the specimen horn and at its supports, thus maintaining a steady vibration. The standing-wave patterns and resonance frequencies of the normal modes are then measured and compared with theoretical results calculated from the wave equations derived in Chapter II. This experimental approach is feasible because it is possible to

construct solid horns with very low internal energy loss and to mount them so that very little torsional-wave energy is lost to the supports.

3.2 The driver

Having decided what type of experiment to perform, we can state some specific design criteria for the driver. The driver should be able to excite all the normal modes within the frequency range of the measurements. The driver should function only to supply the energy dissipated in the vibratory system; that is, it should not appreciably alter the standing-wave patterns and resonance frequencies of the normal modes of the horn. The driver should not interfere with the measurement process either through its physical presence or through the generation of intense electric or magnetic fields which might adversely affect associated electronic apparatus.

First we shall decide where on the specimen horn the driving torque should be applied in order that all the normal modes can be excited. We can adapt some results of Morse* to the present situation. Suppose we drive the horn with a simple-harmonic torque distribution, $T(r,z)e^{j\omega t}$. The spatial distribution $T(r,z)$ can always be expanded in a series of the characteristic functions of the normal modes of the horn. A given normal mode cannot be excited if its characteristic function is missing from the expansion of $T(r,z)$, even if the frequency of the driving torque is exactly the natural frequency of that mode, since there would be no coupling between the driving torque and the normal mode. In particular, if the drive is applied at a "point" (r_o,z_o) which is a node of angular velocity for a normal mode, that mode cannot be excited. A normal mode

---

* pp. 415-17 of Ref. 17, cited on p. 17.

will be maximally excited if the driving point (r_o,z_o) is an antinode of angular velocity. The frequency of maximum excitation is very close to the natural frequency of the mode, provided the losses are small. Being an extremity of both the longitudinal and lateral dimensions of a horn, the edge of a free end is an antinode of angular velocity for all normal modes. A driving torque applied there will be well coupled to all modes. In practice, of course, the drive cannot be applied at only one point, but will be distributed over a small region. If this region is centered on the edge of the end of the horn, then all modes whose wavelengths are long compared with the width of the region can be easily excited.

If the frequencies of maximum amplitude of vibration are to be taken as the natural frequencies of the horn, then it is clear that the applied torque should be independent of the amplitude of vibration. Drawing an analogy between torque and voltage and between angular velocity and current,[19] we see that this means that the driver should approximate an ideal torque source, i.e., a source whose output torque is independent of load.

A driver has been developed which satisfies the above design criteria. It is a form of induction motor which produces torsional drive by means of the interaction with externally applied magnetic fields of eddy currents induced in the specimen horn by the magnetic fields. This arrangement has the advantage that it requires no mechanical coupling of horn and driver.

The conventional induction motor has field windings and a magnetic structure which produce a rotating magnetic field. An electrically

---

19. Olson, H. F., Acoustical Engineering (Van Nostrand, New York, 1957), Chapter 4.

conducting rotor is placed in the magnetic field so that its axis of rotation coincides with the axis of rotation of the magnetic field. If the rotor is not rotating in synchronism with the field, the relative velocity of rotor and field will cause eddy currents to be induced in the rotor. The interaction of the eddy currents and the magnetic field exerts a torque on the rotor which tries to make it follow the inducing field. If now the field windings and pole pieces are arranged to produce a magnetic field whose rotation is oscillatory rather than continuous, an oscillating torque suitable for exciting torsional vibrations will be developed.

Four such eddy-current drivers have been constructed and used in this investigation of torsional horns. The geometric structure of the first two was essentially the same as that of the common four-pole two-phase induction motor (one pole pair per phase). The two pole pairs, each with its own field winding, were symmetrically arranged about the rotor (now a solid horn) so that their magnetic fields crossed orthogonally in the region occupied by the rotor. One field winding was excited with direct current and the other with alternating current of angular frequency ω; thus, the total magnetic field oscillated in direction and magnitude at that frequency.

This simple scheme gave adequate drive, but suffered from several weaknesses. The driver pole pieces enclosed one end of the horn, making it impossible to measure the amplitude of vibration there. The alternating driving current produced a large magnetic field which induced an interfering signal in the amplitude-measurement circuitry of the same order of magnitude as the desired signal. Since the frequency of the

interfering signal was the same as that of the desired signal (hereafter called signal frequency), the desired signal was effectively masked.

The problem of the interfering magnetic field was solved by the use of a different mode of operation of the same basic type of driver. In this mode, both windings are excited with alternating current. Two distinct frequencies are used, one for each winding. The resulting total magnetic field can be decomposed into two components which oscillate rotationally at two other frequencies which are the sum and difference of the driving current frequencies. Either the sum or difference frequency can be tuned to the desired resonance of the specimen horn. Although driving torque is applied at two frequencies, the sharpness of the resonances is such that only one frequency component is observed in the vibration of the horn. Interfering signals are still present in the amplitude-measurement apparatus, but not at signal frequency, so that frequency-selective circuitry can adequately discriminate against them.

The geometry of the field structure was redesigned to allow access to the side of the horn all the way to the end. The poles, instead of encircling the side of the horn, are placed close to the end face of the specimen horn. Fig. 3-1 is a photograph of the two drivers of this type. The magnetic structure is composed of coils of magnet wire wound on ferrite cores assembled from the cores of burned-out television flyback transformers obtained from a cooperative serviceman. Pieces of ferrite were ground to the proper size and shape and cemented together with epoxy adhesive. The two coils on opposite legs form one field winding and are connected in series or parallel aiding. The drivers are mounted on four-inch squares of hardboard for interchangeable installation at the end of

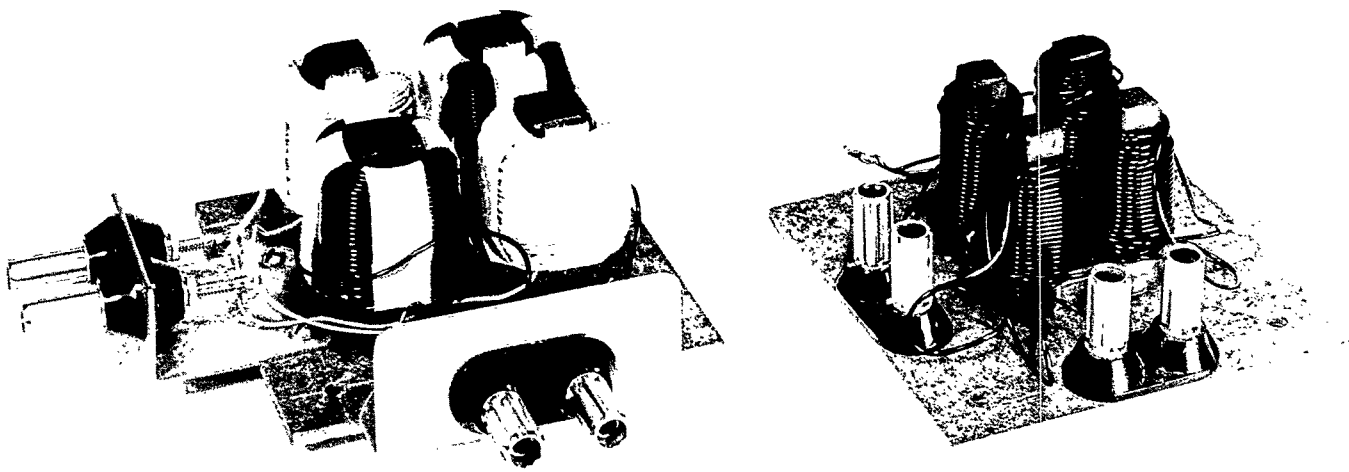

Fig. 3-1. Photograph of two eddy-current drivers. Their sizes may be estimated from the three-quarter-inch spacing of the binding posts.

the specimen horn. (Details of the mechanical system are discussed later in this chapter.)

The change in structure produces two unfavorable effects, neither of which has proven harmful in practice. First, the output torque is not as great for given field currents as it was in the original design. Second, there is a possibility of exciting longitudinal vibrations in ferromagnetic specimen horns by variable reluctance drive at twice the exciting frequencies. (Note the resemblance to a bipolar moving-armature transducer.[20]) Such undesired vibrations were never observed.

An exact general theoretical analysis of the eddy-current driver is not practicable, particularly since the ratio of horn end diameter to driver pole spacing varied over a range of more than four to one due to the wide variety of horns tested. An analysis based on an idealization of the geometry can yield information about the effect of changes in the conductivity and permeability of the horn material upon the induced torque, however. Let us assume an infinite solid cylinder of radius a, relative permeability K, and volume conductivity γ, whose axis is the z-axis of a system of cartesian coordinates. Let us also assume uniform driving fields, an x-directed field of magnetic flux density $B_1 \cos \omega_1 t$, and a y-directed field of flux density $B_2 \cos \omega_2 t$. We can now calculate the torque per unit length induced in the cylinder, assuming the cylinder is kept from moving, by calculating the eddy currents induced by each driving field and the stresses produced by their interaction with the magnetic field within the cylinder.

---

20. Hunt, F. V., Electroacoustics (Wiley, New York, 1954), p. 213.

Smythe[21] gives the magnetic vector potential within an infinite cylinder immersed in a uniform x-directed alternating magnetic field. Adapting his result to our notation and expressing it in cylindrical coordinates r, φ, z (defined by $x = r\cos\varphi$, $y = r\sin\varphi$, $z = z$), we have for the z-component of the vector potential

$$A_1 = \mathrm{Re}\ \frac{4 B_1 K\ I_1(q_1 r)\ e^{j\omega_1 t}\ \sin\varphi}{q_1[(K+1)I_0(q_1 a) - (K+1)I_2(q_1 a)]} \tag{3-1}$$

where Re indicates real part, $q_1 = (j\omega_1 \gamma \mu_o K)^{1/2}$, μ_o is the permeability of free space, and I_0, I_1, and I_2 are modified Bessel functions of the first kind. The x- and y-components of $\underline{A}$ are zero by symmetry. The z-component of the vector potential due to the y-directed field, A_2, is exactly the same as A_1 except that $-\cos\varphi$ is substituted for $\sin\varphi$, ω_2 for ω_1, and $q_2 = (j\omega_2 \gamma \mu_o K)^{1/2}$ for q_1.

Using the standard electromagnetic relations*

$$\begin{aligned} \underline{B} &= \mathrm{curl}\ \underline{A} \\ \frac{d\underline{B}}{dt} &= -\,\mathrm{curl}\ \underline{E} \\ \underline{J} &= \gamma \underline{E}\ , \end{aligned} \tag{3-2}$$

we can write the current density in terms of the vector potential:

$$\underline{J} = -\gamma \frac{d\underline{A}}{dt}\ . \tag{3-3}$$

The induced torque per unit length, denoted by T_ℓ, can now be expressed

---

21. Smythe, W. R., Static and Dynamic Electricity (McGraw-Hill, New York, 1950), p. 418.

* p. 390 of Ref. 21, cited above.

as an integral over the cross section of the cylinder of the electromagnetically induced stress times the "lever arm" r:

$$T_\ell = \int_0^a dr \int_0^{2\pi} d\varphi\, r^2 \left[\underline{J}\times\underline{B}\right]_\varphi \ , \tag{3-4}$$

where the subscript φ denotes the component of the vector in the φ-direction, i.e., the tangential component. If now Eqs. (3-1) through (3-4) are combined, the resulting integral, though terrifying in appearance, will succumb to attack with a variety of Bessel function identities.[22] The result, reduced to a symmetric and moderately simple form, is

$$T_\ell = \frac{4\pi a^2 B_1 B_2 K}{\mu_o}\left\{\mathrm{Re}\left[\frac{G(\omega_1)e^{j\omega_1 t}}{K+G(\omega_1)}\right]\mathrm{Re}\left[\frac{e^{j\omega_2 t}}{K+G(\omega_2)}\right]\right.$$
$$\left. - \mathrm{Re}\left[\frac{e^{j\omega_1 t}}{K+G(\omega_1)}\right]\mathrm{Re}\left[\frac{G(\omega_2)e^{j\omega_2 t}}{K+G(\omega_2)}\right]\right\} , \tag{3-5}$$

where the function $G(\omega)$ is defined by

$$\begin{aligned} G(\omega) &= a\frac{d}{da}\ln I_1[(j\omega\gamma u_o K)^{1/2}a] \\ &= a\frac{d}{da}\ln I_1(qa) \ . \end{aligned} \tag{3-6}$$

Some idea of the behavior of the $G(\omega)$ is obviously necessary for deeper understanding of Eq. (3-5). We can rewrite the argument in terms of the skin depth,

$$qa = (j\omega\gamma\mu_o K)^{1/2}a = (2j)^{1/2}\frac{a}{\delta} \ , \tag{3-7}$$

---

22. Morse, P. M., and H. Feshbach, Methods of Theoretical Physics (McGraw-Hill, New York, 1953), p. 1322-3.

where $\delta = (2/\omega\gamma\mu_o K)^{1/2}$ is the skin depth as usually defined.*

Let us assume ω_1 is the lower of the two driving-current frequencies. In actual operation of the eddy-current driver, the lower frequency $f_1 = \omega_1/2\pi$ was placed between 50 and 100 c/s. The higher frequency $f_2 = \omega_2/2\pi$ was then in the same range as the resonance frequencies of the horns under study, from 2.5 kc/s to 50 kc/s. The driven ends of nearly all the specimen horns were one inch or more in diameter. Consultation of tables[23] of skin depth for various materials shows that for aluminum, brass, and iron, the skin depth δ_2 at frequency f_2 is always much less than the radius, so that the argument of the Bessel function in $G(\omega_2)$ is sufficiently large to warrant use of the asymptotic formula given by Morse and Feshbach** for the Bessel function I_1,

$$I_1(z) \underset{z\to\infty}{\longrightarrow} \frac{e^z}{(2\pi z)^{1/2}} \quad . \tag{3-8}$$

At the lower frequency f_1 the skin depth δ_1 is unfortunately neither much greater nor much less than the radius a. However, f_1 is always sufficiently smaller than f_2 that δ_1 is at least five times greater than δ_2 (and usually more than ten times greater). This means that the eddy currents and magnetic field within the cylinder at f_2 are concentrated in the region near the surface where the magnetic field at f_1 is essentially uniform for variations in r. We shall thus incur small error by assuming that the field at f_1, throughout the range of

---

* p. 393 of Ref. 21, cited on p. 28.

23. Gray, D. E., editor, American Institute of Physics Handbook (McGraw-Hill, New York, 1957) p. 5-90.

** p. 1323 of Ref. 22, cited on p. 29.

integration over r, is constant at its value just within the surface. We can now readily find that approximate values for G are

$$G(\omega_1) = 1$$

and

$$\begin{aligned} G(\omega_2) &= (j\omega_2 \gamma \mu_o K)^{1/2} a \\ &= (2j)^{1/2} \frac{a}{\delta_2} \quad . \end{aligned} \tag{3-9}$$

Inserting these values in Eq. (3-5), and noting that $G(\omega_2) \gg K$, we obtain

$$T_\ell = \frac{2\pi a^2 B_1 B_2}{\mu_o} \left[\frac{K}{1+K}\right]\left[\cos(\omega_2 - \omega_1)t + \cos(\omega_2 + \omega_1)t\right] . \tag{3-10}$$

Equation (3-10) is based on such an unrealistic physical situation that it is useless as a means of actually calculating induced torque. However, we can reasonably expect that it correctly gives the form of the dependence of the torque upon the strength of the inducing fields and upon the electromagnetic constants of the horn material. We note that the conductivity of the cylinder does not explicitly enter into Eq. (3-10). This is due to the fact that the skin depth at f_2 is a small fraction of the radius. The induced torque does depend on the permeability, however. We can group metals used for the construction of horns into two categories: ferromagnetic ($K \gg 1$), and nonferromagnetic ($K = 1$). We see that ferromagnetic substances such as iron and steel should have twice the induced torque which nonferromagnetic metals such as brass and aluminum have. We also note that the induced torque is proportional to the product of the magnitudes of the inducing fields. If

the currents in the driver field coils are small enough that the magnetic core of the driver is not saturated, then we expect the magnetic field strengths to be proportional to the driving currents, and hence the induced torque to be proportional to the product of the amplitudes of the driving currents. Assuming a linear elastic system, the amplitude of vibration should be proportional to the induced torque (all other factors being constant), and hence proportional to the product of the driving-current amplitudes. This was observed to be the case in practice.

A series of measurements was made specifically to determine the properties of the eddy-current driver. Three cylinders, each one inch in diameter, were constructed of brass, soft iron, and aluminum, respectively. The length of the iron cylinder was ten inches, and the lengths of the others were chosen so that the resonance frequencies of all three were nearly equal. Each cylinder was excited at its fundamental resonance frequency with one ampere used in each winding of the driver. The amplitude of vibration was measured at the end of the test cylinder, and the Q of the resonance was measured by the method described in section 3.3.4 of this chapter. The energy stored in the cylinder was calculated from the observed amplitude of vibration and the characteristic function for the fundamental mode of a cylinder. The power input was then calculated from the stored energy and the Q, and then the torque input was found as the ratio of power input to angular velocity. The results of this series of measurements are presented as Table 3-1.

The torque exerted on the iron was indeed approximately twice that exerted on the brass and aluminum. The greater power input to the aluminum cylinder is due to the fact that its characteristic impedance is lower than that of iron or brass; hence for aluminum there is a better

impedance match between driver and cylinder. (Torsional-wave impedance is discussed in Chapter V.)

Table 3-1

Torque and power input from the eddy-current driver to cylinders of various metals

Metal	Resonance frequency kc/s	Power input nanowatts	Torque input micro-ounce-inches
Soft iron	6.357	1.07	0.414
Aluminum	6.553	7.56	0.238
Brass	6.379	0.438	0.235

The eddy-current driver is very inefficient. The electrical power input during these tests was several watts; thus the efficiency is of the order 10^{-9} to 10^{-10}. This driver must be a prime candidate for a prize for the least efficient transducer ever to find a practical use!

A necessary property of the driver is that it react very little on the specimen horn so that the observed frequencies of maximum amplitude of vibration will be essentially the free resonance frequencies of the horn. Two experiments were performed to check this. The first consisted of a series of measurements of the frequency of maximum (forced) vibration of a steel cylinder for various spacings between the driver pole faces and the cylinder. This was based on the premise that varying the driver-cylinder spacing would vary the coupling between driver and cylinder, and as a result vary the magnitude of any effect which the driver had on the observed resonance frequencies. The observed frequencies were constant to within ± 0.1 c/s, the precision of measurement (the frequency was about 7 kc/s). The second experiment was a direct

comparison of the frequency of free vibration with the frequency of maximum forced vibration. The aluminum cylinder used in the experiments described above to measure the torque and power was found to have a very high Q. It was maximally excited at its fundamental resonance, and the frequency of free vibration was measured as the vibration died away. The high Q of the resonance gave a long enough decay time that the frequency could be measured with high precision before the amplitude of vibration fell below the minimum detectable level. No difference was observed between the forced and free resonance frequencies.

The eddy-current driver thus appears satisfactory for its intended use.

3.3 The measurement of torsional standing-wave patterns

A simple approach to the measurement of a torsional standing-wave pattern of a solid horn would be to measure the amplitude of vibration at various points along the horn while holding the driving torque constant. This presupposes that the device used for the measurement of vibration would not alter the amplitude of vibration. For operation at a resonance of high Q, as contemplated here, it would not be surprising if the measurement process introduced sufficient damping to lower the Q noticeably and hence the amplitude as well.

The next degree of sophistication is to monitor the amplitude at a fixed point so that it can be set to the same value for all measurements. This arrangement was tried but it was found to be limited in accuracy. The amplitude at various points was measured by reading a voltmeter; hence, the accuracy can be no better than the calibration of the volt-

meter. Some difficulty was also experienced in holding the amplitude at the reference point sufficiently constant.

Since the standing-wave pattern is only the relative amplitude as a function of position, we need not measure the absolute amplitude of vibration as in the first two methods described above. If we again monitor the amplitude at a reference point, the ratio of the amplitude at any other point may be found by attenuating the larger of the signals from the two points until it is just equal to the smaller. The attenuation required is independent of the absolute amplitude and can be determined with great precision since it depends only on the ratios of resistors. The voltmeter used for the amplitude measurement in the second method above now serves only to indicate the equality of two signals; its calibration errors do not therefore degrade the attainable accuracy. The amplitude of vibration must be stable only for sufficient time to make the balance between the two signals. This imposes a requirement on the frequency stability of the drive, however, since the torsional resonances of solid horns are very sharp.

Suppose we decide that we shall be satisfied if we can measure the relative amplitude along the horn to an accuracy of ±2 percent. If the magnitude of the driving torque does not change with time, then we can tolerate a frequency drift over the range between the points where the resonance curve of the horn is 4 percent down from its peak value. Most of the experimental horns were made of mild steel and their resonances had Q's of approximately 20 000. Assuming the resonance curve is essentially the same as that of a single RLC tuned circuit, we can calculate[24]

---

24. Westman, H. P., editor, Reference Data for Radio Engineers, 4th ed. (International Telephone and Telegraph Corp., New York, 1956), p. 242.

that

$$\Delta f/f = 1.5 \times 10^{-5} , \qquad (3\text{-}11)$$

where Δf is the permissible frequency drift in the time required for amplitude measurement at one point and f is the frequency of vibration. This is a moderately stiff requirement on frequency stability, but it can be met by a high-quality oscillator which is allowed to run continuously so that the problem of warmup drift is eliminated. Surprisingly, however, the resonance frequencies of the specimen horns are not stable enough. The shear modulus in metals decreases with increasing temperature, which causes the shear-wave speed and hence the resonance frequencies to decrease with temperature also. The problem is compounded by the longer time required to make the amplitude balance between the two signals when the amplitude is noticeably drifting. The troublesome temperature change is caused by the Joule heating due to the eddy currents induced by the driver. One solution to this problem is to make the driving torque vary in frequency with the resonance frequency of the horn by using the horn as the frequency-determining element in a self-excited oscillator. The reference signal used for the amplitude comparison can be (and was) the feedback signal. This method was successfully used.

Since the frequencies of the currents in the driver coils are such that it is their sum or difference which is the same as the resonance frequency under investigation, the circuitry necessary for the self-excited oscillator is unusually complex. Fig. 3-2 is a block diagram of the system and Fig. 3-3 is a photograph of the apparatus.

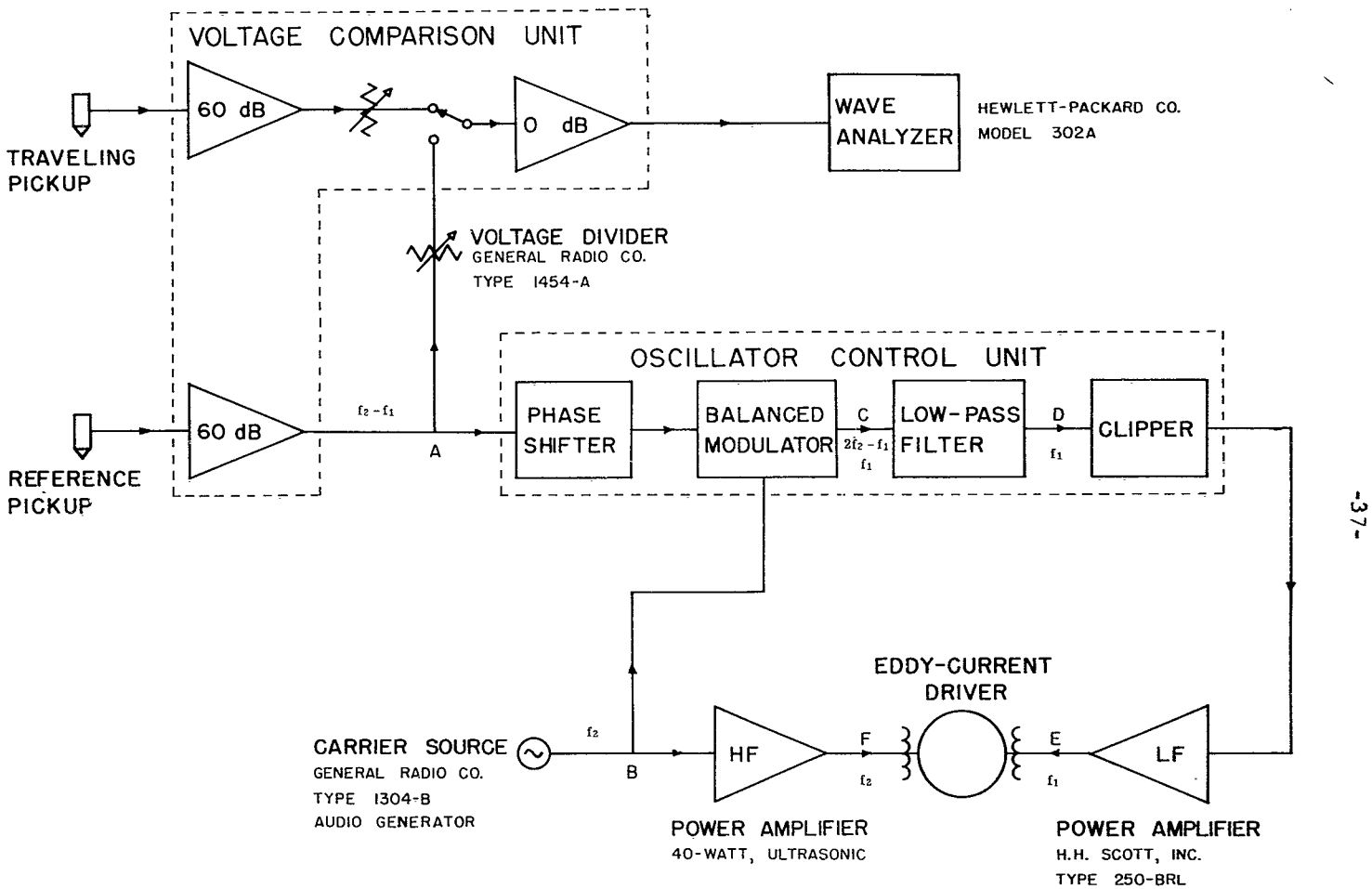

FIG. 3-2 BLOCK DIAGRAM OF SYSTEM FOR THE MEASUREMENT OF TORSIONAL STANDING-WAVE PATTERNS.

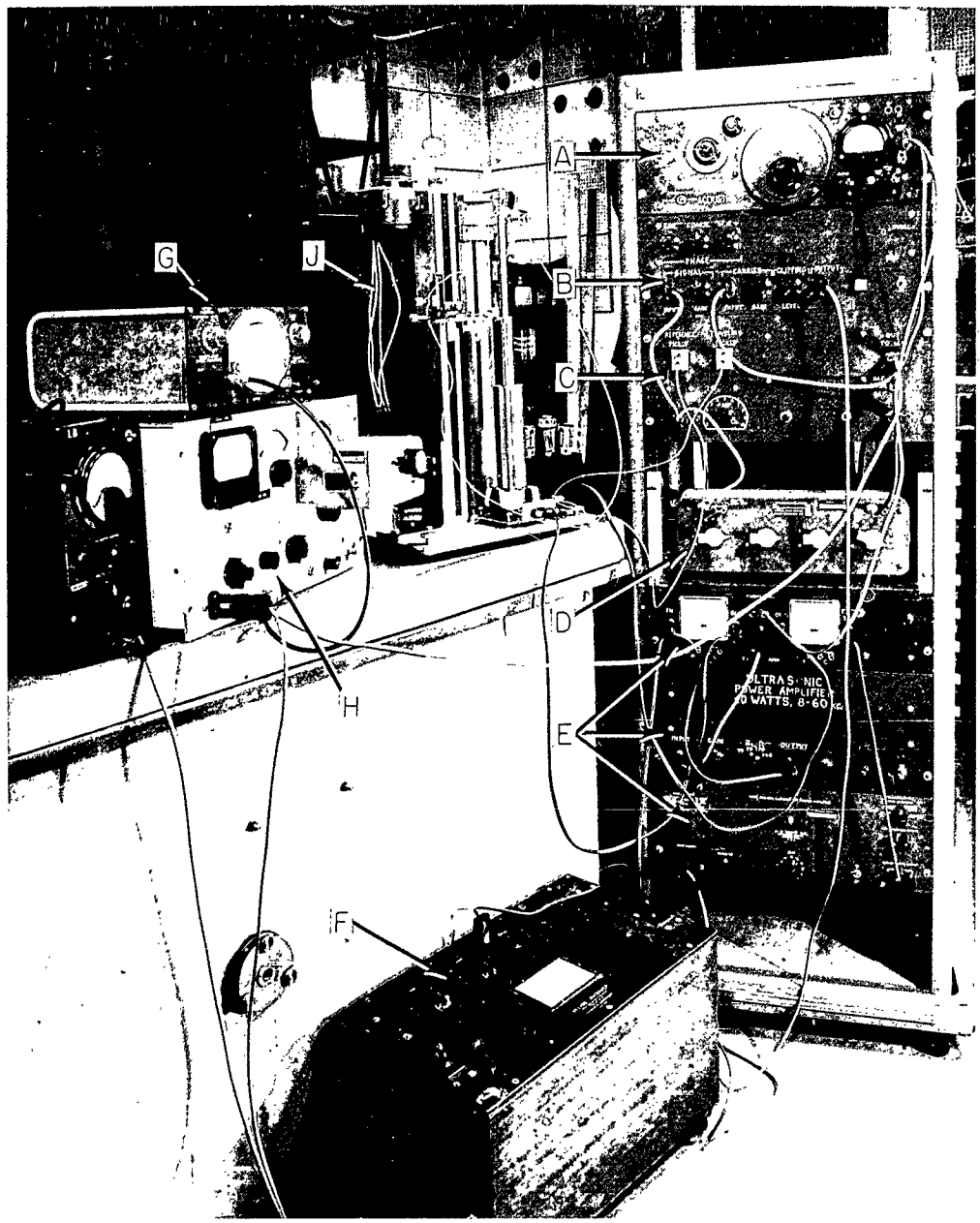

Fig. 3-3. Photograph of the experimental apparatus, showing the carrier source (A), the oscillator control unit (B), the voltage comparison unit (C), the voltage divider (D), the power amplifiers and their metering panel (E), the decade condenser (F), the frequency meter (G), the wave analyzer (H), and the mechanical system (J).

Now we shall see how the circuit oscillates at a resonance frequency of the specimen horn. As above, let f_1 be the lesser and f_2 the greater of the frequencies of the currents in the driver coils. The current at f_2 is obtained from a high-frequency power amplifier driven by a General Radio Co. Type 1304-B Audio Generator tuned to f_2 and designated as carrier source on the block diagram, Fig. 3-2. The current at f_1 is obtained from a low-frequency power amplifier driven by the feedback signal. Suppose that f_2-f_1 is tuned to the resonance frequency of the horn. The driver exerts torques at frequencies f_2-f_1 and f_2+f_1 on the horn, but due to the resonance of the horn, it may be considered to vibrate only at f_2-f_1. The amplified reference signal (point A of Fig. 3-2) is then at frequency f_2-f_1. It is shifted in phase and then mixed with a signal at the carrier frequency f_2 (point B) in the balanced modulator. The output of the balanced modulator (point C) consists of the two modulation products at frequencies $f_2-(f_2-f_1) = f_1$ and $f_2+(f_2-f_1) = 2f_2-f_1$. The low-pass filter attenuates the upper component of frequency $2f_2-f_1$, so that the signal at point D is of frequency f_1. The clipper acts to regulate the amplitude of oscillation, and the clipped signal at frequency f_1 drives the low-frequency power amplifier, thus completing the loop. The phase shifter is used to adjust for zero phase shift around the loop at the resonance frequency of the specimen horn.

The frequency stability of the carrier source need not be particularly good in this system. Small drifts in f_2 are automatically compensated for by the same frequency shift in f_1. Of course, f_1 must lie in the passband of the low-pass filter (<500 c/s), and the phase shift introduced by the change in f_1 must not be great enough to kill the

oscillation. In practice, changes of as much as 50 c/s in f_1 and f_2 are without substantial effect on the oscillation. (This is 5 parts in 10^3 for a resonance at 10 kc/s).

Conventional lateral phonograph pickups were used to detect the vibrations of the specimen horn. One of these, the reference pickup, is fixed in position near the opposite end of the horn from the driver. The other, the traveling pickup, may be placed in contact with any point along the side of the horn by means of the mechanism described in section 3.4. Phonograph pickups were used as the vibration-sensing elements because the particle displacement at the surface is parallel to the surface and not normal to it, and because of their ready availability. In order to minimize stray coupling to the magnetic field of the driver, ceramic pickups (Weathers Stereoramic C-501, wired as lateral pickups) were used in preference to magnetic pickups. Tests with a high-quality magnetic pickup, reputedly one of the best-shielded ones on the market, showed that the unwanted signal was some 40 dB greater, relative to the desired signal, for the magnetic pickup than for the ceramic pickups.

The electrical signals from the two pickups are amplified by two identical amplifiers of 60 dB gain. If the signal from the traveling pickup is larger than that from the reference pickup, it is reduced in steps of 10 percent of full gain until it is less. Then the precision voltage divider, General Radio Co. Type 1454-A, is used to reduce the reference signal until it is just equal to the signal from the traveling pickup. The ratio of gains in the two channels is then the inverted ratio of the amplitudes of the two signals.

The voltage comparison is made by switching the signals alternately to a Hewlett-Packard Model 302A wave analyzer which serves as a tuned

voltmeter. The selectivity of the wave analyzer is great enough so that it successfully discriminates against large interfering signals only 50 to 100 c/s away from the frequency of the resonance under study. An isolation amplifier with a gain of unity and a very high input impedance follows the voltage-comparison switch and serves to keep the capacitance of the cable to the wave analyzer from loading the precision voltage divider and thus impairing its accuracy at the higher frequencies in use.

3.3.1 The voltage comparison unit

Fig. 3-4 is a schematic diagram of the voltage comparison unit. The unit consists of the two matched 60-dB amplifiers, the decade gain switch, the voltage comparison switch, and the unity-gain isolation amplifier, which, together with a common power supply, are all mounted behind a standard 19-inch rack panel $8\frac{3}{4}$ inches in height (see Fig. 3-2).

Each 60-dB amplifier consists of three stages: two cascaded resistance-capacitance coupled pentodes and a triode cathode follower direct-coupled to the second pentode. A large amount of negative feedback is used to stabilize the gain against changes in supply voltages or tube characteristics. It is obtained by cathode-to-cathode feedback from V3 to V1. The feedback ratio is 1/1001 and the loop gain is approximately 22; hence, the gain is predominantly determined by the feedback ratio and is approximately 1000, or 60 dB. The two resistors which determine the percentage of the output voltage fed back, the 10-kΩ and 10-Ω resistors in the cathode circuit of V3, are wirewound to insure good voltage linearity and good stability with time. The 10-Ω resistor is a precision unit and the 10-kΩ resistor is carefully matched to the corresponding resistor in the other 60-dB amplifier.

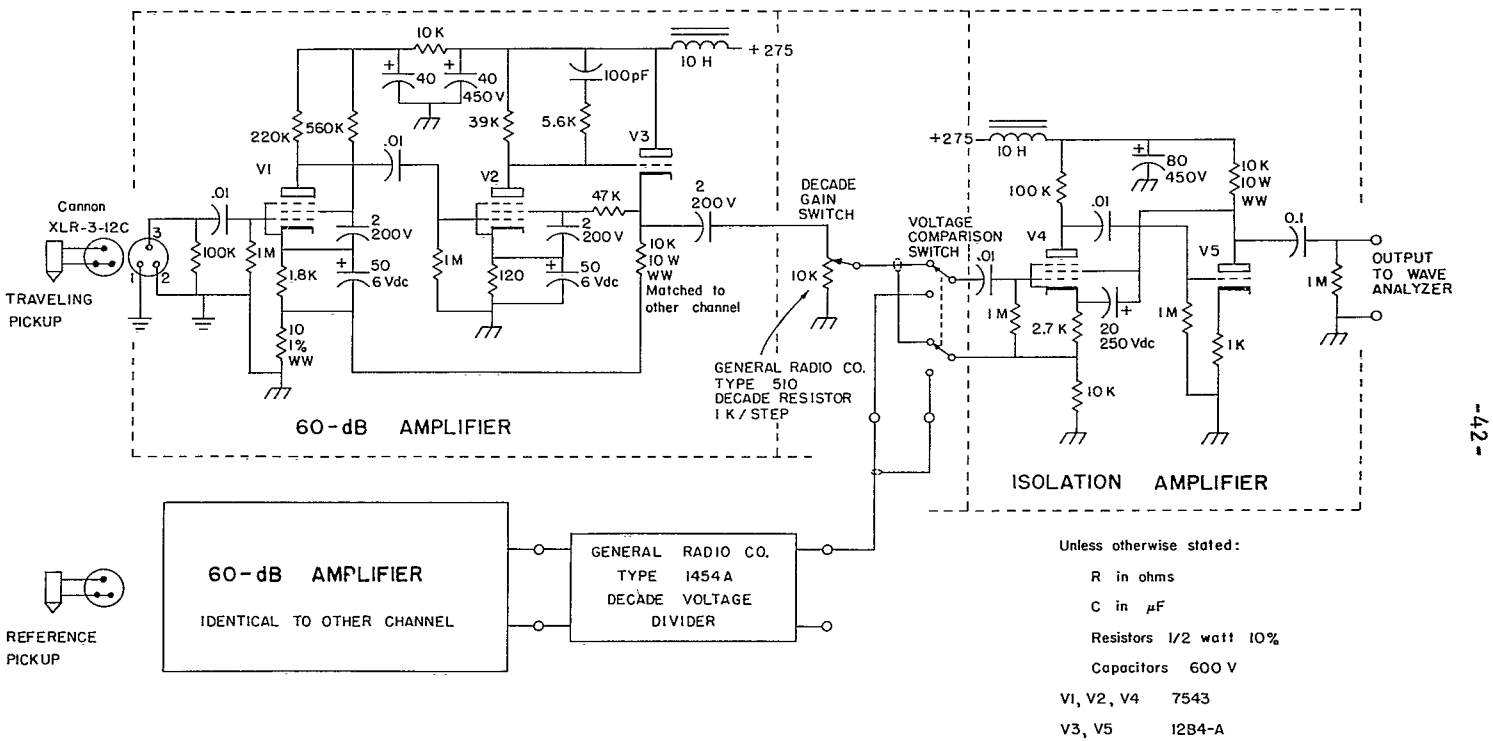

FIG. 3-4 SCHEMATIC DIAGRAM OF VOLTAGE COMPARISON UNIT.

The operating points of V2 and V3 are stabilized by the dc negative feedback obtained by returning the 47-kΩ screen dropping resistor of V2 to the cathode of V3.

Because of the large amount of feedback, special precautions were observed to insure against unwanted oscillations. The high-frequency cut-offs of V1 and V2 are staggered and there is a step network incorporated in the plate load of V2. No instability was observed, although it was found advisable to increase the screen bypass capacitors of V1 and V2 from 0.22 μF to their present value of 2 μF to eliminate a peak in the response at 7 c/s.

The 60-dB amplifiers were tested for relative gain stability by driving both with a common input signal, balancing the outputs using the decade switch and the voltage divider, and checking the balance from time to time over a 24-hour period starting when the amplifiers were first turned on. No change in the relative gains was detected.

The decade gain switch is a General Radio Co. Type 510 precision resistor decade of 1-kΩ per step, wired as a potentiometer. This presents the same load to the traveling-pickup amplifier that the voltage divider presents to the reference-pickup amplifier. The gain of the traveling-pickup channel may thus be accurately adjusted in steps of 10 percent of full gain.

The isolation amplifier following the voltage comparison switch serves primarily to present a very high impedance to the outputs of the decade gain switch and the voltage divider, in order that errors introduced by loading be minimized. The amplifier is a two-stage feedback pair with all the output voltage fed back from the plate of the second stage, a triode, to the cathode of the first stage, a pentode. The

cathode resistor of the first stage is large so that it does not load the second stage unduly. The 100 percent feedback is coupled through the screen bypass capacitor of V4 (the screen is tied directly to the plate of V5). For stability, the low-frequency cutoff of the gain from the plate of V4 to the plate of V5 should be at a higher frequency than the low-frequency cutoff of the gain from the plate of V5 to the cathode of V4. This follows because the feedback to the screen of V4 is positive, as in the feedback connection of a multivibrator. The interstage coupling capacitor and the screen bypass capacitor were chosen with this in mind and no instability was experienced.

The cathode resistor of V4 is tapped at about 4/5 of its resistance from the ground end and the voltage at this point is used to drive the shields on the cables connecting the decade gain switch and the voltage divider to the voltage comparison switch. This reduces the effective cable capacitance by a factor of 5, approximately. If the shields were driven directly from the cathode of V4, in theory the effective cable capacitance could be reduced very nearly to zero. However, should the gain from input to cathode of V4 ever have exceeded unity, then the isolation amplifier would have had a negative input resistance for the shields and instability would have resulted. It was thought preferable to compromise on a capacitance reduction factor of only 5 in order to insure complete stability.

The power supply common to the three amplifiers in the voltage comparison unit is quite conventional except that each amplifier has its own individual filter choke to minimize possible interaction due to coupling through the power supply.

3.3.2 The oscillator control unit

Fig. 3-5 is a schematic diagram of the oscillator control unit. This unit consists of the phase shifter, the balanced modulator, the low-pass filter, the clipper, and a common power supply. All are mounted behind a standard 19-inch rack panel 7 inches in height (see Fig. 3-2).

The phase shifter is the well-known "phase doubler"[25] driven by a split-load phase inverter, V1a. The output of the phase shifter is direct-coupled to the grid of V1b, another split-load phase inverter. The coarse phase control is a four-position switch which selects one of four capacitors for use in the phase-shifting circuit. The four capacitors are chosen to give 90^{o} phase shift at half rotation of the fine phase control at frequencies of approximately 3.5, 9, 18, and 35 kc/s, respectively. The second phase inverter, V1b, is followed by the three-position phase-reversing switch which reverses phase or cuts the phase shifter out of the circuit entirely.

It was originally thought that it might be more convenient to place the phase shifter in the low-frequency part of the circuitry between the balanced modulator and the low-frequency power amplifier. The frequency f_1 is always placed between 50 c/s and 100 c/s; hence the phase shifter would not have to work over such a wide frequency range and it would not need a four-position coarse phase control. However, a drift in the resonance frequency of the specimen horn or the carrier frequency f_2 would cause a change in f_1 of the same number of cycles per second. Even though the drift were a small percentage of f_2, it would be a much larger percentage change in f_1 since f_1 is so much smaller than

---

25. Langford-Smith, F., editor, Radiotron Designer's Handbook (RCA, Harrison, New Jersey, 1953), p. 170.

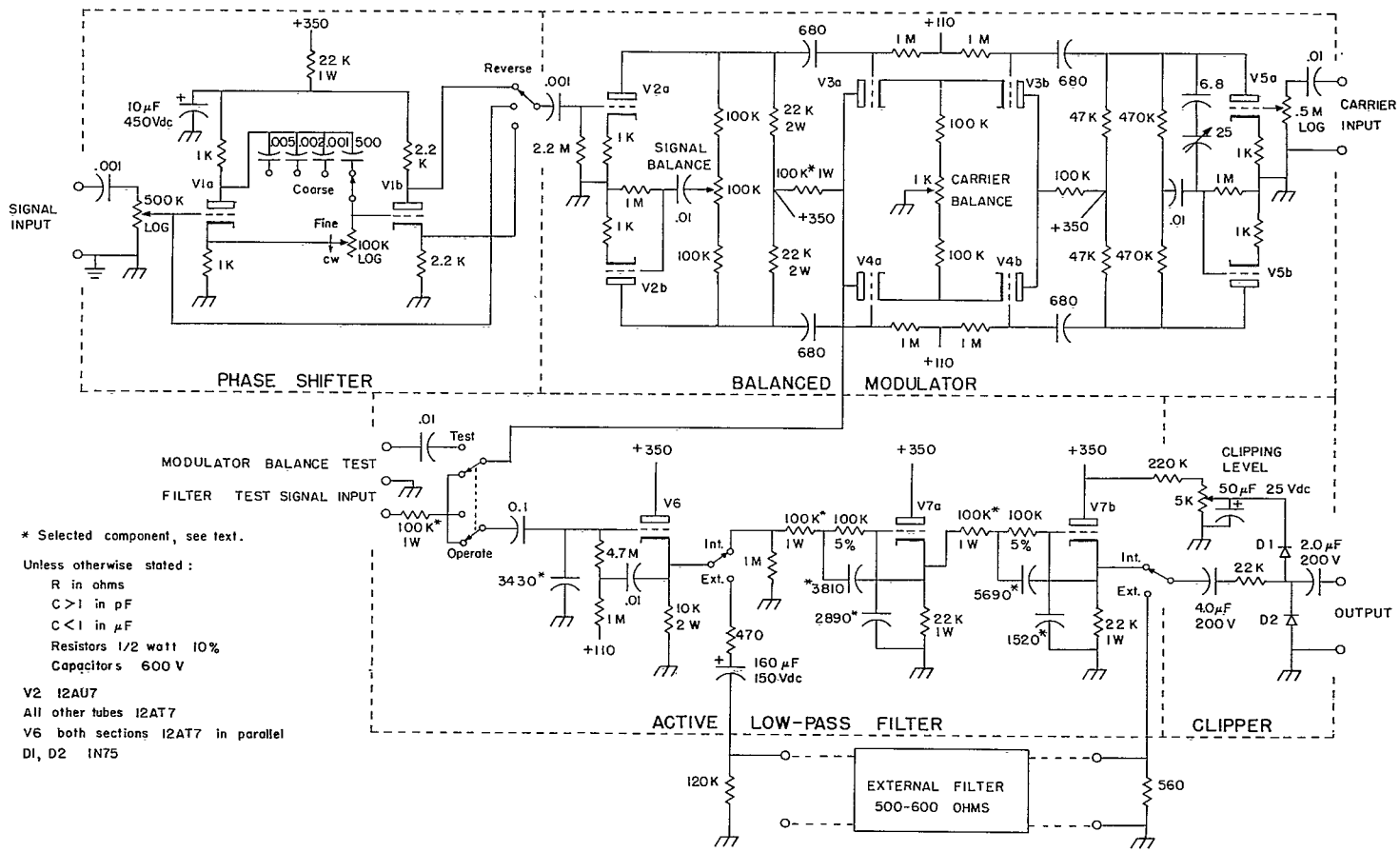

* Selected component, see text.

Unless otherwise stated :
R in ohms
C > 1 in pF
C < 1 in μF
Resistors 1/2 watt 10%
Capacitors 600 V

V2 12AU7
All other tubes 12AT7
V6 both sections 12AT7 in parallel
D1, D2 1N75

FIG. 3-5 SCHEMATIC DIAGRAM OF OSCILLATOR CONTROL UNIT.

f_2. A given frequency drift, then, would cause a greater change in phase shift around the loop if the phase shifter were located in the low-frequency part of the loop rather than in its present location.

The balanced modulator functions as a synchronous switch operated at the carrier frequency f_2. Tubes V5a, an amplifier, and V5b, an anode-follower phase inverter, provide a large push-pull signal at carrier frequency to drive the grids of V3b and V4b. Consider the operation of V3. On the positive half cycle of the carrier signal at the grid of V3b, V3b functions as a cathode follower and drives the cathode of V3a sufficiently positive with respect to its grid that it is cut off for very nearly the entire half cycle. On the negative half cycle of the carrier, V3a serves to hold the cathode voltage of V3b near +110 volts and V3b is cut off by the negative-going swing at its grid. While V3b is cut off, V3a is free to function as a normal amplifier for the signal at its grid, albeit a low-gain amplifier because of the large cathode resistor. If the carrier signal is large, V3a will be switched on and off by V3b at the axis crossings of the signal at the grid of V3b, due to the symmetrical clipping properties of the cathode-coupled clipper[26] from which this circuit was derived. The operation of V4 is exactly the same as that of V3 except reversed in phase with respect to the carrier signal. The output current of the modulator is the sum of the plate currents of V3a and V4a; hence, the output signal is derived alternately from the signals at the grids of V3a and V4a. But these grids are driven in push-pull by the modulating signal (the output of the phase shifter, amplified and inverted in phase by V2) so that the output signal of the

---

26. L. A. Goldmuntz and H. L. Krauss, Proc. IRE 36 (1948), p. 1172.

balanced modulator is just the modulating signal, periodically reversed in phase at the carrier frequency f_2.

In order that the carrier be suppressed at the output, it is necessary that the currents through V3a and V4a in the absence of a modulating signal exactly complement each other, so that their sum, the total plate current at the modulator output, is constant. This means that the currents through the tubes must be just equal in magnitude and opposite in phase. The carrier balance control, a 1-kΩ potentiometer, adjusts the relative magnitudes of the currents by altering the relative sizes of the cathode resistors of V3 and V4. The two 100-kΩ resistors which form the principal parts of these cathode resistors were carefully matched so that the carrier balance control is "right in the middle." If the trimmer capacitor were not between the plate of V5a and the grid of V5b, the anode-follower phase inverter would introduce a slight phase lag in the signal driving V4b. Consequently V3a and V4a would not turn on and off at precisely the same time and a small component at the carrier frequency would appear in the output in phase quadrature to the component balanced out with the carrier balance control. The trimmer capacitor acts as a phase-lead network and can be adjusted to compensate for the phase lag at all frequencies, thus restoring the voltages at the grids of V3b and V4b to exact phase opposition. The maximum capacity of the trimmer is larger than need be, but the unit used was the smallest available at the time of construction.

The signal balance control in the grid circuit of V2b serves to equalize the magnitude of the modulating signals applied to the grids of V3a and V4a, so that the modulating signal does not noticeably appear in the output of the modulator. A small component remains due to the phase

lag of the anode follower, V2b, which could be canceled with a phase-lead network like that described above in connection with the carrier phase inverter. Such compensation was not incorporated here since adequate suppression of the modulating signal was achieved without it.

It can be readily seen from the foregoing discussion, assuming perfect balance in the modulator for suppression of both carrier and modulating signal, that the operation which the modulator performs on the modulating signal is equivalent to multiplication by a square wave at the carrier frequency. If ω and ω_2 are the angular frequencies of modulating signal and carrier, respectively, then we can write the output current of the modulator as

$$i = 2 g_c E \sin(\omega t + \beta) \sum_{n=0}^{\infty} \frac{\sin(2n+1)\omega_2 t}{2n+1}$$

$$= g_c E \sum_{n=0}^{\infty} \frac{\cos[(2n+1)\omega_2 t - \omega t - \beta]}{2n+1} - g_c E \sum_{n=0}^{\infty} \frac{\cos[(2n+1)\omega_2 t + \omega t + \beta]}{2n+1}, \tag{3-12}$$

where $E \sin(\omega t + \beta)$ is the modulating voltage and g_c is a mutual conductance relating input voltage and output current. We have used here the well-known Fourier expansion for a square-wave of peak amplitude $\pi/4$ which switches from negative to positive at $t = 0$.

We assumed in the discussion of the operation of the self-excited system that the output of the modulator contained only two frequencies, the sum and difference of modulating and carrier frequencies. This would be the case if the modulator multiplied the modulating signal by a sine wave at the carrier frequency. In the usual mode of operation, the frequency of the modululating signal is $f = \omega/2\pi = f_2 - f_1$, where f_2 was

identified above as the carrier frequency and f_1 ($\ll f_2$) is the lower field-current frequency of the eddy-current driver. Under these circumstances, we can see from inspection of Eq. (3-12) that the only component of the output current whose frequency is less than the carrier frequency is the first term of the first summation on the right-hand side. We shall name this component i_1:

$$\begin{aligned} i_1 &= g_c\ E\ \cos[(\omega_2-\omega)t-\beta] \\ &= g_c\ E\ \cos[(\omega_2-\omega_2+\omega_1)t-\beta] \\ &= g_c\ E\ \cos(\omega_1 t-\beta)\ , \end{aligned} \tag{3-13}$$

where $\omega_1 = 2\pi f_1$ and $\omega_2 = 2\pi f_2$, as before. Since the carrier frequency lies well above the cutoff frequency of the low-pass filter which follows the balanced modulator, i_1 is the only component of i which will produce a substantial signal at the output of the filter. The introduction of extra terms by the use of square-wave multiplication has thus not altered the essential properties of the system. We also note that g_c is the ratio of the magnitude of the output current at the desired sideband frequency to the magnitude of the input voltage at the modulating frequency. It is therefore the conversion transductance as usually defined.[27]

A test-operate switch was incorporated in the oscillator control unit to permit examination of the unfiltered output of the balanced modulator or the injection of a test signal at the input of the low-pass filter for testing and trouble-shooting. The various balance controls in the modulator were adjusted with the aid of a wave analyzer attached

---

27. Terman, F. E., Electronic and Radio Engineering, 4th ed. (McGraw-Hill, New York, 1955), p. 574.

to the modulator test point. With careful balancing, the carrier suppression of the modulator could be made as high as 57 dB. The various frequency components in the modulator output were found to be nearly in the relation predicted by Eq. (3-12); however, various departures were noted. The sidebands about the harmonics of the carrier frequency [$n \geq 1$ in Eq. (3-12)] decreased in amplitude somewhat faster with increasing frequency than predicted, indicating that V3a and V4a were not switched on and off instantaneously by V3b and V4b, respectively. Also, there were some very weak sidebands centered about the even harmonics of the carrier frequency, showing that the axis crossings of the signals at the grids of V3b and V4b were not uniformly spaced due to second-harmonic distortion of the carrier signal.

In actual operation, the modulating signal contains unwanted components at frequencies f_1 and f_2, as mentioned above in the discussion of the eddy-current driver in section 3.2. It can be seen from Eq. (3-12) that these will produce components in the modulator output at zero frequency and at frequencies above the passband of the low-pass filter. Since the low-pass filter does not actually transmit dc, despite its name, these interfering signals do not affect the operation of the self-excited oscillator system.

The low-pass filter is of the resistance-capacitance active type. Due to their large unbypassed cathode resistors, tubes V3a and V4a in the balanced modulator have very high effective plate resistances. As a result, the output impedance of the modulator is essentially just the resistance of the common plate load resistor of V3a and V4a, and this resistor was used as the first element in the low-pass filter. A capacitor from the grid of V6 to ground forms with this resistor a single RC

low-pass section whose transfer function has a pole on the negative real axis of the complex frequency plane. Two active filter sections follow cathode follower V6, each of which contributes a pair of complex-conjugate poles to the over-all filter transfer function. An internal-external filter switch provides for the use of an external 600-Ω filter in place of these two sections. As noted above in connection with the balanced modulator, the passband of the low-pass filter does not extend down to zero frequency. The input is coupled to the grid of V6 through a capacitor which is necessary for proper biasing of V6.

Each of the active filter sections is of the form shown in Fig. 3-6, below. The amplifiers are cathode followers V7a and V7b; hence the

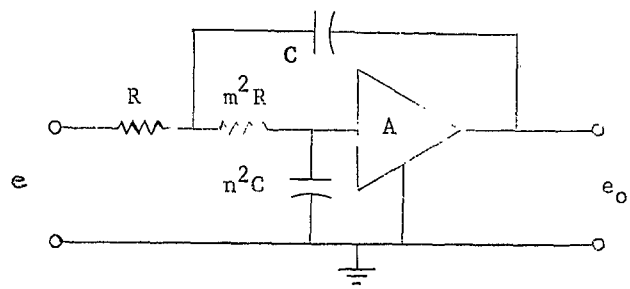

Fig. 3-6. Diagram of Active Low-Pass Filter Section.

gain A is positive but less than unity. Assuming the input admittance and the output impedance of the amplifier are both zero, the transfer function of the filter may be readily calculated and is found to be

$$G(p) = \frac{e_o}{e} = \frac{A}{p^2 + p(mn + \frac{n}{m} + \frac{1-A}{mn}) + 1} = \frac{A}{p^2 + \frac{p}{Q_e} + 1}, \quad (3\text{-}14)$$

where e and e_o are the voltages at the input and the output of the filter, respectively, and $p = mnRCs$ is the normalized complex frequency variable. The quantity Q_e is analogous to the Q of a single RLC tuned circuit.

The transfer function of the filter as a whole was rather arbitrarily chosen to be a fifth-order Butterworth approximation to a constant-time-delay low-pass filter with a cutoff frequency of 500 c/s. The transfer function is the reciprocal of a fifth-degree polynomial in s, which was constructed by standard methods.[28] The roots of the polynomial were found; they consisted of one real root and two complex-conjugate pairs. The two quadratic factors for the complex-conjugate root pairs were normalized to the form of the denominator of the right-hand side of Eq. (3-14), and the necessary circuit constants were determined for the two active filter sections.

This was not a unique procedure, since three constants--m, n, and A--were available for the determination of the one parameter Q_e. The design of the cathode follower determined A, and m was chosen unity because small variations in m are least critical at this value. This left a quadratic in n; the larger solution was chosen in both cases because it was more nearly unity (it was felt that it was advisable to have the circuit-element values neither too large nor too small). The resistor values for both filter sections were then chosen to be 100 kΩ since that is a readily obtainable value and its choice led to reasonable sizes for the capacitors. Those resistors marked with asterisks on the schematic diagram, Fig. 3-5, were carefully matched and are one-watt units in order to be less susceptible to permanent change in value from the heat of soldering. The five capacitors marked with asterisks were either selected units or composed of smaller units connected in parallel

---

28. Guillemin, E. A., Synthesis of Passive Networks (Wiley, New York, 1957), p. 632 ff.

to achieve the design values. A General Radio Co. Type 1650-A impedance bridge was used to pick the capacitors.

If an external filter is used, V6 is heavily loaded but must still be able to handle the maximum output signal of the balanced modulator. It must therefore possess greater power-handling capability than V7a or V7b.[29] For this reason V6 is really two triodes in parallel (both halves of a 12AT7) and is operated with more than twice the quiescent current of V7a and V7b.

The ultimate high-frequency attenuation attainable with these active filter sections is limited by the non-zero output impedance of the cathode followers V7a and V7b. At frequencies high enough so that the capacitors effectively behave like short circuits, the input filter resistor and the output impedance of the cathode follower will act as a voltage divider (see Fig. 3-6). The output impedance of V7a or V7b is about 300 Ω; hence the maximum attenuation in each section is about 50 dB. The frequency response of the filter was measured and did indeed depart from the design figures for frequencies above 2.75 kc/s (attenuation > 70 dB). This was of no consequence in the use of the filter.

The diode clipper which follows the low-pass filter controls the level of oscillation by making the loop gain a decreasing function of signal level. A hard clipper was used rather than a "slow" nonlinearity which would operate only on the envelope of the signal because the time delay associated with a slow nonlinearity frequently leads to difficulties with envelope instability. Since the bandwidth around the oscillating loop is severely limited by the high-Q resonance of the specimen

---

29. T. J. Schultz, Trans. IRE AU-3 (1955), p. 28.

horn
~~loop~~, the extra frequency components introduced by a hard clipper do not materially affect the operation of the feedback loop; the important quantity is the loop gain for the fundamental component of the clipped waveform.[30]

The clipping is symmetric and the clipping level is adjustable on the front panel of the oscillator control unit from 0.3 to 8 volts peak-to-peak. Diodes D1 and D2 (Fig. 3-5) are back-biased by a voltage E, say, from the clipping level control. If we assume that the diodes are identical, the voltage at their junction will be E/2. If now a sinusoidal signal of peak amplitude greater than E/2 is applied to the clipper from the cathode of V7b, then when the positive signal peak exceeds +E/2, diode D1 will be forward-biased and a certain amount of charge will be carried through it. On the negative peak, diode D2 will be forward-biased and some charge will be transported through it. In the steady state, the average forward currents of D1 and D2 must be equal, since all the net charge which moves through D1 must have come through D2 (it cannot have come through the 2-μF and 4-μF blocking capacitors). Thus, the same amount of current flows through D1 on each positive peak as flows through D2 on each negative peak and the clipping is perforce symmetric. Since the junction of the two diodes is clamped to E volts on positive peaks and to ground on negative peaks, the clipping level is clearly E volts peak-to-peak. The 0.3-volt peak-to-peak minimum clipping level is due to the forward voltage drop across the semiconductor diodes (knee voltage).

---

30. Truxal, J. G., Control System Synthesis (McGraw-Hill, New York, 1955), Chapter 10.

In normal operation, the various gain controls around the loop and the clipping level control are adjusted so that there is fairly heavy clipping for steady oscillations. This means that the small-signal loop gain is considerably in excess of unity and the oscillations build up rapidly after the loop is closed. No trouble with envelope instability has been experienced.

3.3.3 Power amplifiers

Two power amplifiers are used to supply the excitation for the eddy-current driver.

The low-frequency amplifier is an H. H. Scott, Inc., Type 250-BRL Laboratory Power Amplifier. It has a rated power output of 50 watts. Although any amplifier with sufficient output power in the 50-100 c/s range could have been used, this unit proved particularly convenient because its wide range of output impedances (0.7 Ω to 600 Ω) permitted the use of eddy-current drivers with field windings of various impedance levels.

The high-frequency power amplifier was constructed specifically for this apparatus. Its circuit is sufficiently straightforward that a short description will explain it adequately. The four tubes in the amplifier are two 12AT7's and two 6L6-GC's. The first 12AT7 is an amplifier direct-coupled to a split-load phase inverter. The second 12AT7 is a push-pull driver for the two 6L6-GC's, which form the push-pull output stage. There is push-pull feedback from the plates of the output tubes to the cathodes of the driver tube. The feedback reduces the gain by approximately a factor of 10 and raises the damping factor to 2. The output transformer is a United Transformer Co. CGU-3, nominally rated at

5 kΩ plate-to-plate, 100 watts, 10 to 50 kc/s. The amplifier will deliver 40 watts into its rated (resistive) load from 8 kc/s to 60 kc/s. The output transformer has four identical secondaries which can be connected to work into rated load impedances of 19, 75, 170, and 300 Ω.

It is possible to use the amplifier at full power output at a single frequency below the normal low-frequency limit of 8 kc/s by shunting a capacitor across the load of the appropriate size to resonate with the inductive reactance of the transformer at that frequency. When a load, such as the eddy-current driver, is inductive, then the capacitor can be adjusted to resonate with the parallel combination of output transformer and load.

The outputs of the two power amplifiers are connected to the driver through a metering and switching panel. Two thermocouple-type ammeters measure the currents in the windings of the driver. A telephone-type lever switch is used to disconnect the two amplifiers from the driver and to disconnect the input signal from the high-frequency power amplifier. Another switch substitutes for the low-frequency power amplifier a filament transformer whose output is adjustable by means of a variable autotransformer in its primary circuit. Thus one winding of the driver can be excited at power-line frequency.

3.3.4 Other apparatus not shown in a block diagram

Several pieces of commercial equipment which do not appear in the block diagram, Fig. 3-2, were used from time to time.

An oscilloscope was always available. During the measurement of a standing-wave pattern it was used to determine the sign of the characteristic function at the measurement point by observing the relative phase

of the signals from the reference and traveling pickups. It was also used to check waveforms at various points around the loop to determine whether the system was oscillating properly. A Tektronix 536 X-Y oscilloscope was in use for some time but it was superseded by a Hewlett-Packard Co. Model 130C which was better suited to these measurements (i.e., it had more gain and less bandwidth than the Tektronix).

Two instruments were employed for the measurement of frequency. A Hewlett-Packard Co. Model 523B electronic counter was used when high precision was needed since it could be read to 0.1 c/s. When a precision of $\pm$ 0.2 percent was deemed adequate, a General Radio Co. Type 1142-A frequency meter was often substituted for the counter.

In connection with the study of the properties of the driver (section 3.2, above), it was necessary to measure the Q's of the resonances of specimen horns. This was accomplished by measuring the decay rate of free vibrations with a Bruel and Kjaer Type 2301 level recorder, and by then calculating the Q from the decay rate and the resonance frequency (discussed in section 3.5).

3.4 The mechanical system

The mechanical system comprises supports for the driver, the specimen horn, and the reference and traveling pickups, as well as a means for positioning the traveling pickup. Fig. 3-7 is a photograph of this part of the apparatus. Two towers (A and B; letters refer to Fig. 3-7) are mounted on a base plate (C). Tower A supports the reference pickup (D) and the top of the solid horn (E). Tower B supports the traveling pickup (F) and the mechanism for positioning it. Its vertical traverse can be driven by an electric motor (G). The eddy-current driver (H) is located beneath the bottom end of the horn.

The base plate is a brass panel of dimensions $12 \times 14 \times \frac{3}{8}$ inches. It is provided with three brass feet, two of which are adjustable in height so that the apparatus may be leveled. The two adjustable feet may be locked in position once the base plate has been leveled.

The specimen horn is mounted on hardened steel point bearings which ride in small dimples centered in the end faces of the horn. The lower bearing, which supports all the weight of the horn, is quite rugged and is screwed firmly to the base plate. The top bearing must withstand only the small lateral forces due to imperfect leveling of the apparatus. It is spring-loaded against the upper end of the horn and is mounted on a sled which can be clamped to tower A at various heights above the base plate. In this manner, specimen horns of lengths 5 to 18 inches can easily be accommodated.

As noted in section 3.2, the eddy-current driver is constructed on a 4-inch square of hardboard. A hole in the center of the hardboard clears the bottom bearing of the horn, and four holes in the corners slip over threaded studs rising from the base plate. The hardboard driver base rests on four coil springs around the studs. Knurled nuts on the studs bear against the top surface of the driver base, thus compressing the coil springs and permitting adjustment of the spacing between the poles of the driver and the end face of the horn.

The traveling pickup can be moved vertically, parallel to the axis of the horn, and laterally, along the extended radius of the cross section of the horn. The pickup is attached to a mechanical stage for a microscope, which provides a lateral movement of approximately 2 inches and a vertical movement of a little more than an inch. The major vertical movement of the pickup is supplied by the motion of a carriage to

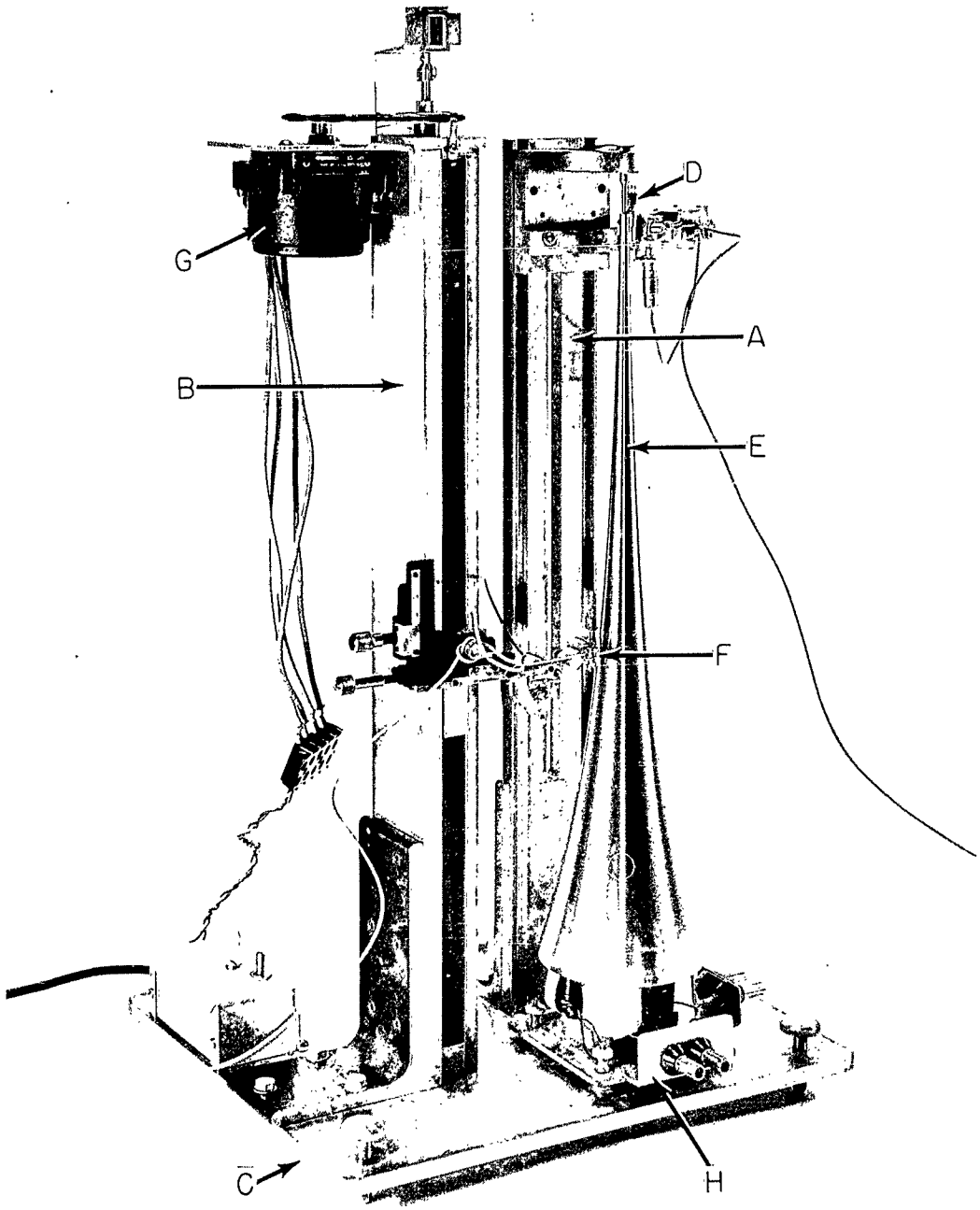

Fig. 3-7. Photograph of the mechanical system. The specimen horn (E) is 18 inches long.

which the mechanical stage is attached. A motor-driven $\frac{3}{8}$-16 stainless-steel lead screw moves the carriage vertically over an 18-inch range. A turns-counting dial for indicating the position of the carriage is driven directly by the end of the lead-screw shaft.

To insure that the traveling-pickup carriage moves accurately in a straight line, its motion is controlled according to kinematic principles.[31,32] The carriage has three spherical feet which ride in two grooves or ways in a bed which forms the major structural member of tower B (Fig. 3-7). The bed is a rectangular bar of cold-rolled steel, $2\frac{1}{2} \times \frac{1}{2}$ inches in cross section and some 22 inches long. The ways comprise one vee groove and one groove of rectangular cross section. In order to insure that they were accurately parallel, the ways were milled into the bed in one series of operations on the milling machine, without removing the bed from the milling table. Two of the spherical feet on the carriage ride in the vee groove, the third on the bottom of the rectangular groove. As long as the feet are maintained in contact with the ways in this manner, the carriage is constrained to move in a straight line.* Since the ways are vertical, gravity cannot be used to hold the carriage to the ways. Three spring-loaded feet push the carriage against the ways by pressing on a "back-up" bar approximately parallel to the ways and on the opposite side of the carriage from the ways. The back-up bar is a rectangular bar of cold-rolled steel of smaller cross

---

31. Whitehead, T. N., Instruments and Accurate Mechanism (Dover, New York, 1954).

32. Elliott, A., and J. H. Dickson, Laboratory Instruments, 2nd ed. (Chemical Publishing Co., New York, 1960), Chapter 6.

* p. 81 of Ref. 32, cited above.

section than the bed but of the same length. It is bolted to the bed through brass spacers at the top and bottom of the ways.

The lead screw which moves the carriage passes through a threaded hole centered in the carriage. This hole has about five complete threads and is elsewhere relieved in order that any warp in the lead screw will not cause binding. The lower end of the lead screw is left free; the upper end passes through the upper spacer between the bed and the back-up bar. A brass collar on the screw shaft bears on the top surface of this spacer and supports the weight of the screw and the carriage. This arrangement insures that the screw exerts no sizable lateral forces which might unseat the carriage from the ways. The lead screw is driven by a geared-down two-phase induction motor (G in Fig. 3-7) coupled to the screw with two pulleys and a rubber O-ring used as a belt. The belt slips when the carriage hits one of its limits, thus preventing damage to the lead screw. A small aluminum box (visible at the left rear of the base plate in Fig. 3-7) contains the phase-shifting capacitor and reversing switch for the motor.

Tower A (Fig. 3-7) is another bed with two parallel ways milled into it. Both ways are vee grooves here. The upper bearing for the horn and the support for the reference pickup are attached to a sled with two cylindrical runners which slide in the ways. The runners are pieces of $\frac{1}{4}$-inch drill rod, milled flat along the sides which are against the body of the sled. When the sled was assembled, each runner was sandwiched between the sled body and its vee groove so that it centered itself in the groove before permanent attachment to the sled body. Thus the runners were made parallel and were spaced the same distance apart as the vee grooves in the bed. When a specimen horn is

installed in the apparatus, the sled is clamped to tower A at the appropriate height by two bolts which pass through a long slot milled through the bed along its center line.

The dimensions are so chosen that the reference pickup always makes contact with the specimen horn about 1/4 inch below the upper end of the horn. At all frequencies and for all materials used experimentally, 1/4 inch is sufficiently smaller than a wavelength that all modes are coupled well to the reference pickup. A rack and pinion allows adjustment of the distance between the reference pickup and the horn axis, so that horns of different diameters can be used.

Tower A and tower B are mounted on the base plate with rugged steel brackets. The bottom faces of the brackets and towers were milled plane after the brackets were attached to the towers so that the towers would be normal to the base plate.

The sensitivity of the phonograph pickups is unfortunately a pronounced function of tracking force. A rise of about 30 percent in output voltage is observed between first contact with a vibrating horn and maximum tracking force (the force at which the stylus has just retreated into the pickup housing). In order to obtain consistent results, then, it is necessary to support the pickups in a manner which permits good reproducibility of tracking force and accurate positioning of the stylus on the surface of the horn as well.

Fig. 3-8 is a photograph which shows in some detail the mounting of the traveling pickup. We can see portions of some of the items discussed above: the bed (A), the lead screw (B), the back-up bar (C), the mechanical stage (D), and the specimen horn (E). The traveling pickup (F) is mounted on a counterbalanced piece of brass which pivots about a

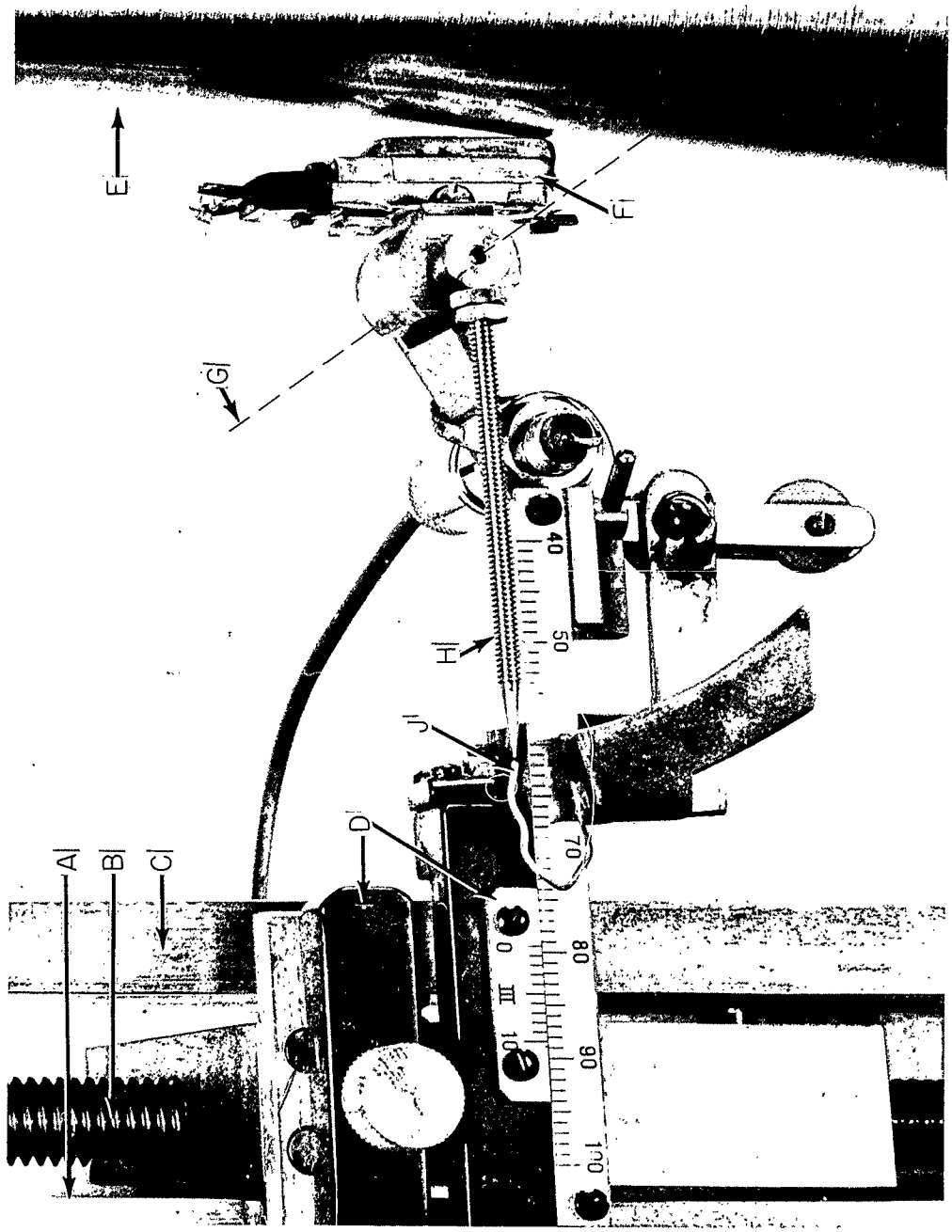

Fig. 3-8. Photograph showing details of the mounting of the traveling pickup (F)

horizontal axis (G). A pointer (H), threaded to receive a drilled and tapped counterweight, if desired, indicates the correct operating position when its tip is directly opposite the end of a wire (J), used as a fiducial point.

Since the axis (G) passes through the center of gravity of the pickup and its brass mounting block, all the tracking force is contributed by the weight of the pointer and the counterweight. Because of the pivot, small errors in the horizontal positioning of the pickup produce small angular variations in the position of the pointer. When the pointer is nearly horizontal, however, the tracking force is essentially independent of such small variations. The pointer can be rotated with respect to the pickup so that the angle between the horn contour and the pickup can be adjusted. If at each measurement point the pointer tip is aligned with the end of the wire (J), the stylus will always be in the same geometrical relation to the lead screw and the position of the lead screw can be used to indicate the vertical position of the stylus.

The reference pickup is mounted in exactly the same manner as the traveling pickup.

3.5 Experimental technique

3.5.1 Measurement of resonance frequencies

A normal mode of a torsional horn is specified by its resonance frequency and characteristic function. Because the resonance frequencies of torsional horns can be easily and precisely measured, they provide a very useful means of checking the agreement between the physical facts and theoretical predictions based on the solution of the equations derived in Chapter II. In Chapter V, the measured resonance frequencies

of exponential horns are used to estimate quantitatively the errors introduced by the assumption of plane wavefronts.

Since at the outset of an experiment the shear-wave speed in the horn material is not known exactly, the resonance frequencies themselves are of little interest; it is rather the ratios of resonance frequencies which are important. Thus a constant percentage error in the frequency measurements would not affect the quality of the experimental results.

It was noted above in section 3.3 that the resonance frequencies of the experimental horns decreased with rising temperature for all metals used. In order to achieve consistent results it was necessary to try to keep the temperature constant during a run of measurements, and in particular to avoid appreciable heating of the specimen horns by the eddy currents induced by the driver. The electronic gear necessary for the measurements was turned on several days in advance of the run so that the room temperature would be stable. (There was a steady-state difference of about 5° C between equipment off and equipment on.) Induction heating by the driver was minimized by operating at as low a signal level as feasible. The self-oscillating system was not used. Instead, one winding of the driver was excited with direct current so that the frequency of the current in the other winding was the frequency of the induced torque. The wave analyzer was operated in its BFO mode, in which it delivers a sinusoidal signal at the frequency to which it is tuned. This signal drove the high-frequency power amplifier which in turn drove the second winding on the driver. The input signal to the wave analyzer was the amplified output of one of the pickups, usually the traveling pickup, placed just at the upper end of the horn so that it was sensitive to all the normal modes. The wave analyzer was then

slowly swept in frequency while its voltmeter was scrutinized for indications of resonances.

As stated in section 3.3, this single-frequency drive produces a spurious component at signal frequency in the output of the phonograph pickup. This interference prevents accurate measurement of the amplitude of vibration, but it does not obscure the presence of resonances. The fact that the rate of change of phase with frequency is a maximum at a resonance frequency can be used to locate the resonance even when the desired signal is as small as one-tenth the interfering signal. For most horns, it proved possible in practice to locate all the resonance frequencies within the frequency range of the wave analyzer ($\leq$ 50 kc/s).

When a resonance is located, the wave analyzer is tuned as nearly as possible to the center of the resonance and the frequency is then measured with the Hewlett-Packard Model 523B electronic counter. The counter operates by counting the number of cycles of its input signal during a standard length of time determined by a built-in frequency standard. The longest available gate time is 10 seconds; thus, frequency may be measured to a precision of 0.1 c/s. Since only the ratios of resonance frequencies are important, a fixed error in the internally generated standard frequency will not affect the significance of the results. However, drift in the standard frequency during a measurement run would introduce errors. The manufacturer specifies that drift in the frequency standard is less than 2 parts in 10^6 per week. Thus for short-term measurements over a few hours, the accuracy of measurement is limited by the 0.1 c/s precision for frequencies less than 50 kc/s. However, the resonance frequencies can rarely be located to within 0.1 c/s. Tests for reproducibility showed that with care the resonances can be

repeatedly found to approximately 2 parts in 10^5. Since comparison of the resonance frequencies of two or several different horns turned from the same (presumably homogeneous) piece of stock requires knowledge of their dimensions, and the accuracy with which the dimensions can be measured is at least an order of magnitude worse than 2 parts in 10^5, we can see that the accuracy attainable in frequency measurements is more than adequate.

3.5.2 Measurement of Q

As a part of the investigation of the properties of the eddy-current driver, it was found necessary to measure the Q's of the resonances of several horns.

A common method for measuring the Q of a resonant system is to measure the bandwidth of the driven system and compute the Q from the formula

$$Q = \frac{f}{\Delta f} , \qquad (3\text{-}15)$$

where f is the resonance frequency and Δf is the bandwidth between the frequencies where the response is 3 dB less than the maximum. If the Q is high, it may be difficult to measure Δf with the desired accuracy. However, for high enough Q, the decay rate of free vibrations is slow enough so that it can be measured and the Q calculated.

The time dependence of a normal mode of free vibration is the same as that of a simple resonator;* hence, if only one normal mode is excited, the envelope of the vibrations after the excitation is removed will decay as $e^{-\omega t/2Q}$, where ω and Q are the natural frequency and the

---

* Chapter VII of Ref. 17, cited on p. 17.

quality factor of the normal mode, respectively.[33] The resonances of solid torsional horns were found to be sharp enough that the determination of Q through measurement of the decay rate of free vibrations was much the better method.

A Bruel and Kjaer Type 2301 level recorder was employed for the measurement of decay rate. The specimen horn was excited by the self-oscillating method and the recorder was driven by the amplified signal from one of the pickups. The oscillating loop was then broken by disconnecting the driver from the two power amplifiers. The logarithm of the ensuing envelope decay was recorded at an appropriate chart drive speed. The decay rate in dB/sec was then calculated from the slope of the recorded decay and the chart speed. Let H be the decay rate in dB/sec. We can easily find Q from H and ω through the following relation:

$$20 \log_{10}\left[e^{-\omega/2Q}\right] = -H \ ,$$

which leads to (3-16)

$$Q = 27.25 \frac{f}{H} \ ,$$

where $f = \omega/2\pi$.

Several decay rates were averaged for each case in order to gain some idea of the reproducibility of the measurements. The spread in decay rates was approximately ± 2 percent.

In addition to the investigation of the properties of the driver, a further object of the measurements of Q was to find out what part of the total damping was contributed by the pickups. For one-inch diameter cylinders of brass and mild steel, the Q was found to be 15 000 to 20 000

---

33. Guillemin, E. A., Introductory Circuit Theory (Wiley, New York, 1953), pp. 247-9).

and was reasonably independent of frequency. The presence of a second pickup in contact with a cylinder lowered the Q by no more than 5 percent. Thus the pickups introduce a noticeable but not significant fraction of the damping for brass and mild steel. However, the Q of the lowest mode of an aluminum cylinder was higher and was limited to approximately 100 000 by the pickup damping with the stylus contact close to the end of the cylinder. In order to reduce the effect of the pickup damping, the point of contact was moved closer to the node at the center of the cylinder. Positioning the contact point anywhere from 1/16 to 1/4 inch from the node always gave essentially the same Q, 304 000; it was therefore felt that the effect of the pickup had been reduced until the losses were predominantly due to other factors.

All of the experimental horns except the one aluminum cylinder were made of brass or mild steel. For virtually all the experimental work performed, then, the damping due to the pickups was not significant.

3.5.3 Measurement of torsional standing-wave patterns

Most aspects of the method used for the measurement of standing-wave patterns have been discussed piecemeal in conjunction with the description in sections 3.2, 3.3, and 3.4 of the equipment constructed for making the measurements. A description of the normal sequence of events in the measurement of a standing-wave pattern follows.

The horn is at first separately excited, not self-excited. The two driver field currents are at the carrier frequency (from the carrier source and the high-frequency power amplifier) and at the power-line frequency, 60 c/s (from the transformer on the metering panel). The carrier frequency is then slowly varied until some indication of resonance

is observed on the oscilloscope, which is monitoring the output of the reference pickup. The circuitry is then reconnected for self-excited oscillation by driving the low-frequency winding of the driver from the low-frequency power amplifier, as indicated in the block diagram, Fig. 3.2. The phase-shifter controls are then adjusted until oscillation commences. The carrier is now slightly changed to place the lower driving current frequency somewhere other than at 60 c/s. Then the phase shifter is readjusted to maximize the amplitude of oscillation. The shunt capacitor across the high-frequency coil of the driver is made to resonate with the inductance of the driver and the output impedance of the high-frequency power amplifier at the carrier frequency. In order that the clipper be the only component limiting the amplitude of oscillation through nonlinearity, the gain controls on the two power amplifiers and the signal gain control and clipping-level control on the oscillator control unit are set to obtain the desired signal levels around the loop.

Now the wave analyzer is tuned to the frequency of vibration of the horn under test. The traveling pickup is moved from point to point, placed in contact with the horn at each point, and the decade gain switch and voltage divider are adjusted until the signals from the two pickups are equal as shown on the wave analyzer. While the traveling pickup is being moved to the next measurement point, the oscillating loop is broken by removing excitation from the driver so that unnecessary induction heating of the specimen horn is minimized.

The settings of the precision voltage divider and the decade gain switch are recorded at each measurement point. Their ratio is the particle displacement on the surface at the measurement point relative

to that at the reference pickup. After the measurement run, these numbers are divided by the radius of the cross section at the measurement point to obtain the relative angular displacement. This result is of course arbitrary to within a multiplicative constant since it corresponds mathematically to the solution of a homogeneous equation. The theoretical standing-wave patterns computed in Chapters IV, V, and VI, with which the experimental results were compared, were always normalized so as to have the value +1 at the top end of the horn. (The top end was always the smaller end wherever the two ends were of different diameter.) A least-squares method was used to find a constant k by which the experimental results could be scaled so that they could be directly compared with the normalized theoretical standing-wave patterns. This method was chosen because it was simple, systematic, and seemed to display the experimental results to best advantage.

This least squares normalization of the experimental data was accomplished in the following way: Let a_n be the non-normalized measured value of the angular displacement at the nth measurement point, and let b_n be the (normalized) theoretical value at the same point. We wish to find the value of k which will minimize the total squared error E given by the equation

$$E = \sum_n (b_n - ka_n)^2 \quad . \tag{3-17}$$

Differentiating with respect to k and equating the derivative to zero, in order to minimize E, we have

$$\frac{dE}{dk} = -2 \sum_n a_n b_n - ka_n^2 = 0 \ , \tag{3-18a}$$

or,

$$k = \frac{\sum_n a_n b_n}{\sum_n a_n^2} \qquad (3\text{-}18b)$$

Having calculated k, we next find all the $A_n = ka_n$, the normalized experimental data, which we then plot to the same scale as the b_n in order to compare experiment and theory (see, for example, Fig. 4-1).

The precision with which the balance between the reference signal and the traveling-pickup signal can be found depends on the signal-to-noise ratios of the two channels. The noise is of two types. The first is the interfering signal induced by the magnetic fields of the driver. This consists of components at discrete frequencies relatively far removed from the passband of the wave analyzer; hence they are not troublesome. The second is broadband noise contributed in part by the amplifiers following the pickups and in part by seismic excitation of the pickups. This type of noise manifests itself as random fluctuations in the voltmeter indication of the wave analyzer. Unless the signal is a great deal stronger than the noise, these fluctuations are the limiting factor in determining the experimental precision. The noise level is quite constant with frequency over the range 5 kc/s to 50 kc/s and rises slowly at frequencies below 5 kc/s.

The signal strength at the terminals of one of the pickups depends on the effectiveness of the coupling between driver and horn, the gain of the horn from the driven end to the pickup, and the sensitivity of the pickup. These factors may be lumped together into the conversion transimpedance ζ, defined as the ratio of the terminal voltage of the pickup at the signal frequency (= horn resonance frequency) to the low-frequency

feedback current in the driver. The signal-to-noise ratio will be proportional to ζ since the noise level is essentially constant over the frequency range of interest.

Since the driver approximates an ideal torque source, ζ will vary inversely with the driving-point impedance of the horn. The driving-point impedance at an end of a torsional horn rises sharply with diameter; thus, the thicker specimen horns are considerably harder to drive than the thinner ones. The shape of the horn and the mode of vibration determine the gain of the horn. This varies widely among the specimen horns from about 0.3 to about 30. The phonograph pickups were basically "displacement pickups"; that is, within the normal frequency range of the pickup, the output voltage was proportional to the displacement of the stylus, not the velocity as with magnetic pickups, for instance. Since the angular velocity of the horn is proportional to the driving current, all other things being equal, we can see that ζ decreases with increasing frequency at a 6 dB/octave rate from this cause alone. In addition, the pickups' displacement sensitivity decreases rapidly above 15 kc/s. Thus, we can say in general that the standing-wave patterns of the higher modes of thick horns cannot be measured with as much precision as those of the lower modes of thin horns.

The precision attained, as indicated by the distribution of repeated measurements, varied from better than 1 percent of maximum angular displacement to some 4 percent. The <u>accuracy</u> was not as good as the precision, primarily due to the fact that the pickup sensitivity depends on temperature. When the traveling pickup is near the bottom of the horn, it is generally warmer than when near the top. The voltage comparison balance between reference and traveling pickups can still be made,

but the variations in pickup sensitivity will in essence have varied the relative gain of the two channels slightly to an unknown degree. The effect is fortunately not too large, and it is believed to introduce no more than 2 percent error.

Any error in the lead screw can cause the measurements to be made at points other than those intended, and consequently can introduce errors in the experimental data. Since other considerations limit the attainable accuracy to about 1 percent of maximum angular displacement, the additional error due to the lead screw must be of at least that order of magnitude to be objectionable. The shortest wavelength in any measured standing-wave pattern was about 4.5 inches. The greatest error will be introduced near the nodes, where the angular displacement is changing most rapidly with distance. Assuming an approximately sinusoidal standing-wave pattern, we can readily calculate with the aid of trigonometric tables that an error in the traveling-pickup placement of .008 inches will cause about a 1-percent error in the measured angular displacement if the wavelength is 4.5 inches. For longer wavelengths, a proportionately greater error in the positioning of the traveling pickup would be tolerable.

The lead screw was checked against an accurate steel scale for large distances and against a traveling microscope for small. The errors observed were considerably less than .008 inches. Thus the lead screw is more than sufficiently accurate for its use.

Chapter IV

HORNS FITTING SEPARABLE COORDINATE SYSTEMS

The "exact" torsional wave equation derived in Chapter II can be solved by the method of separation of variables in some cases. These are cases for which the horn is bounded by coordinate surfaces of a coordinate system in which the Laplacian is separable. This may be shown in the following way.

The torsional wave equation for ψ, assuming sinusoidal time dependence, is, in cylindrical coordinates (r,z,φ),

$$\psi_{rr} + \frac{3}{r}\psi_r + \psi_{zz} + k^2\psi = 0 , \tag{4-1}$$

where $k = \omega/c$ is the wave number, subscripts denote partial derivatives, and ψ is now the angular displacement with the time dependence factored out. We recall that $\psi_\varphi = 0$, and, after some routine crank-turning, we find that (4-1) can be rewritten as

$$\frac{1}{r}\nabla^2(r\psi) + (k^2 - \frac{1}{r^2})\psi = 0 . \tag{4-2}$$

Since torsional waves and torsional horns, as defined here, always possess rotational symmetry, any coordinate system which bounds a torsional horn can always be constructed so that one of the coordinates is an angle φ, the angle of rotation about the axis of the horn. In cylindrical coordinates, the coordinate r is the scale factor h_φ for the angle φ; that is, $rd\varphi = h_\varphi d\varphi$ is an infinitesimal displacement in the φ-direction. Since the Laplacian is invariant under coordinate transformation, we can generalize Eq. (4-2) to all rotationally symmetric coordinates by substituting h_φ for r. We obtain thus

$$\frac{1}{h_\varphi}\nabla^2(h_\varphi\psi) + (k^2 - \frac{1}{h_\varphi^2})\psi = 0 \ . \qquad (4\text{-}3)$$

(The subscript on h_φ identifies only the coordinate, it does not denote a derivative.)

It is obvious that Eq. (4-3) can be separated if the Laplacian is separable and if h_φ is factorable into functions of one coordinate only. Of the eleven coordinate systems for which the Laplacian is separable, five possess rotational symmetry.* For each of these systems, h_φ is suitably factorable. The five systems are cylindrical, spherical, parabolic, oblate spheroidal, and prolate spheroidal coordinates.

Now let (v,w,φ) be the coordinates of a point expressed in one of these systems, and let the separated solution of (4-3) be $\psi = V(v)W(w)$. Only in cylindrical and spherical coordinates can a solution of this form be readily found; in the remaining three systems the situation is complicated by the fact that the separation constant introduced by the separation depends on both V and W. In other words, the solution is separable for the coordinates but not for the separation constant.** Only cylindrical and spherical coordinates will be treated here. The wave equations and the separated ordinary differential equations for the other three systems are given in Appendix A.

Of particular interest are one-parameter solutions, i.e., solutions where ψ is a function of only one space coordinate. As might be expected from the remarks in the preceding paragraph, only in cylindrical and spherical coordinates are there one-parameter solutions. In Appendix A

---

* p. 655 ff. of Ref. 22, cited on p. 29.

** pp. 517-8 of Ref. 22, cited on p. 29.

is a demonstration that in parabolic, prolate spheroidal, and oblate spheroidal coordinates there are no one-parameter solutions.

4.1 Cylindrical coordinates (r,z,φ)

4.1.1 Mathematical analysis

The horn shape fitting cylindrical coordinates which will receive the most attention in this section is the solid right circular cylinder, although some attention will be given to the hollow right circular cylinder.

The wave equation in cylindrical coordinates has already been given as (4-1). If we take

$$\psi = V(r)W(z) \ , \tag{4-4}$$

we readily obtain the two separated ordinary differential equations,

$$V''(r) + \frac{3}{r} V'(r) + \eta^2 V(r) = 0 \tag{4-5}$$

and

$$W''(z) + (k^2 - \eta^2)W(z) = 0 \ , \tag{4-6}$$

where primes denote differentiation with respect to the argument and η is a separation constant to be determined by the boundary conditions.

If we define β by means of the relation

$$\beta^2 = k^2 - \eta^2 \ , \tag{4-7}$$

we can rewrite (4-6) in the more familiar form

$$W'' + \beta^2 W = 0 \ . \tag{4-6a}$$

The boundary condition for a free surface requires that the normal derivative of ψ vanish and leads to the condition

$$V'(r) = 0 \tag{4-8}$$

at surfaces of constant r, and

$$W'(z) = 0 \tag{4-9}$$

at surfaces of constant z.

Case 1: Plane waves

The simplest solution is found when $\eta = 0$. In this case, $\beta = k$ and $V(r) =$ constant, so that

$$\psi = A \exp(\pm jkz) , \tag{4-10}$$

where A is the amplitude of the wave. The plus sign denotes a wave traveling in the negative z-direction and the minus sign a wave traveling in the positive z-direction.

This solution, a one-parameter solution which is a function only of z, is valid for both solid and hollow cylinders. The wavefronts, surfaces on which the phase and amplitude of ψ are constant, are plane cross sections normal to the axis of the horn. The waves propagate in the z-direction with constant amplitude and velocity.

If the horn is a finite cylinder (solid or hollow) of length ℓ, with free ends at $z = 0$ and $z = \ell$, then the standing-wave patterns of the natural modes of free vibration are given by

$$\psi_n = A \cos(n\pi z/\ell) , \quad n = 1, 2, 3, \ldots . \tag{4-11}$$

The corresponding resonance frequencies are

$$f_n = (nc/2\ell) , \quad n = 1, 2, 3, \ldots . \tag{4-12}$$

This simple relationship between the resonance frequencies, the shear-

wave speed, and the length of the cylinder provides a convenient means for the experimental determination of the shear-wave speed in an elastic material, since the cylinder is a geometric form which can be readily and precisely generated on a lathe.

Case 2: Cylindrical waves

If $\eta = k$, there is another one-parameter solution, this one a function of r only. In this situation, $\beta = 0$; therefore, W = constant is a solution of (4-6a) which also satisfies boundary condition (4-9) for any boundary z = constant.

Equation (4-5) is now a form of Bessel equation[34] which yields

$$\psi = A[J_1(kr) + BN_1(kr)]/kr \ , \qquad (4\text{-}13)$$

where J_1 and N_1 are Bessel functions of the first and second kinds, respectively, A is the wave amplitude, and B is a constant to be determined by the boundary conditions. The wave fronts in this case are concentric cylinders centered on the z-axis.

If the horn is a hollow cylinder, B and k must be chosen to satisfy simultaneously boundary conditions of the form (4-8) on the inner and outer surfaces.

If the horn is a solid cylinder, B must be zero in order that ψ be finite on the axis, since N_1 increases without bound for vanishingly small argument. If the radius of the horn is a, then the boundary condition (4-8) is equivalent to the requirement that ka be one of the roots of

$$\frac{d}{dx}\left[J_1(x)/x\right] = 0 \ , \quad (x = ka) \ . \qquad (4\text{-}14)$$

---

34. Jahnke, E., & F. Emde, Tables of Functions (Dover, N. Y., 1945), p. 146.

Using a differential formula given by Jahnke and Emde,* we find that the roots of (4-14) are just the zeros of $J_2(x)$. These are tabulated in Jahnke and Emde and elsewhere. The approximate values of the first few are given in (4-15), below:

$$J_2(k_n a) = 0$$
$$\Longrightarrow \quad k_n a = 0,\ 5.136,\ 8.417,\ 11.620,\ 14.796,\ \ldots \longrightarrow (n+\tfrac{3}{4})\pi\ , \tag{4-15}$$

where n is an integer, the number of the mode. The first root, $k_n a = 0$, is a degenerate case and corresponds to uniform continuous rigid-body rotation of the entire horn.

Case 3: Compound modes

If neither β nor η is zero, then neither V nor W can be a constant, and ψ must therefore be a function of both r and z. The functions V(r) and W(z) have the same form which they had in cases 2 and 1, respectively, except for the changed values of β and η. The wave function ψ is thus given by

$$\psi = A \exp(\pm j\beta z)\ J_1(\eta r)/\eta r \tag{4-16}$$

for the solid cylinder of radius a. The plus and minus again denote propagation toward negative and positive z, respectively. The allowed values for η are determined in the same way as those for k for the purely cylindrical modes. That is, ηa must have one of the values given in (4-15). The propagation constant for the z-direction, β, is then related to η and the frequency through the equation

$$\beta^2 = (\omega/c)^2 - \eta^2\ , \tag{4-17}$$

which is a slightly modified form of (4-7).

---

* p. 145 of Ref. 34, cited on p. 80.

Consider first a cylinder of infinite length in the z-direction (and of radius a). The most notable property of these two-parameter modes is that there is a lower cutoff frequency associated with each of them. In other words, if the frequency of vibration is below the cutoff frequency for a particular mode, that mode will not propagate in the z-direction. The cutoff frequency for a mode with radial eigenvalue η is

$$\omega_c = \eta c \ . \tag{4-18}$$

This is the frequency of the corresponding cylindrical resonance (case 2), at which $\beta = 0$. For lower frequencies, (4-17) shows that β is imaginary; hence, the amplitude of the wave diminishes exponentially in the z-direction, and the phase is everywhere constant. For higher frequencies β is real, corresponding to true wave motion in the z-direction. However, since β is a function of frequency, these modes are dispersive. If the phase velocity c_p is defined by

$$\beta = \omega/c_p \tag{4-19}$$

then, by combining (4-17) and (4-19), we can easily find that

$$c_p^2 = c^2 \Big/ \left[1 - (\eta/k)^2\right] = c^2 \Big/ \left[1 - (\omega_c/\omega)^2\right] \ . \tag{4-20}$$

If we prescribe the angular displacement as a function of r over a plane cross section of the cylinder and ask how this displacement will propagate along the cylinder, we can expand the prescribed distribution in a Fourier-Bessel series in the usual manner, and ψ elsewhere in the

cylinder will be given by a series of terms each of which is of the form of the right-hand side of (4-16).[35]

If the cylinder is not infinite in length, but of length ℓ (from $z = 0$ to $z = \ell$), then for free vibrations β can assume only values allowed by the boundary conditions (4-9) at the ends. The standing-wave pattern for the mnth mode as a function of the space coordinates z and r is then

$$\psi_{mn} = A \cos(m\pi z/\ell)\ J_1(\omega_{cn} r/c)/(\omega_{cn} r/c)\ , \qquad (4\text{-}21)$$

where $m = 1, 2, 3, \ldots$

and ω_{cn} = cutoff frequency for the nth compound mode of the infinite cylinder. Each of these normal modes has associated with it a resonance frequency

$$\omega_{mn} = \sqrt{(m\pi c/\ell)^2 + \omega_{cn}^2} \qquad (4\text{-}22)$$

Case 1 and case 2, plane waves and cylindrical waves, now appear as specializations of case 3 to $n = 0$ and $m = 0$, respectively.

The behavior of torsional waves in an elastic cylinder has much in common with the behavior of sound waves in air enclosed by a rigid cylindrical tube.[36] In both systems, there exist plane waves, purely cylindrical waves, and higher modes which are functions of both r and z. The plane waves can propagate in the z-direction without dispersion and at all frequencies, whereas each of the higher modes, characterized by a cutoff frequency, propagates dispersively and only at frequencies higher

---

35. E. A. Flinn, J. Acoust, Soc. Am. 33 (May 1961), pp. 623-7. See also pp. 48-9 of Ref. 4, cited on p. 2.

36. Lord Rayleigh, Theory of Sound, Vol. II (Dover, New York, 1945), pp. 297-301.

than its cutoff frequency. However, the differential equations describing the behavior of these two systems in the r-direction are different, and as a result, the characteristic functions of r are different.

4.1.2 Experimental verification

In the course of experimentally investigating other shapes of torsional horn, the plane-wave resonance frequencies of many cylinders were measured as a means of determining the shear-wave speed. There was always excellent agreement with the prediction of Eq. (4-12) that the resonance frequencies would be integral multiples of the lowest. A typical case is summarized in Table 4-1, below. By using Eq. (4-12), values of c were calculated from the observed resonance frequencies. The average of these values was used in Eq. (4-12) to find the theoretical resonance frequencies.

Table 4-1

Plane-wave resonance frequencies of a mild steel cylinder radius 0.750 inches, length 9.000 inches

Mode number n	Theoretical f_n kc/s	Experimental f_n kc/s	$\frac{\text{Exp } f_n}{\text{Theor } f_n}$
1	7.0839	7.0864	1.00035
2	14.1677	14.1679	1.00001
3	21.2516	21.2527	1.00005
4	28.3354	28.3344	0.99996
5	35.4193	35.4159	0.99990
6	42.5032	42.4956	0.99982
7	49.5870	49.5814	0.99989

The standing-wave patterns for the first three plane-wave modes of an 18-inch long brass cylinder one-half inch in radius were measured.

These are compared with the corresponding theoretically predicted cosinusoids in Fig. 4-1.

The measurement of the frequencies of cylindrical resonances was not as easy as for the plane-wave resonances. The experimental apparatus could handle specimens of maximum radius 2 inches. The lowest cylindrical resonance in a steel cylinder of this size is at approximately 52 kc/s, just out of range of the wave analyzer. However, brass has a lower shear-wave speed than steel. A brass cylinder 2.000 inches in radius and 5.838 inches in length (and some 23 pounds in weight) was obtained and some of its resonance frequencies were measured. The shear-wave speed was calculated from the length and the measured resonance frequencies of the lowest five plane-wave modes. This was used to predict the resonance frequencies of the cylindrical and compound modes. The first cylindrical mode and the first four of its associated compound modes had resonance frequencies below 50 kc/s. A comparison of predicted and observed resonance frequencies follows in Table 4-2.

Table 4-2

Compound resonances of a brass cylinder
radius 2.000 inches, length 5.838 inches

Mode number mn	Theoretical f_{mn} kc/s	Experimental f_{mn} kc/s	$\frac{\text{Exp } f_{mn}}{\text{Theor } f_{mn}}$
01	35.430	35.461	1.00087
11	36.199	36.249	1.00138
21	38.416	38.160	0.99334
31	41.855	41.820	0.99916
41	46.232	46.199	0.99929

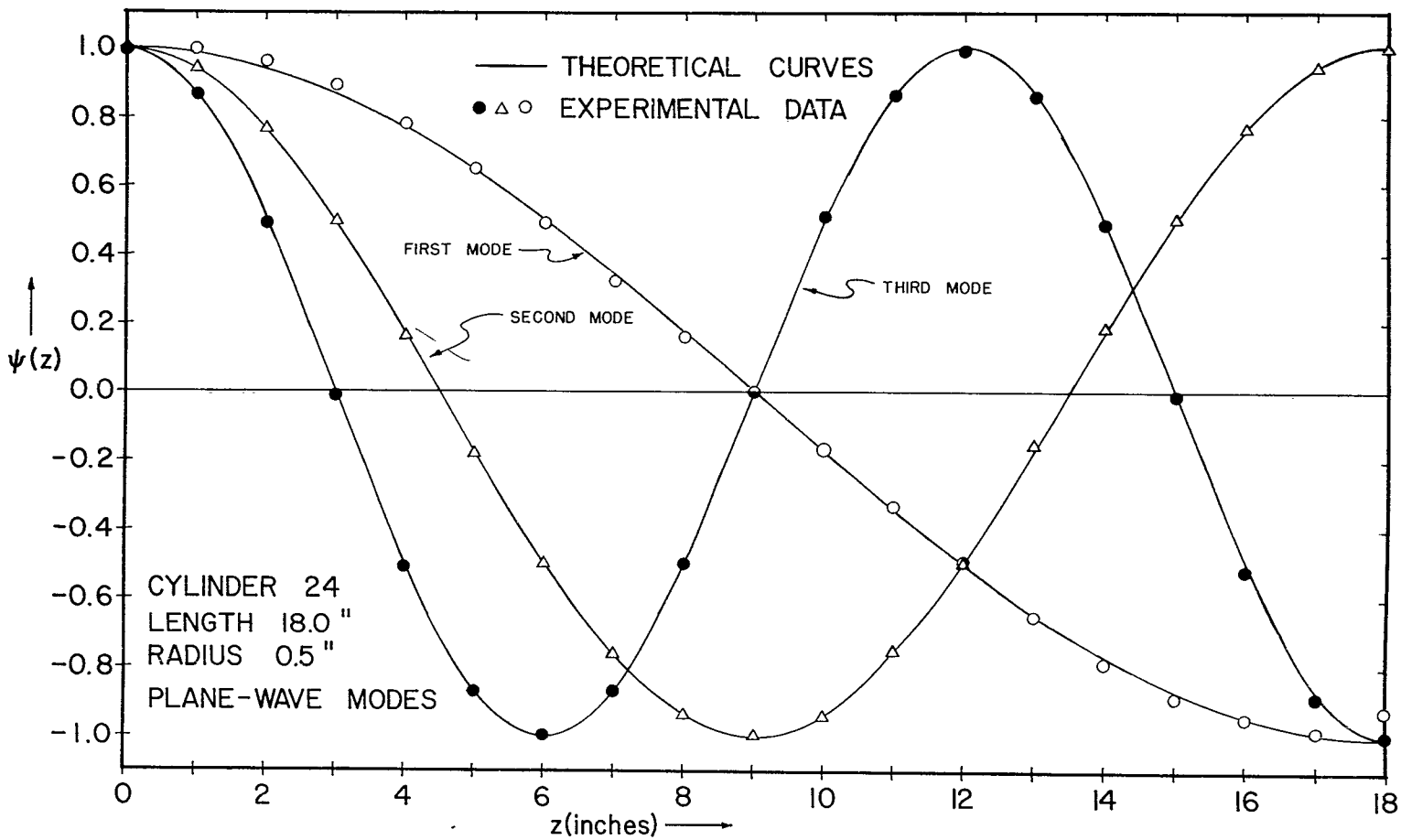

FIG. 4-1 TORSIONAL STANDING-WAVE PATTERNS ON A BRASS CYLINDER.

It is not absolutely certain that the observed resonances belonged to the modes in question. Brass is not as easy to excite as steel, as pointed out in Chapter III, and the large diameter of the specimen would have made it difficult to excite in any event; thus the output from the phonograph pickup was at best not greatly above the noise in this frequency range. The usual method for determining mode number is to count the nodes. The nodes are located by damping the vibrating specimen by touching it with a finger. When the damping is minimal, the finger is on or near a node. This scheme did not work satisfactorily on this thick cylinder, even for the lower plane-wave modes.

The agreement between the predicted and observed resonance frequencies tabulated in Table 4-2 is good enough so that it seems highly probable that these are the first few compound modes. However, it will be observed that the agreement, although good, is an order of magnitude worse than for the plane-wave modes (see Table 4-1).

4.2 Spherical coordinates (r,θ,φ)

4.2.1 Mathematical analysis

Spherical coordinates are suitable for studying conical horns. The side of such a cone is a surface of constant θ, and the ends are spherical caps, surfaces on which r is a constant. Throughout this section, $r = a$ will be taken as the small end of the horn and $r = b$ as the large end. The half-angle of the cone will be denoted by α.

In spherical coordinates,

$$h_\varphi = r \sin\theta \ . \tag{4-23}$$

Making this substitution in (4-3), we can expand the Laplacian and

obtain the torsional wave equation,

$$r^2(\psi_{rr} + \frac{4}{r}\psi_r + k^2\psi) + \psi_{\theta\theta} + 3\cot\theta\ \psi_\theta = 0 \ . \qquad (4\text{-}24)$$

By assuming

$$\psi = V(r)W(\theta) \ , \qquad (4\text{-}25)$$

we can easily separate (4-24) into the two ordinary differential equations

$$V''(r) + \frac{4}{r}V'(r) + \left[k^2 - \frac{(\eta+2)(\eta-1)}{r^2}\right]V(r) = 0 \qquad (4\text{-}26)$$

and

$$W''(\theta) + 3\cot\theta\ W'(\theta) + (\eta+2)(\eta-1)\,W(\theta) = 0 \ , \qquad (4\text{-}27)$$

where η is a separation constant and is introduced in this form for reasons which will become apparent later.

The boundary condition at a free surface now leads to the following conditions on V and W:

$$V'(a) = V'(b) = 0 \ , \qquad (4\text{-}28)$$

and

$$W'(0) = W'(\alpha) = 0 \ . \qquad (4\text{-}29)$$

(The "boundary" condition on the axis of the horn, in this case $\theta = 0$, is discussed in Chapter II.)

Case 1: Spherical torsional waves

If $\eta = 1$, then W = constant is a solution of (4-27) which satisfies boundary condition (4-29) for all α; hence, ψ is a function only of r. Equation (4-26) is another form of the Bessel equation;* ψ is given by

---

* p. 146 of Ref. 34, cited on p. 80.

$$\psi(r) = \frac{A}{(kr)^{3/2}} \left[J_{3/2}(kr) + BJ_{-3/2}(kr) \right] , \qquad (4\text{-}30)$$

where A is the amplitude of the wave and B is a constant determined by the boundary conditions.

It is well known that a Bessel function whose order is half an odd integer is expressible in terms of elementary functions.[37] It is therefore possible to rewrite (4-30) in the more useful form

$$\psi(r) = \frac{C}{(kr)^2} \left(1 + \frac{1}{jkr}\right) e^{-jkr} + \frac{D}{(kr)^2} \left(1 - \frac{1}{jkr}\right) e^{jkr} . \qquad (4\text{-}31)$$

The first term in Eq. (4-31) represents a wave of amplitude C traveling outward away from the origin $r = 0$, and the second term a wave of amplitude D traveling toward the origin. The wavefronts are concentric spherical surfaces of constant r.

Invoking boundary condition (4-28) at the small end, $r = a$, leads to the standing-wave pattern

$$\psi(r) = \frac{A}{(kr)^2} \left[\cos[kr - Q(ka)] - \frac{\sin[kr - Q(ka)]}{kr} \right] , \qquad (4\text{-}32)$$

where $r \geq a$ (the cone does not exist for $r < a$) and the function Q is defined by the equation

$$Q(x) = x - \tan^{-1} 3x/(3 - x^2) . \qquad (4\text{-}33)$$

Equation (4-32) holds even in the limiting case $a = 0$, when the cone is complete to its vertex, although the vertex is a singular point in this

---

37. Whittaker, E. T., and G. N. Watson, Modern Analysis (Cambridge University Press, Cambridge, 1927), 4th ed., p. 364.

case. At a free resonance, the wave number k must be such that ψ as given by (4-32) satisfies boundary condition (4-28) at $r = b$. To find these allowed values of k, we differentiate (4-32) with respect to r, set the derivative equal to zero at $r = b$, manipulate the resulting equation with the aid of some trigonometric identities, and obtain the frequency equation

$$Q(k_n b) - Q(k_n a) = n\pi , \quad n = 1, 2, 3, \ldots , \tag{4-34}$$

where, as usual, n is the mode number.

Before looking for solutions of (4-34), we shall prepare ourselves by examining the behavior of the function Q for various ranges of its argument.

We can evaluate the argument of the arctangent in Eq. (4-33) by long division to obtain the power series

$$\frac{3x}{3 - x^2} = x + \frac{x^3}{3} + \frac{x^5}{9} + \frac{x^7}{27} + \ldots . \tag{4-35}$$

The first two terms of (4-35) are the same as the first two terms of the power series of $\tan x$. This means that $3x/(3 - x^2)$ is a third-order Padé approximant[38] to $\tan x$ (third order because their power series agree through terms in x^3, and the sum of the degrees of numerator and denominator of the rational fraction $3x/(3 - x^2)$ is three). Such Padé approximants are unique; that is, there is no other rational fraction of first degree in the numerator and second degree in the denominator whose power series will agree with the series for $\tan x$ through the first two terms.

---

38. Storer, J. E., Passive Network Synthesis (McGraw-Hill, New York, 1957), p. 272 ff.

Thus the arctangent in (4-33) is very nearly equal to x for small x, and as a result the function Q(x) is very small for $x<1$; e.g., $Q(1) \doteq 0.017$.

In order to look more closely at the behavior of Q for small argument we can repeatedly differentiate Eq. (4-33) and obtain the Taylor series

$$Q(x) = \frac{x^5}{45} - \frac{x^7}{189} + \frac{x^{11}}{2673} - \frac{x^{13}}{9477} + \ldots = \sum_{m=1}^{\infty} \left[\frac{x^{6m-1}}{(6m-1)3^{3m-1}} - \frac{x^{6m+1}}{(6m+1)3^{3m}} \right] \tag{4-36}$$

At the other extreme, for $x \gg 1$, $3x/(3-x^2)$ is a Padé approximant to $\tan(\pi - \frac{3}{x})$, so that an asymptotic formula for large argument is

$$Q(x) = x + \frac{3}{x} - \pi \ , \quad x \gg 1 \ . \tag{4-37}$$

Now we are in a position to obtain some information from Eq. (4-34). If the cone is complete to the vertex, $Q(k_n a)$ is identically zero, and (4-34) becomes

$$Q(k_n b) = 0 \ , \quad n = 1, 2, 3, \ldots \ , \tag{4-38}$$

which has the solutions

$$k_n b = 5.763, 9.095, 12.323, 15.515, 18.689, 21.854, \ldots \quad (n+1)\pi - \frac{3}{(n+1)\pi} \ , \tag{4-39}$$

The asymptotic solution at the right-hand end of (4-39) is obtained from (4-37) and yields answers good to three or more decimal places for $n \geq 7$.

If the cone is almost complete, i.e., if $a \ll b$, then a will be less than a wavelength for the first few resonances, $k_n a$ will consequently be less than 1, and $Q(k_n a)$ will be very small. Therefore, the solutions of Eq. (4-34) will differ very little from those of (4-38). That is, the lower resonance frequencies will be very nearly the same as

those for the complete cone of the same outer dimension b. This can also be argued on physical grounds. Cutting off a piece from the tip of a complete cone will remove only a very small moment of inertia from the end (if the piece is smaller than a wavelength), a loss which can hardly cause great change in the resonance frequencies.

On the other hand, if a is large or if the frequency is very high, so that $k_n a \gg 1$, then Eq. (4-34) approaches

$$k_n(b-a) = n\pi \ , \quad n = 1, 2, 3, \ldots \ , \tag{4-40}$$

which is the same frequency equation as for the plane-wave resonances in a cylinder of length (b - a). In other words, spherical torsional waves many wavelengths from the origin behave in some ways like plane torsional waves; the relationship is similar to that between spherical and plane longitudinal (compressional) sound waves in air.

Case 2: Compound modes

For $\eta \neq 1$, neither V nor W can be constant, save for the trivial case when $k = 0$. Equation (4-26) is still a Bessel equation* and (4-27) becomes a standard form of the Legendre equation[39] with P as dependent variable upon the substitution $W(\theta) = P(\theta)/\sin\theta$. The general solution for ψ is

$$\psi(r,\theta) = \frac{A P_\eta^1(\cos\theta)}{(kr)^{3/2}\sin\theta}\left[J_{(\eta+\frac{1}{2})}(kr) + BJ_{-(\eta+\frac{1}{2})}(kr)\right] , \tag{4-41}$$

where η is determined by the boundary conditions on θ, k and B are

---

* p. 146 of Ref. 34, cited on p. 80.

39. Erdelyi, A., editor, Higher Transcendental Functions (McGraw-Hill, New York, 1953), Vol. I, p. 120.

determined by η and the boundary conditions on r, $P_\eta^1(\cos\theta)$ is an associated Legendre function of the first kind, and $J_{(\eta+\frac{1}{2})}$ and $J_{-(\eta+\frac{1}{2})}$ are Bessel functions of the first kind. A second solution of Eq. (4-24) could be obtained by substitution of the Legendre function of the second kind, $Q_\eta^1(\cos\theta)$, for $P_\eta^1(\cos\theta)$ in Eq. (4-41), but this solution would not satisfy the boundary condition at $\theta = 0$, since $Q_\eta^1(\cos\theta)$ "blows up" at that point. However, $P_\eta^1(\cos\theta)/\sin\theta$ satisfies the boundary condition at $\theta = 0$ for all values of η. We can show this from the derivative relation*

$$W(\theta) = \frac{P_\eta^1(\cos\theta)}{\sin\theta} = \frac{dP_\eta(\cos\theta)}{d(\cos\theta)} \quad , \tag{4-42}$$

which, when differentiated with respect to θ, becomes

$$W'(\theta) = -\sin\theta \frac{d^2P_\eta(\cos\theta)}{d(\cos\theta)^2} \quad . \tag{4-43}$$

Smythe** gives a series expansion for P_η which is valid for all η and which shows that the second derivative of P_η is bounded at $\theta = 0$; thus $W'(0) = 0$ due to the vanishing of $\sin\theta$.

Since $J_{-(\eta+\frac{1}{2})}$ increases without bound for vanishingly small argument, B must be zero for a cone which is complete to the vertex in order to insure that ψ is bounded everywhere. For the sake of simplicity, the following discussion will be restricted to the case of a complete cone.

Let us first find out how η depends on α, the half-angle of the cone. We shall arbitrarily define our cone to have a central angle

---

* p. 148 of Ref. 39 (Vol. I), cited on p. 92.

** p. 147 of Ref. 21, cited on p. 28.

$\alpha \leq \pi/2$. For larger α, the "horn," if such it could be called, would be a sphere with a conical hole in it.

In the limiting case for which $\alpha = \pi/2$, our "cone" becomes a hemisphere, and the allowed values of η are the odd integers, as we shall now see. Using Eq. (4-43), we see that the boundary condition at $\theta = \alpha = \pi/2$, Eq. (4-29), turns into

$$\frac{d^2P_\eta(x)}{dx^2} = 0 \ , \quad x = \cos\theta\Big|_{\theta=\alpha=\frac{\pi}{2}} = 0 \tag{4-44}$$

Assuming that η is an integer, we can make use of Rodrigues' formula* to write

$$\frac{d^2P_\eta(x)}{dx^2} = (2^\eta\,\eta!)^{-1}\,\frac{d^{\eta+2}}{dx^{\eta+2}}\,(x^2-1)^\eta \ , \quad \eta = 1,\ 2,\ 3,\ \ldots \ . \tag{4-45}$$

The quantity $(x^2 - 1)^\eta$ is a polynomial containing only even powers of x; differentiating this polynomial an even or odd number of times will yield a polynomial containing only even or odd powers, respectively. Therefore, we can see from inspection of the right-hand side of (4-45) that $\frac{d^2P_\eta(x)}{dx^2}$ is even or odd** in x according as η is even or odd. All the zeros of Legendre <u>polynomials</u> [$P_\eta(x)$ where η is an integer] are simple and lie in the range $-1 < x < +1$.* By the law of the mean we can

---

* p. 151 of Ref. 39 (Vol. I), cited on p. 92.

** Definition: F(x) is <u>even</u> or <u>symmetric</u> if F(x) = F(-x); F(x) is <u>odd</u> or <u>antisymmetric</u> if F(x) = -F(-x).

Theorem: The zeros of a function F(x) are symmetric about x = 0 if F(x) is even or odd. The proof follows immediately from the definition of even and odd functions: $F(x) = \pm F(-x)$; if F(x) = 0, then F(-x) = 0.

see that the zeros of all the derivatives of a Legendre polynomial will also be simple and lie in the range $-1 < x < +1$. Since by (4-44) $\frac{d^2 P_\eta(x)}{dx^2}$ is to vanish at $x = 0$, and since it has only simple zeros, we can see that it must be an odd function; consequently η must be an odd integer. Thus we have now shown that for $\alpha = \pi/2$, the odd integers are proper values for η. We must now rule out the possibility of non-integral allowed values of η (for $\alpha = \pi/2$) since at the outset we restricted ourselves to integer η. We can see from (4-42) and (4-45) that if η is an odd integer, $W(\theta)$ is an even polynomial in $\cos\theta$ of degree $\eta - 1$. We saw above that all the zeros of any derivative not identically zero of a Legendre polynomial $P_\eta(x)$ are simple and lie in $-1 < x < +1$. By the symmetry properties of $W(\theta)$, then, half its zeros must lie in $0 < \cos\theta < +1$, or $0 < \theta < \pi/2$. That is, $W(\theta)$ has $(\eta - 1)/2$ zeros or nodes in the fundamental domain of the problem, $0 < \theta < \pi/2$. But for $\eta = 1, 3, 5, 7, 9, \ldots$, we have $m = (\eta - 1)/2 = 0, 1, 2, 3, 4, \ldots$, and it follows from the unique relation* bwtween the eigenfunctions and the number of nodes for a Sturm-Liouville system such as this [Eq. (4-27)] and its boundary conditions [(4-29)] that we have found <u>all</u> the eigenvalues and eigenfunctions for the case $\alpha = \pi/2$. We shall henceforth denote by $W_m(\theta)$ the particular eigenfunction associated with η_m, the mth allowed value of η.

We have just seen that for $\alpha = \pi/2$,

$$\eta_m = 2m + 1 , \quad m = 0, 1, 2, 3, \ldots , \tag{4-46}$$

and

$$W_m(\theta) = \frac{P^1_{2m+1}(\cos\theta)}{\sin\theta} = \left.\frac{dP_{2m+1}(x)}{dx}\right|_{x=\cos\theta} . \tag{4-47}$$

---

* p. 454 of Ref. 14 (Vol. I), cited on p. 12.

For $\alpha < \pi/2$, the allowed values of η must change so that the boundary condition at $\theta = \alpha$ is still satisfied, and so that $W_m(\theta)$ has m zeros in $0 < \theta < \alpha$. The lowest eigenfunction, $W_0(\theta) = 1$, does not depend on η, and hence is the same for all α; it is, in fact, the case which gave rise to the spherical torsional waves treated earlier in this section. For the higher values of m with which we are concerned here, we can see that as α decreases from $\pi/2$, the zeros of $W_m(\theta)$ must also decrease in order to remain in $0 < \theta < \alpha$. We can invoke another theorem* of Sturm-Liouville theory which states that the eigenvalues must increase for the zeros to decrease. Thus, $\eta_m > 2m+1$ for $\alpha < \pi/2$.

Values of η_m as a function of α and m were calculated (partly on a Univac I and partly on an IBM 7090) for m = 1, 2, and 3, and for α varying from 10 to 90 degrees in steps of 10 degrees. The numerical method used is outlined in Appendix B. The results are judged accurate to within 1 or 2 in the fourth significant figure for m = 2 and 3, and accurate to four decimal places (five or six significant figures) for m = 1.

We now derive an asymptotic formula for η, valid for small α, whose results we can compare with the results of the machine computations. First we define a new variable $s = \theta/\alpha$. Next we rewrite (4-27) with s as the independent variable and note that because θ is small, $1/\theta$ may be substituted for cot θ. This yields the equation

$$W''(s) + \frac{3}{s} W'(s) + \alpha^2(\eta+2)(\eta-1)W(s) = 0 , \qquad (4\text{-}48)$$

where the primes now denote differentiation with respect to s. The boundary condition (4-29) becomes

---

* p. 454 of Ref. 14, cited on p. 12.

$$W'(0) = W'(1) = 0 \ . \tag{4-49}$$

Equation (4-48) is of the same form as Eq. (4-5), and boundary condition (4-49) is of the same form as (4-8). Equations (4-5) and (4-8) led to cylindrical waves. We should not find this surprising; far from the vertex, a cone of small included angle is hard to distinguish from a cylinder. We can adapt the results of the treatment of Eq. (4-5) and (4-8) in section 4.1.1 and apply them to the present case, obtaining thus

$$\alpha\sqrt{(\eta_m+2)(\eta_m-1)} = 5.136,\ 8.417,\ \ldots,(m+\tfrac{3}{4})\pi,\quad m = 1,\ 2,\ 3,\ \ldots\ . \tag{4-50}$$

Solving by completing the square, we have

$$\eta_m = \sqrt{(\frac{5.136}{\alpha})^2 + \frac{9}{4}} - \frac{1}{2}\ ,\ \sqrt{(\frac{8.417}{\alpha})^2 + \frac{9}{4}} - \frac{1}{2}\ ,\ \ldots\ . \tag{4-51}$$

The angle α is in radians in Eqs. (4-50) and (4-51).

Although Eq. (4-51) was derived using the assumption that α is small, a comparison with the values of η obtained numerically shows that for α as great as $\pi/2$ Eq. (4-51) yields answers in error by not more than 4 percent in the worst case. This suggests the possibility of adding a small correction term to the right-hand side of (4-51) to improve its accuracy. For the case $m = 1$, examination of the discrepancies between the values η_m given by (4-51) and the more precise values given by the IBM 7090 showed that this was indeed possible. The improved formula is

$$\eta_1 = \sqrt{(\frac{5.1356}{\alpha})^2 + \frac{9}{4}} - (\frac{1}{2} + 0.0984 \sin\alpha)\ , \tag{4-52}$$

where α is in radians. Equation (4-52) is more accurate for small α than large. The error in η_1 is never more than 0.0015. This represents

a fractional error of 0.05 percent for $\alpha = \pi/2$ and the error would be even smaller for smaller α. Presumably similar correction terms could be found for higher values of m.

Having now a means for finding appropriate values for η in terms of α, we need to find the values of k for which the r-dependent part of ψ [as given by Eq. (5-41)] satisfies boundary condition (4-28). It is possible to show that for the complete cone, the allowed values of k are always greater than η/b.[40] The only way to get actual values for k seems to be by a direct numerical attack.

The IBM 7090 of the Harvard Computing Center was programmed to calculate kb as a function of α for the lowest compound mode of the complete cone, using the numerical method described in Appendix B to extract the eigenvalues directly from Eqs. (4-26) and (4-27) with their respective boundary conditions (4-28) and (4-29). The computations were performed for α ranging from 5 to 90 degrees in steps of 5 degrees. The results are shown in Fig. 4-2. The lower spherical-wave modes (case 1 for spherical coordinates), which are of course independent of α, are indicated for comparison.

An interesting feature of the compound modes for the complete cone is that the vertex is a node of ψ. [This can be easily seen upon examination of the series expansion* of $J_{(\eta+\frac{1}{2})}(kr)/(kr)^{3/2}$, whose leading term is $(kr)^{\eta-1}$.] One normally expects an increase in the amplitude of vibration toward the small end of a horn, and for the radial modes this does occur. The compound modes, however, all have some wave motion in

---

40. Watson, G. N., Bessel Functions (Cambridge, 1944), p. 468.

* See, for example, p. 4 of ref 39 (Vol. II), cited on p. 92.

the transverse direction, across the axis of the horn, and when the transverse dimensions of the horn become comparable with or less than a wavelength, such wave motion cannot be sustained.

4.2.2 Experimental verification

A cone, designated no. 15, was turned from mild (hot-rolled) steel; its dimensions are a = 0.540 inch, b = 8.114 inches, α = 13.00 degrees. The resonance frequencies of the first five spherical-wave modes lie below 50 kc/s. These were measured and are compared in Table 4-3 with predicted values based on Eq. (4-34). The value of c used in finding the resonance frequencies from the roots of (4-34) was the average of the five values calculated from the observed resonance frequencies for these five modes.

Table 4-3

Comparison of the measured and predicted resonance frequencies for radial modes of cone 15

Mode number n	Theoretical f_n kc/s	Experimental f_n kc/s	$\frac{\text{Exp } f_n}{\text{Theor } f_n}$
1	14.425	14.417	0.99944
2	22.751	22.746	0.99978
3	30.828	30.826	0.99993
4	38.804	38.820	1.00041
5	46.793	46.814	1.00044

Although there is excellent agreement between the calculated and measured frequencies, it is not an impressive as in the case of plane torsional waves in a cylinder. The errors are probably due to inaccuracies in the machining of the cone and in the measurement of its

dimensions. It is more difficult to determine accurately the dimensions of a cone than the length of a cylinder whose ends are plane and parallel.

The standing-wave patterns as functions of r were measured for the first two radial modes. The measured distributions are compared with the predictions of Eq. (4-32) in Fig. 4-3. The agreement here is also very good.

The ratio b/a for cone 15 is approximately 15; thus the cone is close enough to complete so that we can estimate the frequency of the lowest compound mode from Fig. 4-2 and Table 4-3. It is near 60 kc/s and is therefore out of range of the experimental apparatus.

4.3 Conclusions

This chapter has served two purposes. First, we have found all the interesting solutions to the exact torsional wave equation. These solutions reveal that torsional waves in a horn of some particular geometry behave very much like sound waves in air confined by boundaries of the same geometry, except that the order of the characteristic functions is typically one degree higher for the torsional waves. That is, where sound waves in air would be described by a $J_0(kr)$ or $J_{1/2}(kr)$, torsional waves are described by $J_1(kr)$ and $J_{3/2}(kr)$, respectively.

Second, and probably more important, we have seen that the results of experiments upon cylinders and cones agree very well with the predictions of the mathematical analysis. We have then verified that the type of motion predicted by small-signal elastic theory does exist.

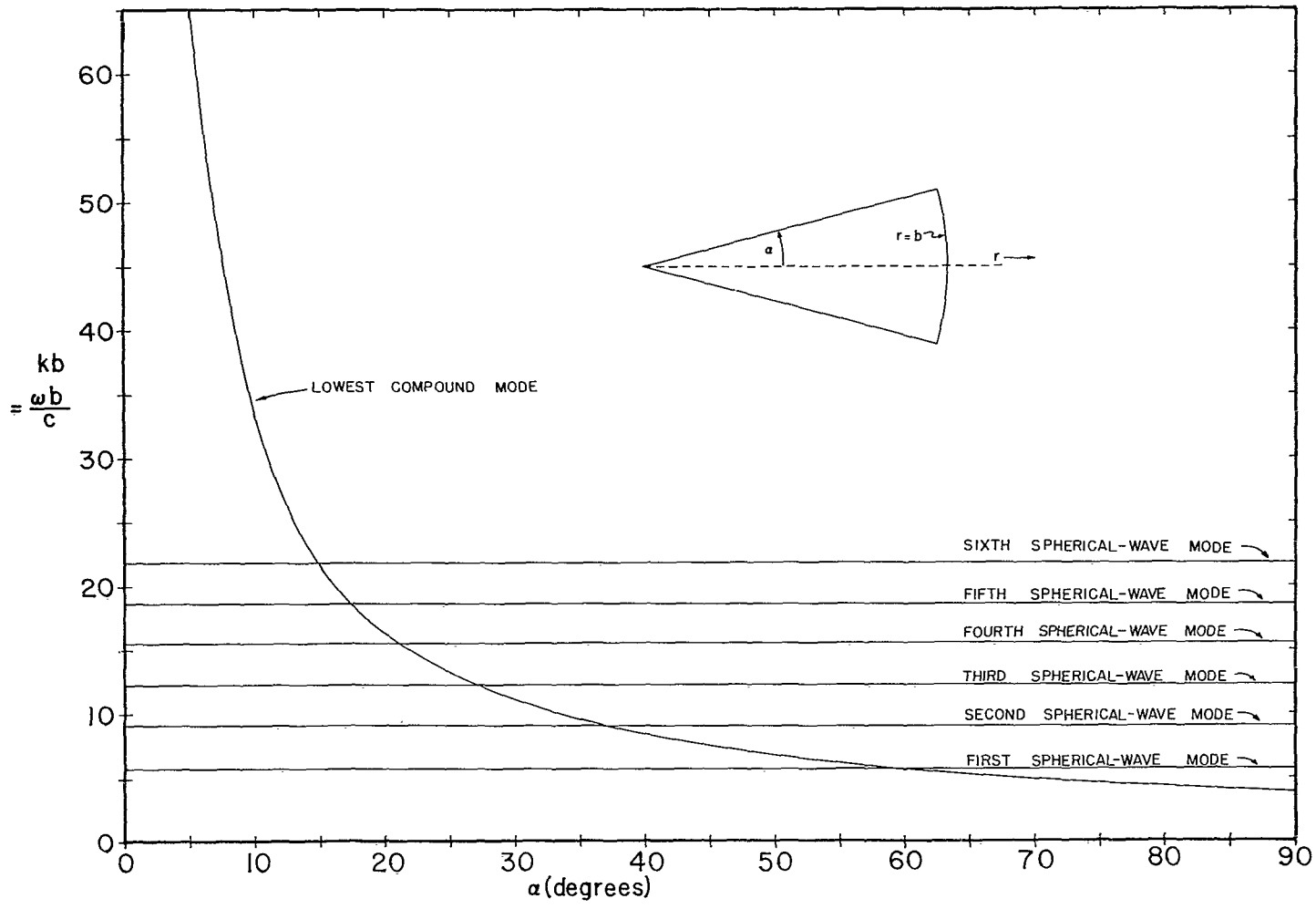

FIG. 4-2 CALCULATED TORSIONAL RESONANCE FREQUENCIES FOR A SOLID CONE.

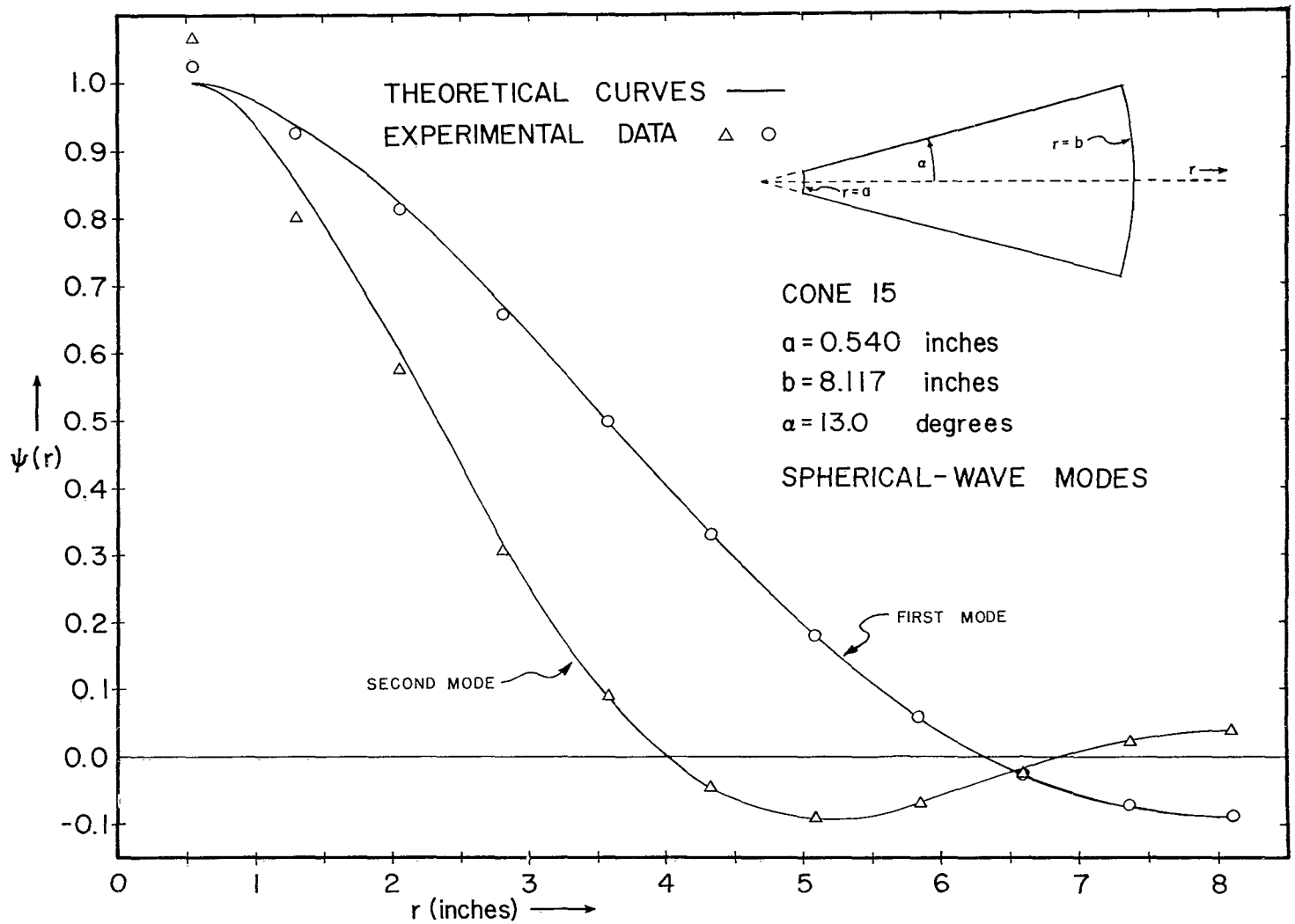

FIG. 4-3 TORSIONAL STANDING-WAVE PATTERNS ON A MILD STEEL CONE.

Chapter V

HORNS OF SMOOTH CONTOUR NOT FITTING SEPARABLE COORDINATES

5.1 Review of plane-wave horn theory

In Chapter II we derived an approximate wave equation based upon the assumption that the wavefronts were plane and normal to the axis of the horn (the z-axis of cylindrical coordinates). The Helmholtz form of this plane-wave equation is

$$\psi''(z) + \frac{I_s'(z)}{I_s(z)} \psi'(z) + k^2 \psi(z) = 0 \ , \qquad (5\text{-}1)$$

where $I_s(z)$ is the polar moment of inertia of the cross section of the horn and primes denote differentiation with respect to z, the argument of ψ and I_s. Solutions of (5-1) should be good approximations to the true wave motion where the slope of the horn contour is small and where the diameter is small compared with a wavelength.

As we noted in Chapter II, this equation is of exactly the same form as the plane-wave horn equation for compressional waves in a fluid or solid, except that the moment of the cross section appears in the torsional-wave equation where the area appears in the compressional-wave equation. Thus we could easily adapt the results obtained for compressional horns by Webster,* Morse,** Mawardi,[41] Beranek,[42] Olson,***

---

* Ref. 3, cited on p. 1.

** pp. 265-88 of Ref. 17, cited on p. 17.

41. O. K. Mawardi, Tech. Memo. No. 4, Acoustics Research Lab., Harvard Univ., 1949; see also O. K. Mawardi, J. Acoust. Soc. Am. 21 (1949), p. 323.

42. Beranek, L. L., Acoustics (McGraw-Hill, New York, 1954), pp. 268-78.

*** pp. 100-15 of Ref. 19, cited on p. 23.

Mason,* and others to the torsional-wave case. The Webster (compressional-wave) horn equation has been solved for a wide variety of horn shapes: cylindrical and conical horns, exponential and catenoidal horns, the so-called Bessel horns (whose contours are powers of z), and others. In this chapter we shall examine in detail only one type of horn contour, the exponential, in an attempt to obtain a quantitative estimate of the degree of approximation afforded by the solutions of the plane-wave equation (5-1). Before moving on to the exponential horn, however, we shall discuss the concept of torsional-wave impedance.

5.2 Torsional-wave impedance

In Chapter III an analogy was drawn between voltage and torque and between current and angular velocity. A logical extension is the definition of impedance for torsional waves as the ratio of torque to angular velocity. Assuming plane wavefronts, so that ψ is a function only of z, we can write the torque[43] transmitted through the plane $z = z_o$ in the direction of increasing z as

$$T = -\mu\, I_s(z_o)\, \psi'(z_o) \quad . \tag{5-2}$$

The angular velocity at the same point is $j\omega\psi(z_o)$, so that we have for the torsional-wave impedance

$$Z = -\frac{\mu\, I_s(z_o)\, \psi'(z_o)}{j\omega\psi(z_o)} = \frac{j\rho c\, I_s(z_o)\, \psi'(z_o)}{k\psi(z_o)} \quad , \tag{5-3}$$

where $k = \omega/c$ and $c^2 = \mu/\rho$, as before. From Eq. (2-31) we can write $I_s(z)$

---

* pp. 156-61 of Ref. 4, cited on p. 2.

43. McLachlan, N. W., Theory of Vibrations (Dover, New York, 1951), p. 106.

for solid, i.e., not hollow, horns in terms of the horn contour, R(z), and obtain thus

$$Z = \frac{j\pi\rho c R^4(z_o)}{2k} \frac{\psi'(z_o)}{\psi(z_o)} \quad . \tag{5-4}$$

It will be instructive to find the driving-point impedance at the end of a cylinder in the two cases where the cylinder is either semi-infinite in extent or of length ℓ.

As we saw in Chapter IV, section 4.1, true plane waves can propagate in a cylinder. Since the cross section is constant, the plane-wave horn equation reduces to

$$\psi'' + k^2 \psi = 0 \ , \tag{5-5}$$

which is just the same as the exact wave equation reduced to the special case of plane waves, Eq. (4-6a). Suppose the cylinder is of radius a and extends along the positive z-axis from $z = 0$ to infinity. If we drive at the end $z = 0$, the wave motion will be a single progressive wave propagating in the direction of increasing z; that is, from Eq. (4-10),

$$\psi = A\, e^{-jkz} \ . \tag{5-6}$$

Using this equation for ψ and performing the necessary differentiation, we obtain for the driving-point impedance

$$Z_{in} = \frac{\pi}{2} a^4 \rho c \ , \tag{5-7}$$

Thus the input impedance of the semi-infinite cylinder is resistive and constant at all frequencies.

If the cylinder extends only from $z = 0$ to $z = \ell$, and the end at $z = \ell$ is free, then the angular displacement is

$$\psi = A \cos k(\ell - z) \ , \tag{5-8}$$

and the input impedance at the end of the finite cylinder is

$$Z_{in} = j \frac{\pi}{2} a^4 \rho c \tan k\ell \ . \tag{5-9}$$

This is purely reactive, as we should expect since we have made no provisions for loss. We note that the input impedance is zero at the natural resonance frequencies of the cylinder [see Eq. (4-12)].

We can also find the input impedance of a conical horn of small included angle using the results obtained in Chapter IV for spherical torsional waves. Let the horn contour be $R(z) = mz$. The plane-wave equation then becomes

$$\psi'' + \frac{4}{z} \psi' + k^2 \psi = 0 \ . \tag{5-10}$$

Here we have the same equation as the exact wave equation reduced for the case of spherical waves, except that the independent variable is now z, (in cylindrical coordinates) instead of r (in spherical coordinates). If the horn extends from $z = a/m$ (so that the radius at the small end is a) to infinity in the direction of increasing z, we know that if the horn is driven at the end, the wave motion will be a progressive wave traveling in the positive z-direction, just as was the case for the semi-infinite cylinder. From (4-31) we have the angular displacement

$$\psi = \frac{A}{(kz)^2} \left(1 + \frac{1}{jkz}\right) e^{-jkz} \ . \tag{5-11}$$

From (5-4) and (5-11), we obtain the input impedance

$$Z_{in} = \frac{\pi}{2} a^4 \rho c \left[\frac{3m}{jka} + \frac{jka}{m + jka} \right] \qquad (5\text{-}12)$$

At high frequencies (large k), the input impedance approaches a pure resistance $\frac{\pi}{2} a^4 \rho c$, which is just the input impedance of the semi-infinite cylinder of the same diameter as the small end of the cone.

These results for cylinder and cone are qualitatively very much the same as those for compressional waves of the same geometry,* except that the resistive component of the input impedance of the conical horn decreases more rapidly with decreasing frequency for torsional than for compressional waves.

The torsional-wave impedance defined here is akin to the mechanical impedance (defined as the ratio of force to particle velocity) often used in the analysis of compressional-wave horns. The specific acoustic impedance (defined as the ratio of pressure to particle velocity), which in a compressional-wave horn is the mechanical impedance divided by the area of the cross section of the horn, is also frequently encountered. We can define an analogous specific torsional impedance as the ratio of stress to particle velocity in a torsional wave. A derivation similar to that shown above [Eqs. (5-2) to (5-4)] yields the result that the specific torsional impedance is just the torsional-wave impedance divided by the moment of the cross section. Thus once again the moment of the cross section plays the same role for torsional horns as the area does for compressional-wave horns.

---

* p. 238 of Ref. 17, cited on p. 17.

Elsewhere in this report, the term impedance applied to torsional waves always means the ratio of torque to angular velocity.

5.3 The exponential horn

5.3.1 The plane-wave equation and its solutions

Let the driven end of our exponential horn be at $z = 0$ and let its radius be a. The horn contour is

$$R(z) = a\, e^{z/2h} , \tag{5-13}$$

where h, the flare constant, is the increase in z in which the cross-sectional area of the horn increases by a factor of e. Using Eq. (2-31) again to find I_s in terms of R, we can readily obtain the plane-wave equation for an exponential solid torsional horn:

$$\psi'' + \frac{2}{h}\psi' + k^2\psi = 0 . \tag{5-14}$$

By assuming a solution of the form $\psi = e^{bz}$, we can verify that the general solution to (5-14) is

$$\psi = e^{-z/h}(A\, e^{-j\beta z} + B\, e^{j\beta z}) , \tag{5-15}$$

where

$$\beta^2 = k^2 - (1/h)^2 . \tag{5-16}$$

For $k^2 > (1/h)^2$, β is real and there is true wave propagation; A and B represent the amplitude of waves propagating in the positive and negative z-directions, respectively. For $k^2 < (1/h)^2$, β is imaginary, and the angular displacement is in phase everywhere. (Note the mathematical similarity to the propagation of compound modes in a cylinder, pp. 81-2.)

There is, therefore, a cutoff frequency at which $\beta = 0$, namely,

$$\omega_c = |c/h| \ , \tag{5-17}$$

below which there is no wave propagation.

If we take the horn to extend from $z = 0$ to infinity in the positive z-direction, the wave motion above the cutoff frequency will consist of a single progressive wave traveling in the positive z-direction, so that $B = 0$ in (5-15). We can then find from (5-4) that the input impedance for $h > 0$ (diameter increases with z) is

$$Z_{in} = \frac{\pi}{2} a^4 \rho c \left[\sqrt{1 - (\omega_c/\omega)^2} - j(\omega_c/\omega) \right], \quad \omega > \omega_c \ . \tag{5-18}$$

At high frequencies, this impedance, like the input impedance of an infinite conical horn, approaches the purely resistive input impedance of a cylinder of the same end diameter. At zero frequency, the input impedance must be zero (since no torque is required to maintain even an infinite horn in uniform rotation). We therefore choose the appropriate sign on the square root in (5-18) to fulfill this condition and obtain the input impedance for frequencies far below the cutoff frequency:

$$Z_{in} = -j \frac{\pi}{2} a^4 \rho c \left(\frac{\omega}{2\omega c}\right) , \quad \omega \ll \omega_c \tag{5-19}$$

If the horn diameter diminishes with z, $h < 0$, the input impedance turns out to be just the complex conjugate of the impedance for $h > 0$.

Let us now consider the problem of reflections from a free end of an exponential horn. Suppose the end at $z = 0$ is free; then the incident and reflected waves will have the same amplitude at the end (due to the total reflection), which means $A = B$ in (5-15). Thus we can write the

angular displacement in the form

$$\psi = A\, e^{-z/h} \cos(\beta z - \gamma) \ , \tag{5-20}$$

where we must now choose γ so that $\psi'(0) = 0$ (boundary condition at a free end: normal derivative of ψ vanishes). Taking the derivative and equating it to zero, we obtain

$$\cot \gamma = h\beta = \pm \sqrt{(\omega/\omega_c)^2 - 1} \quad , \quad (\omega > \omega_c) \ . \tag{5-21}$$

The magnitude of the phase shift on reflection depends only on the ratio ω/ω_c, but the sign depends on the sign of h, i.e., on whether the end is larger or smaller in diameter than the rest of the horn.

We see that the phase shifts due to reflections at the two ends of a freely vibrating finite exponential horn just cancel, so that the natural frequencies must be those for which the length of the horn is an integral number of half wavelengths at the phase velocity. That is,

$$\beta_n \ell = n\pi \ , \quad n = 1, 2, 3, \ldots \ , \tag{5-22}$$

which can easily be solved for the natural frequencies with the aid of (5-16):

$$\omega_n = c\left[(n\pi/\ell)^2 + (1/h)^2\right]^{1/2} \ , \quad n = 1, 2, 3, \ldots \ , \tag{5-23}$$

where ℓ is the length of the horn.

The corresponding standing-wave patterns are of the form of (5-20), where β and γ are restricted to the values allowed by (5-21) and (5-22). Since for the normal modes $\beta\ell$ is an integral multiple of π, then

$$\left|\cos(-\gamma)\right| = \left|\cos(\beta\ell - \gamma)\right| \ , \tag{5-24}$$

and we can see from (5-13) and (5-20) that the "gain" of the horn, the ratio of the magnitudes of the angular displacement at the two ends, is the same for all modes, namely,

$$G = e^{|\ell/h|} = (b/a)^2 , \qquad (5\text{-}25)$$

where b and a are the radii of the large and the small ends of the horn, respectively.

Standing-wave patterns were measured for several exponential horns. Some typical results are presented in Fig. 5-1. The specimen horn in this case was 18 inches in length and its end diameters were 1 and 4 inches. The agreement between theory and experiment is very good. It thus appears that, within the limits of experimental error, the plane-wave approximation is a valid means of predicting the standing-wave patterns for an exponential horn of moderate flare and diameter.

5.3.2 Validity of the plane-wave approximation

Due to the limited accuracy with which standing-wave patterns can be measured, their measurement is of little use in investigating the accuracy of analytical results based on the plane-wave assumption. Fig. 5-1 demonstrates this very well. Resonance frequencies, however, can be very accurately measured. It was stated in Chapter II that the resonance frequencies predicted by using the plane-wave assumption cannot be lower than the actual resonance frequencies. This fact provides a means by which we can quantitatively estimate the error incurred by assuming plane wavefronts.

We shall first define wavefronts a little more carefully than heretofore, and then attempt to deduce the qualitative behavior of waves

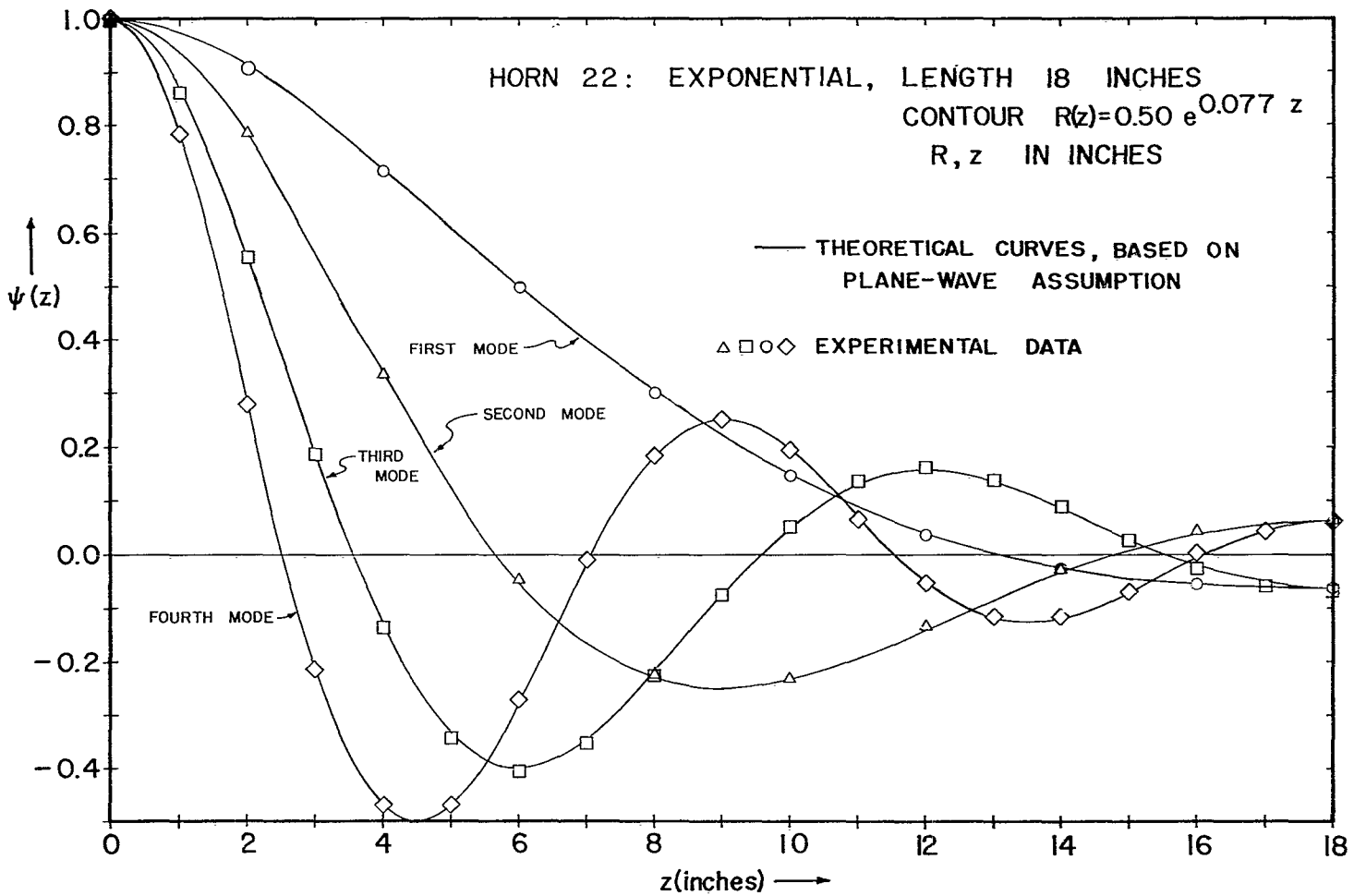

FIG. 5-1 TORSIONAL STANDING-WAVE PATTERNS ON A MILD STEEL SOLID EXPONENTIAL HORN.

propagating along a horn with progressively increasing flare such as an exponential horn. Wavefronts can be taken to mean surfaces on which the properties of the wave are constant, that is, surfaces where amplitude and phase are the same everywhere. This is a very restrictive definition. If such surfaces exist in a given horn, then a coordinate system could be constructed in which these wavefront surfaces are coordinate surfaces. The wave motion could then be exactly described as a function of only one space coordinate. But in Chapter IV we saw that the only such one-parameter waves are plane, cylindrical, and spherical waves. Thus in the general case of a horn of arbitrary contour, there are no surfaces on which the amplitude and phase of a progressive wave are both constant.

Suppose, however, that the slope of the contour does not change much in a wavelength [$R''(z)$ is small]. Then any piece of the horn shorter than a wavelength will not look too different from a truncated cone. We know that true one-parameter waves (spherical waves) can propagate in a cone, and we therefore suspect that if the diameter is not much greater than a wavelength, the wave motion in any small section of the horn will not differ too much from the spherical waves which would propagate in a cone of the same angle of flare. Thus it seems reasonable to suppose that in horns meeting the geometrical conditions outlined above, there exist "wavefront" surfaces on which the amplitude and the phase are reasonably constant, and that such surfaces are more or less spherical so as to be normal to the surface of the horn (see Chapter II for the boundary condition at a free surface).

Let us now consider reflections from the large end (assumed free) of a typical horn (exponential, say); the horn is terminated in a plane normal to the axis. This situation is depicted in Fig. 5-2.

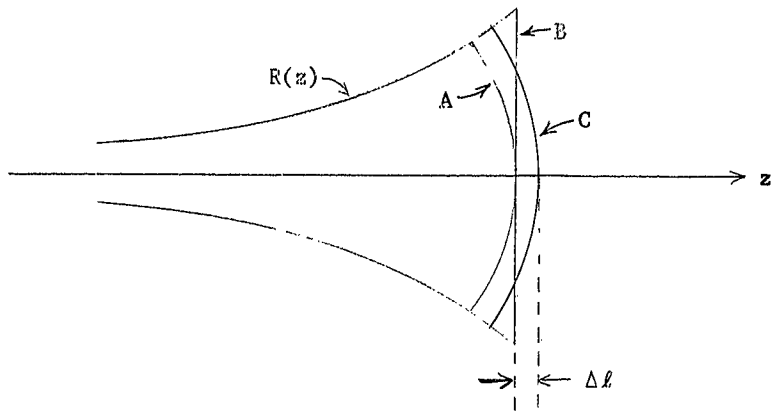

Fig. 5-2. Reflection from the large end of a horn. The end correction.

Surface A is the last "wavefront" contained within the horn; surface B is the plane end of the horn. Since this discussion is restricted to frequencies low enough so that the diameter is never large compared with a wavelength, the "left-over" region bounded by surfaces A, B, and R(z) will be much thinner than a wavelength. Being at the end of the horn, it will vibrate essentially as a rigid body and could be replaced by any other piece with the same moment of inertia, at least as far as the rest of the horn is concerned. In particular, we could construct a "wavefront-shaped" piece, terminating the horn in surface C. This "fits" the assumed shape of the incident wave and, as can be seen from Fig. 5-2, effectively lengthens the horn by an amount $\Delta\ell$.

The same sort of argument can be employed at the small end of the horn, resulting in a negative "end correction" (since the small end should be slightly concave to fit the wavefront). The end correction at the small end will of course be much smaller than that at the large end, since the wavefronts are so much more nearly plane at the small end.

If we could derive an approximate wave equation based on the assumption that the amplitude and phase are constant on each of some set of suitable curved surfaces (for an exponential horn they are parabolic[44]), we would expect that the resonance frequencies of a horn whose end faces are plane would be very close to the frequencies predicted by the approximate wave equation for a horn which is longer than the actual horn by the end corrections.

In the case of the cone, we do not need an approximate wave equation since spherical waves are an exact solution. A cone was fabricated with plane end faces and its resonance frequencies measured for the lowest five modes. Except for the shape of the end faces, this cone, designated as no. 14, was essentially identical with cone 15, described in Chapter IV. An "effective length" for this cone was defined as the length of the cone (of the same included angle but terminated in spherical caps) which would have had the same resonance frequency. The effective length was calculated for each of the five modes and then the end correction found by subtracting the physical length. These values are compared in Table 5-1 with the end correction calculated from the geometrical considerations of Fig. 5-2. The end correction calculated from the resonance frequencies is reasonably constant for the different modes and is in fairly good agreement with the end correction calculated from the moment of inertia of the end slice bounded by A, B, and R(z) in Fig. 5-2. The physical length of cone 14 was 7.590 inches; thus, the discrepancy in the corrections calculated in these two ways represents some 0.1 percent of the length. An error of only .002 inches in the measurement

---

44. J. Holtsmark, J. Lothe, S. Tjøtta, and W. Romberg, Archiv for Mathematik og Naturvidenskab 53, no. 8 (1955).

Table 5-1

End correction for a cone

Mode no.	$\Delta\ell$, inches	
1	0.140	Calculated from the geometry, $\Delta\ell = 0.135$ inches
2	0.142	
3	0.143	
4	0.146	
5	0.148	
average	0.144	

of the diameter at the large end of the cone would ~~would~~ cause this discrepancy.

However, in general we do not have even an approximate wave equation based on curved wavefronts. Such an equation could presumably be constructed for an arbitrary horn contour, though it would be tedious and it would have to be done separately for each type of contour. We do have Eq. (5-1), an approximate wave equation based on plane wavefronts, and, as we have seen, it can be solved for a wide variety of contours. We now hypothesize that the resonance frequencies of a freely vibrating horn can be described by a frequency equation derived using the plane-wave assumption if instead of the physical length of the horn we use an effective length in this frequency equation. Because the resonance frequencies predicted from the plane-wave assumption are upper bounds on the actual resonance frequencies, we can see that the effective length cannot be shorter than the physical length of the horn. In other words, we assume that by modifying the input data of an admittedly approximate equation, we can make the equation yield the correct answers.

An experimental program was undertaken to verify this hypothesis. Five exponential horns were made of mild (hot-rolled) steel. Their lower resonance frequencies were carefully measured using the techniques described in Chapter III. For each mode, an effective length was calculated by using the measured resonance frequency, shear-wave speed, and the mode number with a frequency equation based on the plane-wave assumption. Data are presented showing the constancy of the effective length with frequency. Table 5-2 gives the identification numbers and nominal dimensions of the experimental horns. (Note that the four physical dimensions given are not independent. Any three would suffice to describe an exponential horn completely.)

Table 5-2

Nominal dimensions in inches of experimental exponential horns

Horn no.	Length ℓ	Small-End Radius a	Large-End Radius b	Flare Constant h
16	18.000	0.125	2.000	3.246
17	9.000	0.125	0.500	3.246
18	9.000	0.500	2.000	3.246
19	9.000	0.125	2.000	1.623
22	18.000	0.500	2.000	6.492

The first seven resonance frequencies of the 9-inch horns and the first fourteen resonance frequencies of the 18-inch horns fell within the range of measurement (≤ 50 kc/s). A calibration cylinder for determining the shear-wave speed was turned from each piece of stock used for the exponential horns. After the resonance frequencies of the exponential horns and calibration cylinders were measured, the shear-wave speed

was calculated and used with (5-23) and the nominal value of h to calculate the effective length for each mode from its measured resonance frequency. The results were far from encouraging. The effective lengths as calculated showed a wide variation with frequency; worse yet, some were shorter than the physical lengths of the horns, in one case by nearly 1.5 inches. However, it was noted that the worst offenders were horns 16, 17, and 19, which were more subject to large percentage errors in their dimensions since they were of smaller diameter at their small ends. Careful measurement of the end diameters and the actual lengths of the five horns revealed departure from the nominal dimensions in the right directions to account for the observed discrepancies. A means of correcting the frequency equation to allow for machining error was then sought.

The following sequence of operations takes place in the fabrication of a specimen horn. A table of radius versus length at 0.2-inch intervals along the horn is made up. Using this table, a step-wise approximation to the horn contour is milled into the edge of a $\frac{1}{8}$-inch sheet of brass or aluminum. The steps are then filed down by hand until they just disappear. The edge of this sheet or template is thus supposed to be the horn contour. The template is then clamped in a tracing attachment on a large lathe and a piece of stock, already roughed out to approximate shape, is mounted between centers in the lathe. The feeler arm of the tracing attachment moves along the edge of the template and guides the cutting tool along a path parallel to it. On successive cuts the cutting tool is moved toward the axis until the diameter at one end of the horn is measured to be its designated value. The ends of the horn are then faced off.

The contour of the resulting horn can be in error even if the contour of the template is perfect (an unlikely possibility). The cutting tool might be set at the wrong distance from the axis, giving a constant error in the horn radius, and the "axis" of the template (the line from which the contoured edge of the template is measured) might not be parallel to the axis of the lathe, giving a "conical error" in the finished horn. Assuming no errors in the template, we can then write the actual contour of the horn in the form

$$\begin{aligned} R(z) &= a(e^{z/2h} + mz + \epsilon) \\ &\doteq a[e^{(m+1/2h)z} + \epsilon] \end{aligned} , \tag{5-26}$$

where m and ϵ are the error terms. We can write the second form where m is essentially incorporated into a modified flare constant because m is small. If we assume that the value of h has been adjusted to include the effect of m, we have

$$R(z) = a(e^{z/2h} + \epsilon) \quad . \tag{5-27}$$

We shall use (5-27) to obtain a correction term to the frequency equation (5-23).

For a horn of contour (5-27), the plane-wave equation is

$$\psi'' + \frac{2}{h(1+\epsilon e^{-z/2h})}\psi' + k^2\psi = 0 \ , \tag{5-28}$$

where the small end of the horn (radius a) is at $z = 0$ and the horn extends to $z = \ell$ in the positive z-direction. This is very much like (5-14), the plane-wave equation for a true exponential, except that the flare "constant" is now a slowly varying function of z. To the degree

of accuracy contemplated here, we can assume that the solution of (5-28) is of the form (5-15), where the propagation constant β is now a function of z found from (5-16) by using $h(1+\epsilon e^{-z/2h})$ instead of h. The phase shifts due to reflections at the two ends $z = 0$ and $z = \ell$ as given by (5-21) will no longer cancel since β is not constant.

We can find the resonance frequencies of our modified exponential horn by noting that β is the rate of change of phase with distance. If we integrate β over the length of the horn twice and include the phase shift due to reflection at the ends, we will have "followed" a wave through a complete circuit of the horn. Those frequencies for which the total phase shift is an integral multiple of 2π will be the resonance frequencies. We obtain thus

$$\omega_n = c\left[\left(\frac{n\pi}{\ell}\right)^2 + \left(\frac{1}{h}\right)^2 - \frac{6\epsilon(b-a)}{b\,h\,\ell}\right]^{1/2}, \quad n = 1, 2, 3, \ldots, \qquad (5\text{-}29)$$

where a and b are the radii of the small and large ends of the horn, respectively. The first two terms within the brackets are the same as those in Eq. (5-23); the third term incorporates the correction for the constant error in the radius, ϵa. By measuring a, b, and ℓ, we can calculate ϵ and h for use in (5-29).

Fig. 5-3 shows the effective length, ℓ_e, versus frequency for the five experimental horns. The effective length was calculated using (5-29) with the measured resonance frequencies and physical dimensions. The actual length of each horn is indicated for comparison. Also shown is the mean of the effective lengths weighted by mode number. This weighted mean was deemed a more reliable estimate of length than the average. Equation (5-29) shows that the effect of any error in the contour is

less for the higher modes than for the lower. For large n, the first term within the brackets dominates, and this term depends only on the length of the horn and the mode number. The variation of ℓ_e shown in Fig. 5-3 also shows that the higher modes give a more consistent estimate of effective length.

Fig. 5-3 also indicates that there probably are errors in the dimensions of the horns beyond those corrected in Eq. (5-29). The effective lengths for the first mode of horn 16 and for the second mode of horn 17 are less than the physical lengths of these horns. Nevertheless, it is clear from Fig. 5-3 that the concept of effective length is a useful one for the investigation of the accuracy of the plane-wave assumption. The horns with smaller flare angles (nos. 17 and 22) have effective lengths closer to their physical lengths than horns of more pronounced flare (nos. 16, 18, and 19), thus indicating a closer agreement with plane-wave theory, as expected.

Having demonstrated the existence of an "end correction" for torsional horns, we would now like to know in what way it depends on the parameters of the horn. We expect (from Fig. 5-2) that the end correction is a larger percentage of the radius of the end for horns of large flare angle than for horns of small flare angle. The simplest assumption we can make is that the end correction is directly proportional to the radius of the end and to the slope of the contour at the end. Let us now see how well the experimental data on exponential horns can be described under this assumption.

Differentiating (5-13) to find the slope of the contour of an exponential horn, we have

$$R'(z) = \frac{a}{2h} e^{z/2h} = \frac{1}{2h} R(z) \quad . \tag{5-30}$$

If the radius of the large end is b, then we have hypothesized that the end correction there is proportional to $b^2/2h$. The end correction at the small end (where the radius is a) is similar but negative as discussed above on p. 114. We wish, then, to find out if the effective length for a finite exponential horn exceeds the physical length by

$$\ell_e - \ell = \Delta\ell \propto \frac{b^2 - a^2}{2h} \quad . \tag{5-31}$$

In Fig. 5-4, $\Delta\ell$ (from the weighted mean of the individual ℓ_e's) is plotted against $(b^2 - a^2)/2h$ for the five horns tested. The vertical bars mark off ±1 standard deviation. A straight line can be drawn through the origin which passes within one standard deviation of the mean effective length for all five horns. The slope of this line is approximately 0.2 (note the difference in vertical and horizontal scales), so that

$$\Delta\ell \doteq 0.2 \, \frac{b^2 - a^2}{2h} \quad . \tag{5-32}$$

In this chapter we have sought and found a measurable discrepancy between the predictions of resonance frequencies by plane-wave horn theory and the observed behavior of torsional horns. We have interpreted the discrepancy in terms of an effective length which gives a better fit between the plane-wave predictions and the observed facts. Since errors in the radius of a horn of a few thousandths of an inch were found to cause substantially greater change in the resonance frequencies than the departure from plane wavefronts, the use of a length correction [such as Eq. (5-32) for exponential horns] in the prediction of resonance frequencies will not offer any improvement over the plane-wave theory unless machining errors can be reduced by an order of magnitude.

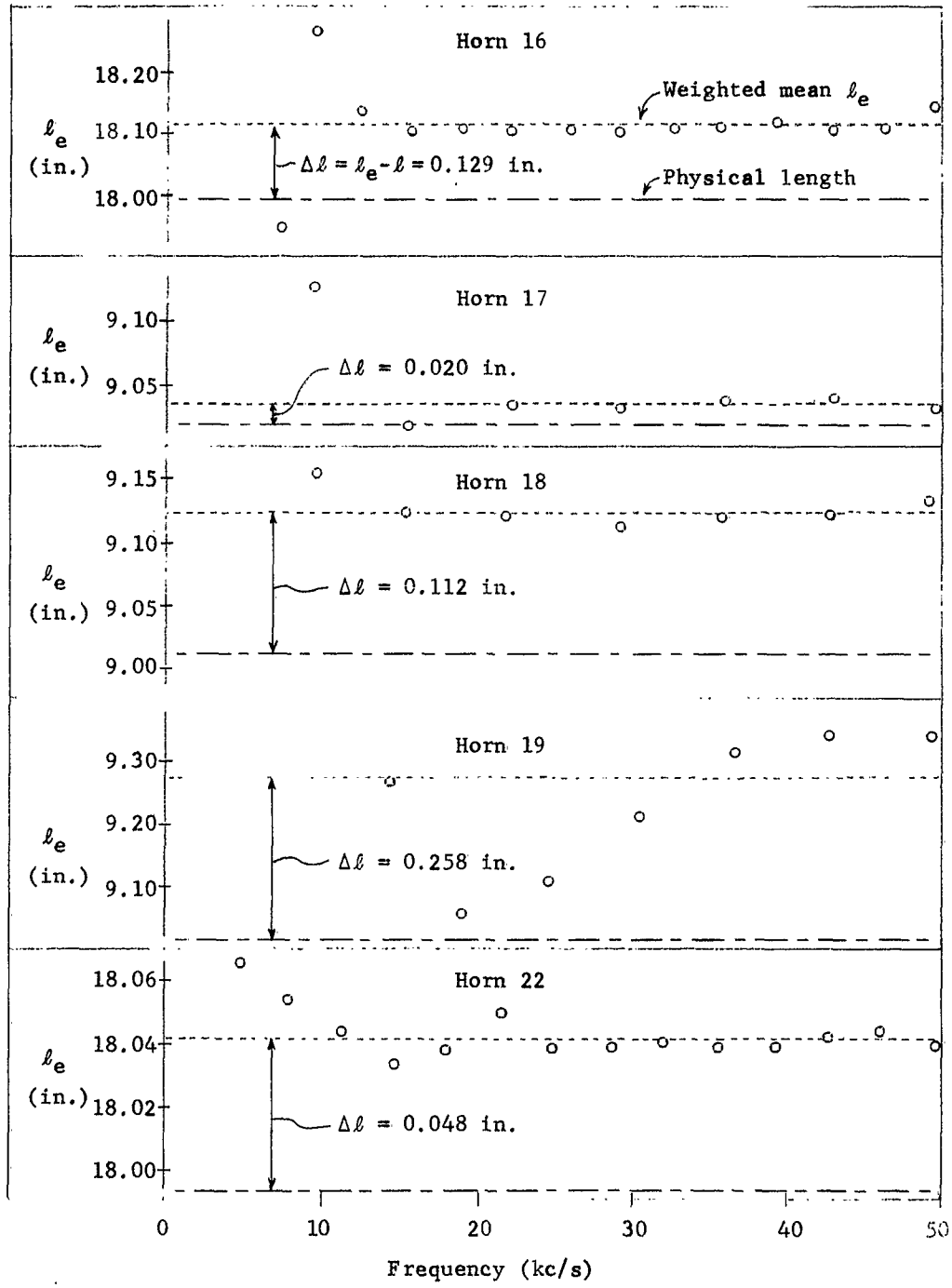

Fig. 5-3. Effective length versus frequency for five exponential horns. Note different vertical scales.

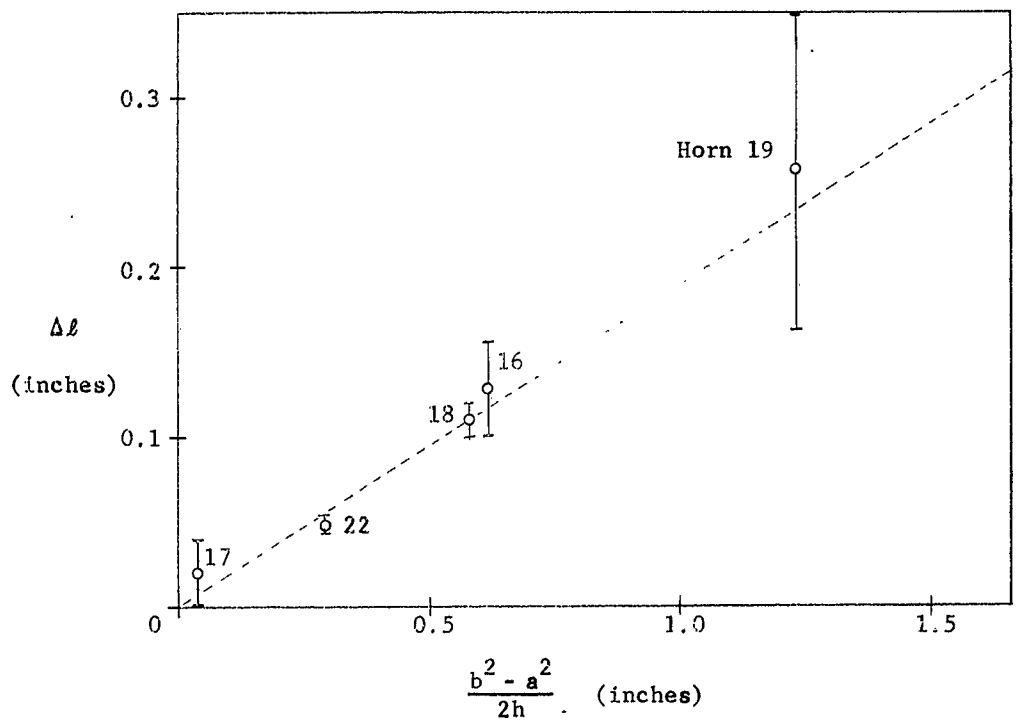

Fig. 5-4. Dependence of length correction upon horn dimensions for exponential horns. The weighted mean and standard deviation are taken from Fig. 5-3.

Chapter VI

HORNS OF PIECE WISE-SMOOTH CONTOUR

6.1 General remarks

We can consider standing waves on a finite (lossless) horn in free vibration to be composed of two progressive waves traveling in opposite directions. The two progressive waves are necessarily of equal intensity at any given point so that there is no net energy flow in either direction. We have hitherto discussed horns wherein these progressive waves are reflected only at the boundaries. For axially propagating waves, the directed energy flux due to one of the progressive waves is then the same through any cross section, since all the energy in the wave travels the full length of the horn. The introduction of a discontinuity in the horn contour or its slope, however, permits partial reflection from an internal point. The energy stored in the progressive waves need not be uniformly distributed over the length of the horn.

We can readily extend the appropriate methods of Chapter V to the analysis of piecewise-smooth horns. Within each section of the horn, the wave motion can be found from the wave equation suitable for the contour of that section. The differences in the solution are the result of the different boundary conditions: one or both ends are not free but are joined to other sections of the same horn. We can easily see what conditions are to be satisfied at an internal boundary. The angular displacement must be continuous or the horn would fracture, and by Newton's third law, the torque must be continuous since each section must exert an equal and opposite torque on the other.

A plane-wave solution found in this way will not in general satisfy the boundary condition for a free surface along the side of the horn, particularly in the vicinity of a discontinuity (infinite slope of contour), but we should expect that it would adequately describe the gross features of the vibration. Just as with the plane-wave approximation for smooth horns, the resonance frequencies calculated for piecewise-smooth horns will be upper bounds on the actual resonance frequencies, since constraining the wave motion to be a function only of distance along the horn is equivalent to stiffening the horn material internally to make the wavefronts plane.

6.2 Coupled cylinders

The experimental investigation of non-smooth horns was restricted to coupled cylinders of different diameters. These were easy to make accurately, and their modes of vibration display those features noted above not found in smooth horns. Furthermore, the plane-wave solution within each section is an exact solution in this case.

6.2.1 The double cylinder

Suppose we have two coupled cylinders of lengths ℓ_1 and ℓ_2 and radii R_1 and R_2, respectively, such that $R_1 < R_2$. Let the axis of this double cylinder coincide with the positive z-axis of a system of cylindrical coordinates and let the smaller end be at $z = 0$. Arbitrarily choosing the amplitude of the angular displacement at the small end to be unity (the same normalization we have previously employed), and assuming that only the plane-wave mode of vibration exists in each cylindrical part, we can write the standing-wave pattern for free vibrations:

$$\begin{aligned} \psi &= \cos kz \ , \qquad 0 \le z \le \ell_1 \ , \\ &= B \cos k(L-z) \ , \quad \ell_1 \le z \le L = \ell_1 + \ell_2 \end{aligned} \tag{6-1}$$

where k is the wave number, B is the amplitude in section 2, and L is the total length of the horn. Continuity of angular displacement at the step gives us

$$\cos k\ell_1 = B \cos k\ell_2 \ , \tag{6-2}$$

and continuity of torque gives [using Eq. (5-2)]

$$\sin k\ell_1 = -B \left(R_2/R_1\right)^4 \sin k\ell_2 \ . \tag{6-3}$$

Dividing (6-3) by (6-2) to eliminate B, we obtain the frequency equations

$$\tan k\ell_1 + (R_2/R_1)^4 \tan k\ell_2 = 0 \ , \quad \cos k\ell_1 \neq 0 \ , \tag{6-4a}$$

or

$$\cos k\ell_1 = 0 \ . \tag{6-4b}$$

Having solved (6-4) for the values of k, we can find the corresponding values of B from (6-2) or (6-3).

The case $\ell_1 = \ell_2 = L/2$ is of particular interest. It can be seen by inspection of (6-4) that the resonance frequencies are the same as those of the uniform cylinder of the same over-all length, L:

$$k_n L = n\pi$$

or

$$\omega_n = \frac{n\pi c}{L} \ , \quad n = 1, 2, 3, \ldots \ . \tag{6-5}$$

For the odd modes, (6-2) vanishes identically, and (6-3) gives

$$B = -(R_1/R_2)^4 \ , \quad n = 1, 3, 5, 7, \ldots \ . \tag{6-6}$$

For the even modes, (6-3) vanishes, and (6-2) gives

$$B = 1 , \quad n = 2, 4, 6, 8, \ldots . \tag{6-7}$$

The gain of the horn is $|1/B|$, or $(R_2/R_1)^4$ for the odd modes and unity for the even modes. It should be noted that for the same end diameters the gain of an exponential torsional horn is $(R_2/R_1)^2$ for all modes.

In its fundamental mode of vibration, this type of horn is known as "double quarter-wave" for obvious reasons. It is widely used for the longitudinal vibrators used in commercial ultrasonic machining devices. It has the advantage of greater ease of manufacture and greater gain than an exponential horn of the same end diameters (or, alternatively, greater lateral stiffness for a given gain due to its greater thickness). A disadvantage is that the stress has a relatively large peak at the step which limits the maximum tip velocity attainable before the elastic limit of the horn material is exceeded. A torsional double quarter-wave horn has been used experimentally for ultrasonic welding.*

Three double cylinders were constructed and investigated experimentally. Table 6-1 gives their dimensions as well as a comparison of the measured and theoretical gains for the first two modes of each. The measured gains agree with the predicted values within the precision of measurement.

The first twenty resonance frequencies for each horn were measured and compared with values predicted from the resonance frequencies of a calibration cylinder cut from the same piece of stock. The observed

---

* Personal communication from Mr. E. A. Neppiras, Mullard Laboratories, England. See also Ref. 6, cited on p. 2.

Table 6-1

Properties of double-cylindrical horns

For all horns: $R_2 = 0.500$ inches, $\ell_1 = \ell_2 = L/2 = 9.000$ inches

Horn no.	R_1, inches	Mode no.	Measured Gain	Theoretical Gain
29	0.325	1	85.2	89.6
		2	0.952	1
30	0.500	1	15.7	16.0
		2	0.975	1
31	0.700	1	4.23	4.16
		2	1.02	1

resonance frequencies for the even modes were in good agreement with the theoretical frequencies from Eq. (6-5). The odd resonance frequencies were found to be very nearly in the ratios 1:3:5: etc., but were a constant percentage lower than the theoretical values: 2.4 percent for horn 29, 2.0 percent for horn 30, and 1.7 percent for horn 31.

This behavior is not too surprising. It can be explained by reference to Fig. 6.1. For arbitrary values of k and B, ψ as given by (6-1) satisfies everywhere except at the step the boundary condition that the normal derivative of ψ vanish at the surface. Values of k and B are found which insure the continuity of torque and angular displacement across S_2 without regard to the fact that the normal derivative of ψ must vanish on the annular ring S_1 since it is a free surface. For all the even modes, however, there is an antinode of ψ at the step so that $\psi' = \frac{d\psi}{dz}$, the normal derivative on S_1, does vanish. The plane-wave solution for the even modes is then the exact solution since it satisfies the exact wave equation and boundary conditions everywhere.

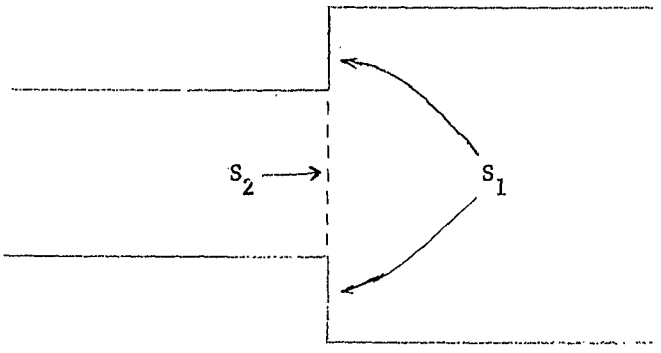

Fig. 6-1. The junction of two coupled cylinders.

All the odd modes have a node of ψ at the step and consequently the plane-wave solution does not satisfy the boundary condition there. However, since Mother Nature always sees to it that the boundary conditions <u>are</u> satisfied, there must be compound modes at the step which "patch up" the solution there. The frequency range of these measurements is well below the cutoff frequencies for the compound modes; hence, these modes do not propagate but die away exponentially with distance (see Chapter IV, section 4.1.1). Thus the presence of these modes will not appreciably affect the gross features of the standing-wave patterns (such as the gain) but will alter the resonance frequencies since these compound modes will change the energy distribution.

The observed fact that the odd resonance frequencies are a fixed percentage lower than predicted while the even resonance frequencies show good agreement with theory cannot continue to hold indefinitely for higher and higher modes since it would eventually lead to the result that an odd mode had a lower resonance frequency than the next lower even mode. The pattern of resonance frequencies must change, therefore,

at frequencies high enough so that the wavelength is comparable to the diameter of the horn, i.e., near or in the range of the cutoff frequencies for the compound modes. The influence of the compound modes would then not be restricted to the immediate vicinity of the step.

6.2.2 The triple cylinder

Let us now consider the triple cylinder: three cylindrical sections of lengths ℓ_1, ℓ_2, and ℓ_3 and radii R_1, R_2, and R_3, respectively. Let us take $L = \ell_1 + \ell_2 + \ell_3$ and choose $\psi(0) = 1$. If, as before, the small end of the horn is at $z = 0$ and the axis of the horn coincides with the positive z-axis, we can write

$$\begin{aligned} \psi &= \cos kz && 0 \le z \le \ell_1 \\ &= B_2 \cos(kz - p) , && \ell_1 \le z \le \ell_1+\ell_2 \\ &= B_3 \cos k(L - z) , && \ell_1+\ell_2 \le z \le L \end{aligned} \tag{6-8}$$

where the four constants k, p, B_2, and B_3 must be determined by the continuity of torque and angular displacement at the two internal boundaries $z = \ell_1$ and $z = \ell_1+\ell_2$.

The continuity of angular displacement gives

$$\cos k\ell_1 = B_2 \cos(k\ell_1 - p) \tag{6-9}$$

and

$$B_2 \cos[k(\ell_1+\ell_2) - p] = B_3 \cos k\ell_3 . \tag{6-10}$$

The continuity of torque gives

$$R_1^4 \sin k\ell_1 = B_2 R_2^4 \sin(k\ell_1 - p) \tag{6-11}$$

and

$$-B_2 R_2^4 \sin[k(\ell_1+\ell_2) - p] = B_3 R_3^4 \sin k\ell_3 . \tag{6-12}$$

We can divide (6-11) by (6-9) and (6-12) by (6-10) to obtain two equations from which B_2 and B_3 have been eliminated. Solving these two equations for $\tan(k\ell_1 - p)$ and equating the resulting two expressions, we obtain the frequency equation

$$R_1^4 \tan k\ell_1 + R_2^4 \tan k\ell_2 + R_3^4 \tan k\ell_3 = \left[\frac{R_1 R_3}{R_2}\right]^4 \tan k\ell_1 \tan k\ell_2 \tan k\ell_3 \qquad (6\text{-}13)$$

Once we have found k from (6-13), we can retrace our steps and solve sequentially for p, B_2, and B_3.

If ℓ_2 is one-quarter wavelength, and $R_1 R_3 = R_2^2$, so that the impedance in the second section is the geometric mean of the impedances of the end sections, we have the well-known quarter-wave matching section.* Under these conditions, there is no net reflection of a wave impinging on the quarter-wave section.

Five horns were built to test the operation of a quarter-wave matching section. The dimensions were chosen so that each horn was just one wavelength long at its second resonance. The matching section was made one-quarter of the total length. If there is no net internal reflection by the matching section, then conditions at the ends, in particular the gain, should not be affected by changes in the position of the matching section along the horn. The gain was therefore chosen as a useful index of the performance of the matching section as it was moved from one end of the horn to the other. Table 6-2 gives the dimensions and a comparison of the measured gain and the theoretical gain.

Since in this mode of vibration the energy reflected from the two ends is the same, we can use the torsional-wave impedance of a cylinder

---

* p. 120 of Ref. 19, cited on p. 23.

Table 6-2

Properties of horns for testing quarter-wave matching section

For all horns: $R_1 = 0.250$, $R_2 = 0.500$, $R_3 = 1.000$, $\ell_2 = 4.50$ inches

Horn no.	ℓ_1 (inches)	ℓ_3 (inches)	Measured Gain	Theoretical Gain
8	13.50	0	15.1	16
9	9.00	4.50	16.1	16
10	6.75	6.75	17.3	16
11	4.50	9.00	16.0	16
12	0	13.50	16.4	16

to find that the gain should be $(R_3/R_1)^2$, the same as that of an exponential horn of the same end diameters.

There is reasonable agreement between theory and experiment. Since the operation of a quarter-wave matching section depends on multiple reflections canceling each other, it seems likely that small inaccuracies in the dimensions of these horns could have a more pronounced effect on the wave transmission than comparable machining errors in, say, an exponential horn.

We have in this chapter examined the effects of a discontinuous contour upon the transmission of torsional waves. Discrepancies between experimental data and theoretical predictions based on a simplified analysis have been explained in terms of coupling to more complicated modes at the boundary. Finally, we have tested the operation of a torsional-wave analog of the quarter-wave matching section often used to couple two uniform transmission lines of different impedance.

Chapter VII

SUMMARY AND CONCLUSIONS

7.1 Results of the present investigation

The work reported here has been an attempt to develop the theory of the propagation of torsional waves in solid horns and to verify experimentally the adequacy of the theoretical description of torsional wave motion.

The theoretical analysis assumes that the horns are made of a lossless, homogeneous, isotropic elastic material. Experimental horns were made of brass and mild steel, materials which have low internal losses and whose elastic properties are sensibly homogeneous and isotropic in the frequency range of the experimental apparatus.

The mathematical tools needed for the analytic study of torsional horns are derived in Chapter II. These consist of two differential equations and their associated boundary conditions. One of these wave equations is "exact," but cannot be readily solved except for cylindrical and conical horns. The other wave equation is approximate since it is assumed at the outset that the wavefronts are plane cross sections of the horn, a circumstance which is not generally true. This equation, not surprisingly, is very similar to the plane-wave horn equation often used in the analysis of horns for compressional waves in a fluid or a solid, and, like the compressional wave equation, it can be solved for a wide variety of horn contours. The boundary condition at a free surface for use with either wave equation is that the normal derivative of the angular displacement must vanish there.

The apparatus and techniques used for the experimental study of torsional horns form the subject matter of Chapter III. It was found desirable to measure resonance frequencies and standing-wave patterns at resonance of finite horns, and thus to simulate the normal modes of vibration of a freely vibrating lossless horn.

Standing-wave patterns are measured by maintaining the specimen horn in steady vibration at one of its natural resonance frequencies, by power supplied by an eddy-current driver, and then comparing the amplitude of vibration at measurement points on the surface of the horn to the amplitude at a fixed reference point. Two conventional phonograph pickups are used to sense the vibration of the horn: a reference pickup fixed near one end of the horn and a traveling pickup which can be placed in contact with any point along the horn contour.

Resonance frequencies are found by varying the frequency of excitation and noting those frequencies at which the amplitude of vibration of the horn is a maximum. An electronic counter is used for precise measurement of the frequencies.

The eddy-current driver is a form of induction motor designed for the excitation of torsional horns. It exerts an oscillating torque on the specimen horn, without being mechanically connected to the horn, at frequencies which are the sum and difference of the two frequencies at which the drive coils are energized. An approximate analysis of the driver indicates that it should exert about twice the torque on a ferrous specimen horn that it exerts on a nonferrous horn, all other things being equal. This was tested experimentally and found to be very nearly correct. The results of the experiment are presented in tabular form in Chapter III.

The definition of torsional waves, in Chapter III, as rotationally symmetric shear waves led to the restriction that the boundary of a torsional horn be a surface of revolution. Thus torsional horns can be classified by their profile contours. It was found convenient to divide horn contours into three categories: smooth contours fitting separable coordinates, smooth contours not fitting separable coordinates, and piecewise-smooth contours characterized by one or more points of discontinuity in the contour or its slope. Chapters IV, V, and VI are devoted to selected horns of these three types, respectively.

In Chapter IV the exact wave equation is separated and solved for the normal modes of cylinders and cones. Experimental data in the form of resonance frequencies and standing-wave patterns are presented throughout the chapter in graphical and tabular form and are compared with theoretical predictions. The agreement between theory and experiment is very good to excellent in all cases. Thus the exact wave equation provides a good description of the behavior of real torsional waves.

Chapter V deals with plane-wave horn theory. The concept of impedance for torsional waves is presented and the driving point impedances of infinite cones, cylinders, and exponential horns are worked out and compared. The impedance is found to vary as the fourth power of the radius, which can be compared with variation as the square of the radius for the analogous mechanical impedance in compressional-wave horns. The exponential horn is singled out for close scrutiny to determine quantitatively the errors incurred by use of the plane-wave assumption. Measurements on a family of five exponential horns revealed that solutions of the plane-wave equation agreed with the observed standing-wave patterns within the experimental precision. The predicted resonance frequencies

were noticeably different from those measured, however, although the discrepancy is small. The frequency equation derived by use of the plane-wave assumption can be modified to provide a more accurate description of the observed facts. The modification consists of replacing the physical length of the horn by an effective length which incorporates a correction due to the non-infinitesimal flare angle of the horn. The length correction at each end of the horn is shown to be approximately proportional to the product of the slope of the contour and the radius at that end. However, it was found that the variation in resonance frequencies produced by relatively small machining errors far outweighs the change due to the use of the effective length rather than the physical length. The concept of effective length is thus not of great utility in predicting resonance frequencies, and the plane-wave horn theory in practice provides an adequate description of the behavior of exponential horns of moderate flare and radius.

The introduction of a discontinuity in the horn contour or its slope can cause partial reflections of progressive waves from an internal point of the horn. A study of the effect of a discontinuity in contour forms the subject of Chapter VI. The plane-wave analysis of Chapter V is extended to piecewise-smooth horns by imposing the requirements that torque and angular displacement be continuous across a discontinuity in the contour or its derivative. The results obtained in this manner are compared with experimental results for double and triple cylinders. The error in the resonance frequencies predicted by plane-wave theory is found to be worst when the step in contour occurs at a node of angular displacement. This behavior is qualitatively explained in terms of mode conversion at the step.

7.2 The future

We have seen that tapered solid rods excited torsionally do indeed display the characteristics commonly associated with compressional-wave horns. The methods of analysis developed for compressional waves have been successfully adapted to torsional horns. In particular, the simplifying assumption of plane wavefronts has provided a means for analyzing a wide variety of horn contours. We have seen that the accuracy of the solution thus obtained is good enough so that other factors -- machining errors and temperature variation -- produce errors of at least the same order of magnitude as the errors introduced by the plane-wave assumption. It thus appears that the problem of analysis of torsional horns has been satisfactorily solved.

The problem of synthesis still remains. Suppose we are given a set of specifications for gain and/or resonance frequencies and/or driving-point impedance, how can we synthesize the dimensions of a horn which will fill the specifications? If, as seems likely, the synthesis is not unique, how can we decide which of all the solutions is the best? It would appear that the techniques of electric-circuit synthesis could probably be adapted to some aspects of the design of distributed systems such as horns for guiding mechanical energy in one form or another. The digital computer has found application in the optical industry for the design of lens systems. Its use for the design of acoustic devices appears to be an interesting possibility.

Another possible extension of solid-horn theory would be to consider the simultaneous use of two different types of vibration (such as torsional and longitudinal) to produce particle displacement in three dimensions instead of in a plane or a line. Such a complex motion could

prove very useful in certain types of ultrasonic machining. Torsional horns as such would probably be limited in application to ultrasonic spot welding or polishing and burnishing. The design of a horn to satisfy the requirement that a longitudinal resonance and a torsional resonance occur at the same frequency would be an interesting problem.

It is the author's hope that the work described in this report can provide a useful starting point for attack upon problems such as these.

Appendix A

SEPARABLE COORDINATE SYSTEMS NOT PERMITTING ONE-PARAMETER SOLUTIONS

In addition to the cylindrical and spherical coordinates discussed in Chapter IV, there are three more separable coordinate systems with rotational symmetry. These are parabolic, prolate spheroidal, and oblate spheroidal coordinates.

In all three systems, φ is the azimuth angle and hence does not appear in the differential equations for ψ, since ψ is not a function of φ. First we tabulate for the three coordinate systems the differential line element, ds (in terms of the scale factors and differentials of the coordinates), the torsional wave equation, and the two ordinary differential equations into which it separates; then we show that none of these three systems possesses a one-parameter solution for ψ. As usual, $k = \omega/c$.

Parabolic coordinates: (v,w,φ)

$$ds^2 = (v^2 + w^2)(dv^2 + dw^2) + v^2 w^2 d\varphi^2 \tag{A-1}$$

The torsional wave equation for ψ is

$$\psi_{vv} + \frac{3}{v}\psi_v + \psi_{ww} + \frac{3}{w}\psi_w + k^2(v^2 + w^2)\psi = 0 . \tag{A-2}$$

If $\psi = V(v)\,W(w)$, we obtain the following separated ordinary differential equations, wherein λ is a separation constant:

$$\frac{d^2V}{dv^2} + \frac{3}{v}\frac{dV}{dv} + (k^2v^2 - \lambda)\,V = 0 \tag{A-3}$$

$$\frac{d^2W}{dw^2} + \frac{3}{w}\frac{dW}{dw} + (k^2w^2 + \lambda)\,W = 0 \tag{A-4}$$

Prolate spheroidal coordinates: (μ,θ,φ)

$$ds^2 = D^2(\cosh^2\mu - \cos^2\theta)(d\mu^2 + d\theta^2) + D^2\sinh^2\mu \sin^2\theta d\varphi^2 \qquad (A\text{-}5)$$

D is a shape parameter with the dimensions of length.

The torsional wave equation for ψ is

$$\psi_{\mu\mu} + 3\coth\mu\ \psi_\mu + \psi_{\theta\theta} + 3\cot\theta\ \psi_\theta + (kD)^2(\cosh^2\mu - \cos\theta)\ \psi = 0. \qquad (A\text{-}6)$$

If $\psi = V(\mu)\,W(\theta)$, we obtain the following separated equations:

$$\frac{d^2V}{d\mu^2} + 3\coth\mu\,\frac{dV}{d\mu} + \left[(kD\cosh\mu)^2 - \lambda\right]V = 0 \qquad (A\text{-}7)$$

$$\frac{d^2W}{d\theta^2} + 3\cot\theta\,\frac{dW}{d\theta} - \left[(kD\cos\theta)^2 - \lambda\right]W = 0 \qquad (A\text{-}8)$$

Oblate spheroidal coordinates: (μ,θ,φ)

$$ds^2 = D^2(\sinh^2\mu + \cos^2\theta)(d\mu^2 + d\theta^2) + D^2\cosh^2\mu \sin^2\theta d\varphi^2 \qquad (A\text{-}9)$$

D is again a shape parameter.

The torsional wave equation for ψ is

$$\psi_{\mu\mu} + 3\tanh\mu\ \psi_\mu + \psi_{\theta\theta} + 3\cot\theta\ \psi_\theta + (kD)^2(\sinh^2\mu + \cos^2\theta)\ \psi = 0. \qquad (A\text{-}10)$$

If $\psi = V(\mu)\,W(\theta)$, we obtain the following separated equations:

$$\frac{d^2V}{du^2} + 3\tanh\mu\,\frac{dV}{du} + \left[(kD\sinh\mu)^2 - \lambda\right]V = 0 \qquad (A\text{-}11)$$

$$\frac{d^2W}{d\theta^2} + 3\cot\theta\,\frac{dW}{d\theta} + \left[(kD\cos\theta)^2 + \lambda\right]W = 0 \qquad (A\text{-}12)$$

Both prolate and oblate spheroidal coordinates approach spherical coordinates as $D \rightarrow 0$.

It is now easily seen that none of these three systems allows a one-parameter solution for ψ. Such a solution would require that either V or W equal a (nonzero) constant. Bearing in mind that k and λ are constants and not functions of position, we see from examination of Eqs. (A-3), (A-4), (A-7), (A-8), (A-11), and (A-12) that unless both k and λ are zero, none of these equations is satisfied by a constant. The case k = 0 is a degenerate situation in which the only motion of the horn is continuous rigid-body rotation. Therefore, there are no one-parameter solutions.

Appendix B

NUMERICAL CALCULATION OF EIGENVALUES

In Chapter IV, numerical data calculated with the aid of the programmed digital computer were presented in graphical form. It is the purpose of this appendix to indicate the major features of the numerical analysis involved.

The problem was to find the resonance frequencies of the compound modes of a cone, or, in mathematical terms, to find the eigenvalues of a differential-equation-plus-boundary-conditions system. The differential equation in question is Eq. (4-24) and its associated boundary conditions (4-28), which are

$$V''(r) + \frac{4}{r} V'(r) + \left[k^2 - \frac{\lambda}{r^2}\right] V(r) = 0 \qquad \text{(B-1)}$$

and

$$V'(a) = V'(b) = 0 \qquad \text{(B-2)}$$

where $k = \omega/c$, the wave number, is the eigenvalue to be determined, and λ is itself the eigenvalue of Eq. (4-27) and its boundary conditions (4-29), namely,

$$W''(\theta) + 3 \cot \theta \, W'(\theta) + \lambda W(\theta) = 0 \qquad \text{(B-3)}$$

and

$$W'(0) = W'(\alpha) = 0 \qquad \text{(B-4)}$$

The cone is bounded by $r = a$ at the small end, $r = b$ at the large end, and $\theta = \alpha$ along the sides. In order to keep in touch with the notation of Chapter IV, we should note that λ is an abbreviation for $(\eta + 2)(\eta - 1)$.

In order to find the proper values of λ, and hence η, from Eqs. (B-3) and (B-4), the continuous domain $0 \leq \theta \leq \alpha$ was replaced by the $N+1$ points $\theta_i = i\alpha/N$, $i = 0, 1, 2, \ldots, N$. The differential equation was replaced by a difference equation obtained by approximating the derivatives with the three-point difference formulas

$$W'(\theta_i) \equiv W_i' = \frac{W_{i+1} - W_{i-1}}{2h} + R_1 \quad , \tag{B-5}$$

and

$$W'(\theta_i) \equiv W_i'' = \frac{W_{i+1} - 2W_i + W_{i-1}}{h^2} + R_2 \tag{B-6}$$

where $W_i \equiv W(\theta_i)$, $h \equiv \alpha/N$ = mesh spacing, and the remainder terms R_1 and R_2, which are neglected in the formation of the difference equation, are both[45] of the order of h^2. The fact that R_1 and R_2 are of order h^2 will prove useful later.

The approximating difference equation is

$$(1 - \frac{3}{2} h \cot \theta_i) W_{i-1} + (\lambda h^2 - 2) W_i + (1 + \frac{3}{2} h \cot \theta_i) W_{i+1} = 0 \tag{B-7}$$

and the boundary conditions (B-4), using difference formula (B-5), become

$$W_{-1} = W_{+1} \quad \text{and} \quad W_{N-1} = W_{N+1} \tag{B-8}$$

We now have a difference equation and boundary conditions whose solution will be a good approximation to the solution of (B-3) and (B-4) if h is small.

If the boundary conditions (B-8) are used to eliminate the W_{-1} and W_{N+1} terms from the difference equation (B-7) for $i = 0$ and $i = N$, respec-

---

45. Kunz, K. S., Numerical Analysis (McGraw-Hill, New York, 1957), Chapters 4 and 7.

tively, then the set of equations represented by Eq. (B-7) may be conveniently cast in the matrix form

$$\begin{bmatrix} B & C_0 & 0 & \cdots & \cdots & 0 \\ A_1 & B & C_1 & 0 & \cdots & 0 \\ 0 & A_2 & B & C_2 & 0 \cdots & 0 \\ \cdots & & & & 0 & \\ & 0 & & & & \\ 0 & \cdots & \cdots & 0 & A_{N-1} B & C_{N-1} \\ 0 & \cdots & \cdots & \cdots & 0 \quad A_N & B \end{bmatrix} \begin{bmatrix} W_0 \\ W_1 \\ W_2 \\ \\ \\ W_{N-1} \\ W_N \end{bmatrix} = \begin{bmatrix} 0 \\ 0 \\ \\ 0 \\ \cdot \\ \\ 0 \end{bmatrix} \qquad \text{(B-9)}$$

where $A_i = 1 - \frac{3}{2} n \cot \theta_i$, $i = 1, 2, 3, \ldots, N-1$, and $A_N = 2$, $B = \lambda h^2 - 2$, and $D_i = 1 + \frac{3}{2} h \cot \theta_i$, $i = 1, 2, 3, \ldots, N-1$, and $C_0 = 2$.

Now we have a set of linear, homogeneous, simultaneous equations which can have a nontrivial solution only if the determinant of their coefficients vanishes. It is now apparent that we seek those values of λ for which the determinant of the square matrix in (B-9) will vanish. We should note that the determinant is a polynomial of degree $N+1$ in B and hence will vanish for at most $N+1$ different values of λ, whereas the original differential equation has an infinite number of eigenvalues. The process of substituting the difference equation for the differential equation is physically equivalent to substituting a lumped mechanical system with $N+1$ degrees of freedom for the (continuously distributed) cone. Since we expect the lumped mechanical system to be a good approximation to the cone only for wave-lengths "sufficiently greater than a lump," so also we should expect that the roots of the determinant will

provide much better approximations to the lower eigenvalues of the differential equation than to the higher ones.

Examining the form of the determinant, we see that it is "tri-diagonal"; that is, the only nonzero terms are on the diagonal and immediately adjacent to it on either side. This is a direct consequence of our use of three-point approximations to the derivatives in setting up the difference equation. A tri-diagonal determinant is quite easy to evaluate. Denoting by D_i the ith upper left-hand principal minor, we can expand in minors of the ith row or column and obtain

$$D_i = B\, D_{i-1} - A_i C_{i-1} D_{i-2} \qquad \text{(B-10)}$$

Starting with $D_0 = B$ and $D_1 = B^2 - A_1 C_0$, we can apply (B-10) repeatedly until we obtain D_N, the value of the whole determinant. This procedure can be readily adapted to machine calculation.

The errors in the calculated eigenvalues arise from two sources. The first is the fact that the roots of the determinant are not exactly equal to the eigenvalues of the differential equation for finite N. The second is roundoff error in the computer, which limits the accuracy attainable in finding the roots of the determinant. The first type of error can be made as small as desired by increasing N; the second, however, increases as N increases. Therefore, there is some optimum value of N for which the accuracy is the greatest. This can be determined experimentally by calculating one or more eigenvalues for various values of N.

An IBM 7090 was the computer used for most of the calculations. The optimum value of N was empirically found to be approximately 100. The values of the eigenvalue η (reminder: $\lambda = \eta^2 + \eta - 2$) were found with an accuracy of three to four significant figures for N = 100. However, it was possible to gain about two more significant figures in accuracy by estimating the error and introducing a correction. It was noted above that the remainder terms in (B-5) and (B-6), the difference-formula approximations to the first and second derivatives, were both of order h^2. We might suspect that the error in the calculated eigenvalues would then also be of order h^2. Assuming this to be true, we could then calculate an eigenvalue for two different values of h (i.e., two values of N), plot eigenvalue versus h, and construct a parabola through these two points which would cross the h-axis normally and at a much more accurate estimate of the eigenvalue.

This procedure is very difficult to justify on other than empirical grounds. It was tried in cases for which the answers were known, using N = 50 and N = 100, and it yielded an improvement in accuracy of approximately a factor of 100 over N = 50, with an increase of only a factor of three in computer time used. It was therefore incorporated as a feature of the program.

Exactly the same method was used to find the eigenvalue k in Eq. (B-1), except that a new dependent variable $G(r) = r^{1-\eta} V(r)$ was introduced to avoid difficulties at the origin r = 0 due to the singularity there. This transformation gives the differential equation

$$G''(r) + \frac{2(\eta + 1)}{r} G'(r) + k^2 G(r) = 0 \ . \qquad \text{(B-11)}$$

The boundary conditions on G(r) are now mixed:

$$(\eta - 1)\, G(b) + bG'(b) = 0$$

and

$$(\eta - 1)\, G(a) + aG'(a) = 0 \ , \quad a \neq 0 \ ,$$

or

$$G'(0) = 0 \ , \quad a = 0. \tag{B-12}$$

The problem was normalized in such a way that the number calculated was the dimensionless product $k(b - a) = k\ell$. The parabolic error-estimating scheme described above was found to work here, also.

The results of these computations are presented as Fig. 4-2, Chapter IV.

LIST OF REFERENCES

1. U. S. Patent No. 2,044,807, issued June 23, 1936, to Atherton Noyes, Jr., assignor to G. W. Pierce. Application filed on June 30, 1933.

2. U. S. Patent No. 2,514,080, issued July 4, 1950, to W. P. Mason. Application filed on January 10, 1945.

3. A. G. Webster, "Acoustical Impedance and the Theory of Horns and of the Phonograph," Proc. Natl. Acad. Sci. U. S. 5 (1919), p. 275.

4. Mason, W. P., Physical Acoustics and the Properties of Solids (Van Nostrand, New York, 1958). See also W. P. Mason and R. F. Wick, "A Barium Titanate Transducer Capable of Large Motion at an Ultrasonic Frequency," J. Acoust. Soc. Am. 25 (1951), p. 209.

5. L. G. Merkulov, "Design of Ultrasonic Concentrators," Soviet Phys. - Acoustics 3 (1957), p. 246.

6. E. A. Neppiras, "Very high energy ultrasonics," Brit. J. Appl. Phys. 11 (1960), p. 143.

7. E. A. Neppiras and R. D. Foskett, "Ultrasonic Machining," Philips Tech. Rev. 18 (1956-7), p. 325. See also E. A. Neppiras, "A high-frequency reciprocating drill," J. Sci. Inst. 30 (1953), p. 72.

8. R. W. Pyle Jr., "Torsional Horns," paper I9, Sixtieth Meeting of the Acoustical Society of America, October 20-22, 1960. An abstract of this paper appears in J. Acoust. Soc. Am. 32 (1960), p. 1504.

9. A. V. Kharitonov, "Torsional Ultrasonic Concentrators," Soviet. Phys. - Acoustics 7 (1962), p. 310.

10. L. O. Marakov, "Theoretical Investigation of Selected Torsional Oscillating Systems," Soviet Phys. - Acoustics (1962), p. 364.

11. Sokolnikoff, I. S., Mathematical Theory of Elasticity (McGraw-Hill, New York, 1956).

12. Kolsky, H., Stress Waves in Solids (Oxford University Press, London, 1953).

13. L. Pochhammer, J. reine angew. Math. 81 (1876), p. 324.

14. Courant, R., and D. Hilbert, Methods of Mathematical Physics (Interscience, New York, 1953), Vol. I.

15. Forsythe, A. R., Calculus of Variations (Dover, New York, 1960).

16. Kaplan, W., Advanced Calculus (Addison-Wesley, Cambridge, Mass., 1953).

17. Morse, P. M., Vibration and Sound (McGraw-Hill, New York, 1948), 2nd ed.

18. Temple, G., and W. G. Bickley, Rayleigh's Principle (Dover, New York, 1956).

19. Olson, H. F., Acoustical Engineering (Van Nostrand, New York, 1957).

20. Hunt, F. V., Electroacoustics (Wiley, New York, 1954).

21. Smythe, W. R., Static and Dynamic Electricity (McGraw-Hill, New York, 1950).

22. Morse, P. M., and H. Feshbach, Methods of Theoretical Physics (McGraw-Hill, New York, 1953).

23. Gray, D. E., editor, American Institute of Physics Handbook (McGraw-Hill, New York, 1957).

24. Westman, H. P., editor, Reference Data for Radio Engineers (International Telephone and Telegraph Corp., New York, 1956), 4th ed.

25. Langford-Smith, F., editor, Radiotron Designer's Handbook (RCA, Harrison, New Jersey, 1953).

26. L. A. Goldmuntz and H. L. Krauss, "The Cathode-Coupled Clipper Circuit," Proc. IRE 36 (1948), p. 1172.

27. Terman, F. E., Electronic and Radio Engineering (McGraw-Hill, New New York, 1955), 4th ed.

28. Guillemin, E. A., Synthesis of Passive Networks (Wiley, New York, 1957).

29. T. J. Schultz, "Triode Cathode-Followers for Impedance Matching to Transformers and Filters," Trans. IRE AU-3 (1955), p. 28.

30. Truxal, J. G., Control System Synthesis (McGraw-Hill, New York, 1955).

31. Whitehead, T. N., Instruments and Accurate Mechanism (Dover, New York, 1954).

32. Elliott, A., and J. H. Dickson, Laboratory Instruments (Chemical Publishing Co., New York, 1960), 2nd ed.

33. Guillemin, E. A., Introductory Circuit Theory (Wiley, New York, 1953).

34. Jahnke, E., and F. Emde, Tables of Functions (Dover, New York, 1945).

35. E. A. Flinn, "Exact Transient Solution of Some Problems of Elastic Wave Propagation," J. Acoust. Soc. Am. 33 (1961), p. 623.

36. Lord Rayleigh, Theory of Sound (Dover, New York, 1945).

37. Whittaker, E. T., and G. N. Watson, Modern Analysis (Cambridge University Press, Cambridge, 1927), 4th ed.

38. Storer, J. E., Passive Network Synthesis (McGraw-Hill, New York, 1957).

39. Erdelyi, A., editor, Higher Transcendental Functions (McGraw-Hill, New York, 1953), Vols. I & II.

40. Watson, G. N., Bessel Functions (Cambridge University Press, Cambridge, 1944).

41. O. K. Mawardi, "Sound Propagation in Horns: General Theory," Tech. Memo. No. 4, Acoustics Research Lab., Harvard Univ., 1949. See also O. K. Mawardi, "Generalized Solutions of Webster's Horn Theory," J. Acoust. Soc. Am. 21 (1949), p. 323.

42. Beranek, L. L., Acoustics (McGraw-Hill, New York, 1954).

43. McLachlan, N. W., Theory of Vibrations (Dover, New York, 1951).

44. J. Holtsmark, J. Lothe, S. Tjøtta, and W. Romberg, Archiv for Mathematik og Naturvidenskab 53, no. 8 (1955).

45. Kunz, K. S., Numerical Analysis (McGraw-Hill, New York, 1957), Chapters 4 and 7.

Distribution List[†]

Office of Naval Research (Code 468)
Department of the Navy
Washington 25, D. C. (2)

Bureau of Ships (Code 688)
Department of the Navy
Washington 25, D. C. (2)

Armed Services Technical Information Agency
Arlington Hall Station
Arlington 12, Virginia (10)

Bureau of Naval Weapons
Code RU-22 (Oceanographer)
Washington 25, D. C.

Bureau of Ordnance (ReUlc)
Department of the Navy
Washington 25, D. C.

Bureau of Aeronautics
Department of the Navy
Washington 25, D. C.

Commanding Officer
Office of Naval Research Branch Office
495 Summer Street
Boston 10, Massachusetts

Commanding Officer
Office of Naval Research Branch Office
Box 39, Navy No. 100
FPO, New York (2)

Commanding Officer
Office of Naval Research Branch Office
The John Crerar Library Building
88 East Randolph Street
Chicago 1, Illinois

Commanding Officer
Office of Naval Research Branch Office
1030 East Green Street
Pasadena 1, California

Commanding Officer and Director
David Taylor Model Basin
Washington 7, D. C.

Stanford Research Institute
Department of Physics
Stanford, California
Attn: Sonics Section

New Zealand Joint Services Mission
3101 Cleveland Avenue, N.W.
Washington 8, D. C.

Superintendent
U. S. Navy Postgraduate School
Monterey, California
Attn: Prof. L. E. Kinsler

Bell Telephone Laboratories
Whippany, New Jersey
Attn: Dr. W. A. Tyrell

John Carroll University
University Heights
Cleveland 18, Ohio
Attn: Dr. E. F. Carome

Melpar, Inc.
Applied Science Division
11 Galen Street
Watertown 72, Massachusetts
Attn: Mrs. Lorraine T. Nazzaro, Librarian

Gordon McKay Laboratory of Applied Science
Harvard University
Cambridge 38, Massachusetts (2)

Gordon McKay Library
Pierce Hall
Harvard University
Cambridge 38, Massachusetts (2)

Commander
U. S. Naval Air Development Center
Johnsville, Pennsylvania

Director
U. S. Naval Research Laboratory
Technical Information Division
Washington 25, D. C. (6)

Director
U. S. Naval Research Laboratory
Sound Division
Washington 25, D. C.

Commander
U. S. Naval Ordnance Laboratory
Acoustics Division
White Oak
Silver Spring, Maryland

Commanding Officer and Director
U. S. Navy Underwater Sound Laboratory
Fort Trumbull
New London, Connecticut

Commanding Officer and Director
U. S. Navy Electronics Laboratory
San Diego 52, California

Director
U. S. Navy Underwater Sound Reference Laboratory
Office of Naval Research
P. O. Box 3629
Orlando, Florida

Commanding Officer
U. S. Navy Mine Defense Laboratory
Panama City, Florida

Commander
New York Naval Shipyard
Brooklyn 1, New York
Attn: Material Laboratory (Code 912b)

CROTLS, Stop 39
Air Force Cambridge Research Center
Army Base
Boston, Massachusetts
Attn: John Armstrong

U. S. Naval Academy
Annapolis, Maryland
Attn: Library

Dr. J. R. Smithson
Electrical Engineering Department
U. S. Naval Academy
Annapolis, Maryland

Western Reserve University
Department of Chemistry
Cleveland, Ohio
Attn: Dr. E. Yeager

Convair
Division of General Dynamics Corporation
San Diego 12, California

Library
Scripps Institution of Oceanography
La Jolla, California

U. S. Atomic Energy Commission
Technical Information Service Extension
P. O. Box 62
Oak Ridge, Tennessee
Attn: I. A. Warheit

Director
Defense Research Laboratory
University of Texas
Austin, Texas

Institute for Defense Analyses
Communications Research Division
von Neumann Hall
Princeton, New Jersey

Chief, Physics Division
Office of Scientific Research
Hq. Air Research and Development Command
Andrews Air Force Base
Washington 25, D. C.

Chief, Physics Division
Office of Scientific Research
Hq. Air Research and Development Command
P. O. Box 1395
Baltimore, Maryland

Commander
Wright Air Development Division
Wright-Patterson Air Force Base
Ohio
Attn: Bioacoustics Branch
(Aerospace Medical Laboratory)

Office of Chief Signal Officer
Department of the Army
Pentagon Building
Washington 25, D. C.

Los Alamos Scientific Laboratory
P. O. Box 1663
Los Alamos, New Mexico
Attn: Dr. G. L. Campbell

Director
National Bureau of Standards
Connecticut Avenue and Van Ness St., N.W.
Washington 25, D. C.
Attn: Chief of Sound Section

National Science Foundation
1520 H Street, N.W.
Washington, D. C.

Woods Hole Oceanographic Institution
Woods Hole, Massachusetts
Attn: A. C. Vine

Brown University
Department of Physics
Providence 12, Rhode Island

University of California
Department of Physics
Los Angeles, California

University of California
Marine Physical Laboratory of the Scripps Institution of Oceanography
San Diego 52, California

Catholic University of America
Department of Physics
Washington 17, D. C.

Director
Hudson Laboratories
Columbia University
145 Palisades Street
Dobbs Ferry, New York

Lamont Geological Observatory
Columbia University
Torre Cliffs
Palisades, New York

Chief, Office of Ordnance Research
Box CM, Duke Station
Durham, North Carolina

Massachusetts Institute of Technology
Department of Physics
Cambridge 39, Massachusetts
Attn: Prof. Ingard

Director
Ordnance Research Laboratory
Pennsylvania State University
University Park, Pennsylvania

[†]One copy unless otherwise specified.